63-3-5

RADC-TDR-62-618

MULTIMEGAWATT BROADBAND MICROWAVE TUBES AND RELATED STUDIES

FIRST ANNUAL REPORT

September 1, 1961 to October 31, 1962

TECHNICAL DOCUMENTARY REPORT NO. RADC-TDR-62-618

December 1962

Rome Air Development Center
Research and Technology Division
Air Force Systems Command
United States Air Force
Griffiss Air Force Base, New York

Project No. 5573, Task No. 557303

(Prepared under Contract No. AF 30(602)-2575 by the Microwave Laboratory, W. W. Hansen Laboratories of Physics, Stanford University, Stanford, California)

ASTIA NOTICE:

Requests for additional copies by Agencies of the Department of Defense, their contractors, and other Government agencies should be directed to the:

ARMED SERVICES TECHNICAL INFORMATION AGENCY
ARLINGTON HALL STATION
ARLINGTON 12, VIRGINIA

Department of Defense contractors must be established for ASTIA services or have their "need-to-know" certified by the cognizant military agency of their project or contract.

PATENT NOTICE:

When Government drawings, specifications, or other data are used for any purpose other than in connection with a definitely related Government procurement operation, the United States Government thereby incurs no responsibility nor any obligation whatsoever and the fact that the Government may have formulated, furnished, or in any way supplied the said drawings, specifications or other data is not to be regarded by implication or otherwise as in any manner licensing the holder or any other person or corporation, or conveying any rights or permission to manufacture, use, or sell any patented invention that may in any way be related thereto.

EXISTENCE OF PROPRIETARY INFORMATION NOTICE:

This document is furnished under U.S. Government Contract No. AF 30(602)-2575 and shall not be released outside the Government (except to foreign Governments subject to these same limitations) nor be disclosed, used, or duplicated for procurement of manufacturing purposes, except as otherwise authorized by said contract, without the permission of the Microwave Laboratory. This legend shall be marked on any reproduction thereof in whole or in part.

DISPOSITION NOTICE:

Do not return this copy. Retain or destroy.

FOREWORD

This report describes the results achieved under Contract AF 30(602)-2575 during the contract year of September 1, 1961 to October 31, 1962.

The general overall objectives of this contract are to conduct theoretical and experimental investigations of microwave tubes with a view toward the development of tubes capable of at least 10 megawatts of peak power, average power approaching 50 kilowatts, bandwidths approaching 30 percent, gains of 35 db and efficiencies of 40 percent; and to conduct theoretical and experimental investigations of other related microwave devices.

The predecessor to this contract was AF 30(602)-1844 and the earlier work for a number of the projects included herein has been reported under Contract AF 30(602)-1844.

During the course of this contract year, three quarterly memoranda were written and distributed:

(1) Quarterly Memorandum No. 1, for the period 1 September to 30 November 1961 (Microwave Laboratory Report No. 881, January 1962).

(2) Semi Annual Technical Note; jointly Quarterly Memorandum No. 2, for the period 1 December 1961 to 28 February 1962 (Microwave Laboratory Report No. 903, March 1962).

(3) Quarterly Memorandum No. 3, for the period 1 March to 31 May 1962 (Microwave Laboratory Report No. 933, July 1962).

This Annual Report summarizes the materials reported in these three quarterly memoranda and describes the work done in the final quarterly period as well.

At the time of this Annual Report there were 11 projects active under this contract:

I. Long Slot TWT

II. Ten Megawatt Cloverleaf TWT

III. Tapered Cloverleaf TWT

IV. Centipede TWT

V. Electron Stick

VI. Hollow Beam Electron Guns

VII. Extended Interaction Klystrons

VIII. Nonperiodic Dielectric-lined High-power TWT

IX. Fast Wave Tubes

X. Electron Beam Interaction with a Cesium Plasma

XI. Transverse Wave Devices

The first 8 of these projects were active during the year and were reported regularly in the quarterly memoranda. The last three are new projects recently assigned to this contract. These three projects have not been reported under this contract prior to this time. The background and history of each is reported herein.

Three of these projects will be terminated as of 31 October 1962, and the fourth one will be reorganized:

AIR FORCE. Cato Show Prtg. Co. 5/7/63 - 246

1. Ten Megawatt Cloverleaf TWT
2. Tapered Cloverleaf TWT
3. Electron Stick
4. Centipede TWT

These projects will therefore not be reported again as such after this Annual Report. The "Centipede TWT" project will be re-organized because a major part of the work has been completed. Future reports on this latter project will appear under a different title.

The Responsible Investigator for this contract is Professor Marvin Chodorow.

ABSTRACTS

I. Long Slot TWT

During the past year a study of various methods of selectively loading the upper passbands of a periodic circuit has been made. This has resulted in a loading scheme which is a composition of various other types and appears to merit testing in an amplifier at high power levels. The attenuation is accomplished by means of resonant slots which radiate into a lossy waveguide which is essentially nonpropagating by virtue of the high attenuation per wavelength. The coupling through the slots is, therefore, discrete and the total attenuation is found by multiplying that from one slot by the total number of slots. Cold tests on the slow-wave structure so loaded have indicated values of attenuation per cavity in excess of the small signal gain. Thus, regenerative oscillations should be suppressed and backward-wave oscillations inhibited unless the circuit is made excessively long. Attenuation in the amplification band is minimal because the radiating slots are not resonant at these frequencies and the lossy waveguide is well below cutoff so there is no propagation through the loss material.

II. Ten Megawatt Cloverleaf TWT

The effort on this project has been reduced this past year in order to develop project I above more fully. After some modifications are made, measurements will be made; and then the project will be terminated.

III. Tapered Cloverleaf TWT

This project was recently completed and a final report has been written. The abstracts from the final report is included herein.

IV. Centipede TWT

The suppression of unwanted modes has been the principal objective of the work using the centipede structure. The analysis and cold test of externally coupled waveguides which are cut off at the operating frequency and the related centipede structure studies have been completed. A similar theoretical and experimental study which allows for coupling throughout the operating frequency range is current and is adapted for evaluation using the electron stick. It is expected that these methods will allow the tube performance characteristics to be optimized without the previous limitations of the stability requirements. The methods and techniques used here should be applicable to nearly all similar types of traveling-wave tubes.

V. Electron Stick

The electron stick is a tool for evaluating high power traveling-wave tube or klystron type circuits without the construction of a complete tube. Another particularly important advantage of this device is that the circuit under test is outside the vacuum envelope so that individual circuit parameters may be varied in a controlled manner. The electron stick with all of the associated mounting mechanisms adapted for use with several circuits has been completed. This electron stick has nearly 100 percent beam transmission and has been operated at 120 kv with a beam power in excess of 10 megawatts.

VI. Hollow Beam Electron Guns

Over the past year the work on this project has been concerned with two main areas. One is the continuation of our work on a general method for obtaining gun designs by the method of analytic continuation for axisymmetric flows in which the initial conditions are the cathode current density and cathode shape. During the year we developed the method for determining analytically the electrodes required to form these flows. Further work was done on the investigation of cathode shapes which would be useful from a practical viewpoint.

The other area of work this year was on the development of a high precision method of calculation to be used as an alternate to the method of analytic continuation. The theory for this was worked out in detail and also tested on a digital computer for the two-dimensional Laplace equation. Further computer calculations indicated the method was also valid for more complicated electron gun design equations.

VII. Extended Interaction Klystrons

"Cold"-test properties of the SSM line, both in single-deck and double-deck configurations, are closely predicted by means of Dashenkov's method. Possible improvement of basic circuit characteristics has been explored.

VIII. Nonperiodic Dielecric-Lined High-Powered TWT

The objective of this project has been to design and then construct an S-band TWT having an rf structure of a homogeneous beryllium-oxide tube bonded to an outer copper shell. The design work has been completed and the construction has proceeded as far as possible without using the beryllia. Further work has been deferred pending the availability of the electron stick (see Section VI).

IX. Fast Wave Tubes

Cyclotron resonance interaction to produce backward-wave oscillation and amplification has been investigated at S-band, and a tube directly scaled to 1 mm wavelength was built and tested. This tube has a similar beam injection scheme as that used in the S-band. A long, homogeneous, and millisecond-pulse magnetic field at 100,000 gauss was achieved by a special design of a single-layer helical coil similar to Bitter's type. The design of the coil and associated pulser is discussed briefly. Rectangular waveguide with inner dimensions of 1 mm x 0.7 mm was used for the rf circuit. Beam transmission as high as 120 ma through such intensive field is reported.

X. Electron Beam Interaction with a Cesium Plasma

This project is reported herein under this contract for the first time, so a review of previous work and nomenclature is given. The plasma-beam interaction is examined by considering the special case of the plasma and beam filling the drift tube. The phase characteristics of a plasma column of nonuniform cross section are studied both analytically and numerically. Dispersion relations are derived for the plasma column containing a turning-point. An experiment has been set up to check the propagation theory developed.

XI. Transverse Wave Devices

The objective of this new project is to study a possible approach to broadband high-power amplifiers which involves interaction between an electron beam and a circuit in the presence of an axial dc magnetic field. The work to date has been primarily theoretical. Abstracts from five papers are reported herein. Significant progress has been made in establishing a theory for transverse wave propagation on electron beams of finite diameter; some of the important results are summarized.

PUBLICATION REVIEW

This report has been reviewed and is approved.

Approved:

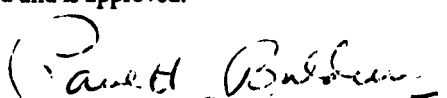

ARTHUR J. FROHLICH
Chief, Techniques Laboratory
Directorate of Aerospace Surveillance & Control

Approved:

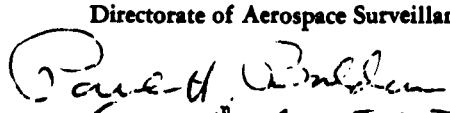

JAMES B. BRYANT, Col, USAF
Director of Aerospace Surveillance & Control

TABLE OF CONTENTS

LIST OF FIGURES

INTRODUCTION

A number of the objectives for this contract have either been achieved or surpassed or they can be easily achieved on the basis of knowledge that has been accumulated. In the portion of the contract related to the development of broadband megawatt tubes, including the cloverleaf, centipede and long-slot structures, objectives such as a peak power output of 10 megawatts, 30 percent efficiency, 30 db gain, bandwidth of 20 percent, and high average power at 3000 Mc have essentially been accomplished. In other respects, however, the evolution of the program has indicated areas where there are still difficulties which should be emphasized. One area that received considerable emphasis was related to the achievement of most of the above objectives, *i.e.*, that of adequate stability. Additional objectives which include new design procedures for high perveance hollow beam electron guns, different types of interaction circuits for high power tubes, and new interaction mechanisms such as transverse wave devices for high power applications are discussed separately below.

(1) A new model of the long-slot tube has been designed and the features which should provide adequate stability have been incorporated. This tube has given the largest bandwidth of this class of tubes. In fact, one version of the long-slot structure had a measured 2-to-1 cold bandwidth.

(2) Eight megawatts of peak power have been obtained with the 10 Mw cloverleaf tube with adequate stability. This project is almost complete and will be terminated on completion of current tests with a confined flow type electron gun instead of the initial Brillouin flow gun to obtain a direct comparison of results from the two different types of electron confinement.

(3) The tapered cloverleaf tube illustrates a promising approach to achieve an optimum combination of stability and efficiency. The tapering of the circuit velocity and frequency of the output section eliminated the band-edge oscillations. The tests and analysis have been completed and the final technical report is in preparation. It is now expected that other studies involving tapering and related features will be incorporated in programs involving the electron stick. When the technical report on this project is completed and distributed this project will be terminated.

(4) The circuit which has given the best all around satisfactory tube performance, namely the centipede circuit, has been used to evaluate methods of obtaining tube stability, *i.e.*, freedom from oscillations. The distributed attenuation used to date to suppress oscillations has, in general, degraded the tube performance characteristics. A number of different methods have been studied in detail which will couple the unwanted modes and frequency ranges into a region external to the operating circuit in such a way that the operating frequency range of the circuit is not affected. The advantages of such schemes are immediately apparent: the excessive attenuation in the operating band is eliminated, the rf fields at the operating frequencies do not see this kind of attenuation and thus can give no peak or average power limitations, and, in general, the tube performance characteristics can be optimized without the limitations imposed by stability requirements. These methods have undergone extensive cold test measurements and the results are extremely promising. Although the vehicle being used is the centipede circuit, the general idea of coupling an auxiliary waveguide to a traveling-wave tube and the techniques involved would be applicable to other circuits as well.

(5) The "electron stick" will be used to test many of the ideas described in several paragraphs in this Introduction. Operating at a low duty cycle, nearly 100 percent beam transmission has been obtained for a peak beam power of over 10 megawatts at 120 kv. Much of the cold test work on circuits adapted for testing on the electron stick is complete. The experiments in this category include the testing of the centipede circuit and external coupling mechanisms, the dielectric loaded waveguide, and the stub-supported meander line which is to be used as the output section of an extended interaction klystron. The work on this project as a separate project has now been terminated. The electron stick will be used, however, as a very useful tool in many other experiments.

(6) One large common factor in obtaining optimum tube performance characteristics in any klystron or traveling-wave tube is the design and control of the electron beam. The hollow beam electron gun program has been concerned with new methods for the design of electron beams with high convergence and high perveance. Now methods have been developed which permit computer calculations to determine completely the geometry of the gun electrodes without recourse to the electrolytic tank. These methods permit, for example, the design of electron guns using nonspherical cathodes with curvilinear trajectories and in which the convergence can be much greater than conventional. There may be many possible important applications of this completely new class of cathode designs.

(7) The investigation of the stub-supported meander line circuit for use as an extended interaction klystron at the megawatt level is continuing. This circuit seems to have the proper cold characteristics for such an application as well as for a high power TWT. The cold test measurements and evaluation are well along, and the design and construction are underway to adapt usual reentrant klystron cavities as the input and intermediate cavities with the stub-supported meander line as the extended interaction output. The design is for use on the electron stick.

(8) Another new approach to the design of broadband high power tubes is the use of a waveguide containing a hollow dielectric with the electron beam passing through the hole in the dielectric. Calculations and cold test measurements show that the bandwidth and impedance are comparable to those of periodic circuits. Since the circuit is nonperiodic, the usual difficulties due to backward wave oscillations at cutoff frequencies and higher order modes should be avoided. With the use of beryllium oxide as the dielectric and a metal helix such as in the electron stick, both the problems of heat dissipation and the charging of the dielectric surface should be adequately solved. The initial experiments will use the electron stick.

(9) A completely different way of generating high power in the millimeter wave region is reported on for the first time in this contract. The fast wave tube consists of a rotating beam traveling along the axis of a smooth waveguide. A transverse wave interaction occurs at the frequency of rotation of the electron beam. An S-band tube of this type has been operated successfully at this laboratory. Using pulsed magnetic fields of 100 kilogauss, a tube designed to operate at a wavelength of about one millimeter is under test but thus far no oscillations have been observed. The use of such a simple circuit certainly is the attractive feature at these high frequencies.

(10) The interaction of an electron beam with a plasma has been investigated both theoretically and experimentally. At this laboratory, gains as high as 15 db/cm were observed on a tube at S-band. The detailed study includes not only the basic interaction of the beam with the plasma, but also the methods coupling rf energy to the system. The types of devices possible from this relatively new and unexploited area could make great contributions where high powers and high frequencies are required.

(11) A basic theoretical analysis of transverse waves on an electron beam in an axial dc magnetic field has led to an approach for the design of broadband high power amplifiers. These devices depend on the interaction between the transverse motion of electrons and transverse electric fields of a uniform circuit. There are many possible variations of this kind of interaction which do not have the usual limitations in frequency and power level of conventional devices. Furthermore, the predicted efficiency of these devices is high. The preliminary design work is under way to experimentally evaluate these predictions.

In summary, the program for the year has consisted of the completion of the work on portions of the program such as the ten megawatt cloverleaf tube, the tapered cloverleaf tube, the centipede structure studies and the cold-test evaluation of external coupling to the centipede circuit. The long-slot tube has been redesigned to satisfy the stability requirement. The electron stick project, with its associated mounting which makes it possible to evaluate many different devices, has been completed. The extended interaction stub-supported meander line, the uniform dielectric-loaded waveguide, and the centipede structure with different types of circuit modifications and/or coupled waveguides are currently being designed and constructed for

test on the electron stick. The hollow beam gun study has developed extremely flexible methods of designing highly convergent cathodes and will continue.

In addition, some radically new approaches have been added to the program during the year which explore the possibilities of obtaining suitable combinations of high frequency, high power, bandwidth, high gain and efficiency. Included here are the fast wave tubes, the electron beam interaction with a cesium plasma, and the transverse wave devices. It is anticipated that these latter programs will be continued. In general, all of the parts of the above program have been appropriately reported in publications and technical reports, although the last three projects described above are new and are reported herein for the first time under this contract.

I. LONG SLOT TWT

A. Introduction

Tests on the first model of the long-slot coupled-circuit traveling-wave tube indicated its potentialities as a broad-band, high power amplifier with good electronic efficiency.[1] In addition to the usual upper-passband and pulse-edge oscillations which occasionally plague amplifiers utilizing periodic structures as the slow wave circuit, this tube exhibited a low frequency oscillation associated with the passband arising from the coupling slots which are resonant at a frequency below the operating passband. Methods of suppressing the latter oscillations were readily devised, but a truly effective method of suppressing those associated with the upper passband, without affecting the overall amplifier performance, has been more elusive.

During the past year a study of various methods of selectively loading the upper passbands of a periodic circuit has been made. This has resulted in a loading scheme which is a composition of various other types and appears to merit testing in an amplifier at high power levels. The attenuation is accomplished by means of resonant slots which radiate into a lossy waveguide which is essentially nonpropagating by virtue of the high attenuation per wavelength. The coupling through the slots is, therefore, discrete and the total attenuation is found by multiplying that from one slot by the total number of slots. Cold tests on the slow-wave structure so loaded have indicated values of attenuation per cavity in excess of the small signal gain. Thus, regenerative oscillations should be suppressed and backward-wave oscillations inhibited unless the circuit is made excessively long. Attenuation in the amplification band is minimal because the radiating slots are not resonant at these frequencies and the lossy waveguide is well below cutoff so there is no propagation through the loss material.

B. Discussion

Suppression of unwanted oscillations in high power traveling-wave amplifiers has been the subject of many studies during the past several years and several methods have been attempted with various degrees of success.[1] These methods have generally involved the addition of attenuation to the slow-wave circuit in a judicious manner such that more loss is provided at the oscillation frequencies than in the described amplification band. Typical ratios of such differential attenuation range from 2:1 to as much as 4:1 depending on the field configuration in the oscillating mode compared to the amplification mode. However, the attenuation must be distributed over most of the length of the slow-wave circuit to suppress oscillations in the upper mode, so even the relatively low loss in the fundamental passband may adversely affect the electronic efficiency. In addition, the power levels of high power amplifiers are sufficient to cause appreciable heating of the loss material, thus restricting the type and size of materials which can be used.

The long-slot traveling-wave tube exhibits oscillations in the "slot" passband and the upper passband simultaneously. Although the latter can be suppressed when the rf drive is sufficient to saturate the beam, it is still necessary to suppress them completely in order to have a really useful amplifier. For sake of clarity, the propagation characteristics of several of the modes are shown in Figure 1. Oscillations in the slot passband were measured at a frequency somewhat above the π mode of the lowest passband which is that which would be measured with all long slots in the coupling irises. Since the amplifier consists of alternately two long and two short slots[1] and the long ones are at each end of the amplifier, it is difficult if not impossible to observe any oscillations associated with the "short" slots. It is assumed that such oscillations are present, however, so measurements were made to determine the mechanism of oscillation and a means devised to eliminate them. It was determined that these were monotron oscillations due to the nature of the construction utilizing two different slot lengths, and it was found that the addition of Kanthal in the vicinity of the slot lowered the Q sufficiently to preclude such oscillations. The effect on the operating passband was negligible insofar as additional attenuation is concerned.

---

[1]Second and Third Annual Reports for Contract AF 19(602)-1844, Microwave Laboratory Report Nos. 773 and 854, Stanford University (January 1961 and February 1962).

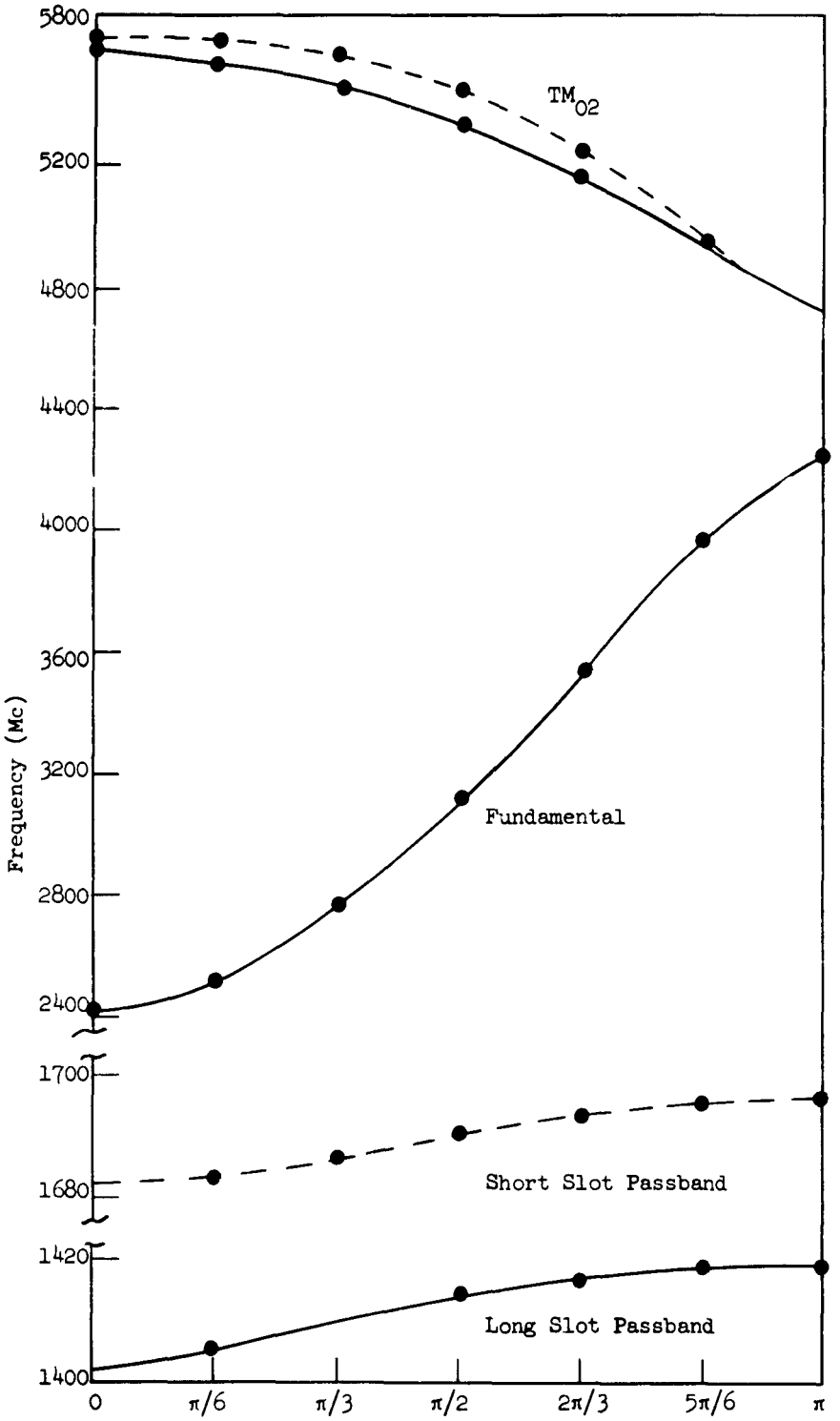

FIGURE 1. Propagation characteristic of several passbands measured for both "long" slot and "short" slot sections.

It was indicated in the last quarterly report[2] that misalignment due to rotation of the cavities can cause large reflections in the upper (TM_{02}) passband. Thus, oscillations at these frequencies may be due to these instead of reflections from the couplers or disk attenuators which are normally well matched in the operating passband. In fact, the measured oscillation frequencies as a function of beam voltage are nearly constant and one is led to believe that they are caused by large reflections in a region that is relatively free from attenuation such as one might obtain from a misaligned cavity near the tube input and/or output. The cavities which are sprayed with Kanthal provide attenuation which has relatively little reflection, so a mismatched coupler should not provide such a fixed frequency oscillation especially in this tube where the mismatch is bad over most of the upper passband. However, it is possible that a peculiar set of conditions happen to exist in this amplifier (it is the only model tested to date) and the oscillations are the result of this combination. Figure 2 shows a typical plot of $\triangle f$ in the TM_{02} passband, which is proportional to the circuit impedance, measured on a length of structure identical to that used in the amplifier. It is apparent that the impedance increases as the frequency increases (βL decreases) so that at a certain frequency the gain of the amplifier, with a high reflection coefficient at the coupler or sever termination, is sufficient to cause regenerative oscillations. One would expect them to be almost independent of voltage as far as frequency is concerned.

Because of inadequate knowledge of the cause of the upper passband oscillations it was decided to design the attenuator to provide sufficient loss to suppress all of them regardless of their nature. Thus, the studies were directed toward obtaining an attenuator located external to the slow-wave structure and coupled to it in a manner such that negligible loss is provided in the operating passband but high loss is provided in the passband which gives rise to oscillations. Locating the loss externally permits direct cooling of the loss material should this prove necessary. However, if the attenuation is sufficiently low in the fundamental band, heating should be no problem. It is assumed, of course, that all oscillations are suppressed so no rf power is absorbed at frequencies where the loss is high.

A series of measurements were made on the long-slot coupled structure in which a radiating slot was cut into the outer wall as shown in Figure 3. This slot was designed to be resonant near the lower cutoff frequency (π mode) of the upper (TM_{02}) passband. Thus, maximum energy is lost from the slow-wave circuit through the slot in the vicinity of this resonant frequency, but the loss is a rather slowly varying function of frequency and is of considerable magnitude over a range of several hundred megacycles. In order to prevent resistive loss from extending into the fundamental passband, a waveguide which has a cutoff frequency near, but somewhat below the π mode of the TM_{02} passband was incorporated external to the radiating slot and extending parallel to the axis of the tube. This slot would then be shorted in effect at frequencies below the cutoff of the waveguide.

Reflections from the single slot caused by the detuning of the cavity containing it resulted in inconclusive measurements of attenuation of the power transmitted through the section. A probe was located at each end of a six cavity section and was well matched (VSWR $<$ 2:1) when the radiating slot was covered by metal. Although the VSWR was not especially high when the slot was uncovered, it was sufficient to cause any attenuation measurements to be invalid. Therefore, a new structure was devised utilizing the slots shown in Figure 4, but with one slot cut in the wall of each cavity of a nine-cavity section. In order to prevent coupling between adjacent slots, each cavity was rotated so that the slots in the adjacent cavities were 120° apart. A continuous rotation of 120° in the same direction from cavity to cavity provided a structure which had slots appearing in the same azimuthal position every third cavity. Thus, very little coupling should occur between slots even if the waveguide were not heavily loaded since the phase conditions are not proper.[3]

Since the circuit used in the amplifier is comprised of cavities coupled by both long and short slots (coupling slots are cut into the plates as shown in Figure 3 and are not to be confused with the radiating slot

[2]Quarterly Memorandum No. 3 for Contract AF 30(602)-2575, Microwave Laboratory Report No. 933, Stanford University, (July 1962).

[3]N. Rynn, "On the Periodic Coupling of Propagating Structures," IRE Trans., *ED-6*, 325-329 (July 1959).

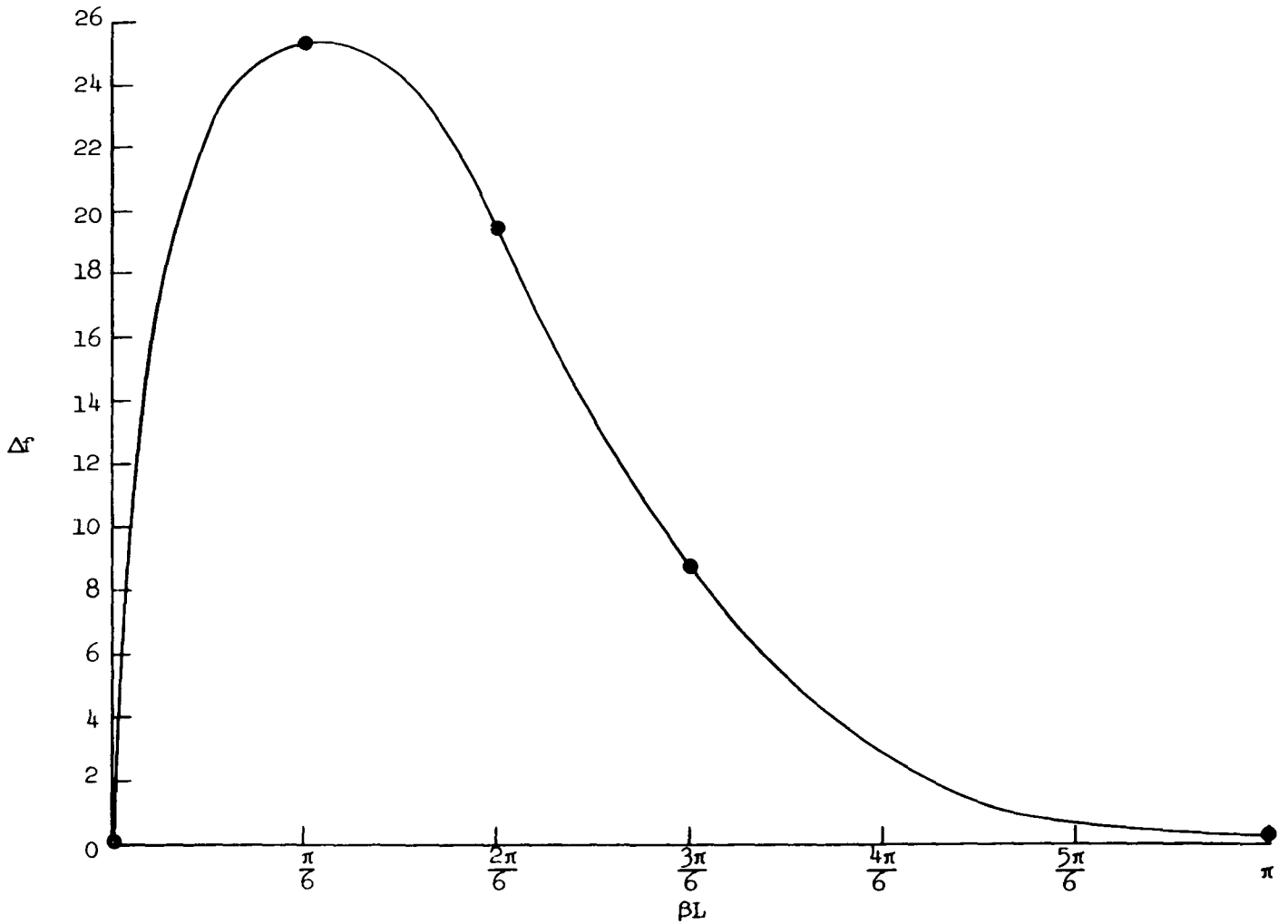

FIGURE 2. Frequency perturbation of axial E field in the TM_{oe} passband of long-slot structure. Perturbing rod is 0.025 in. diameter sapphire.

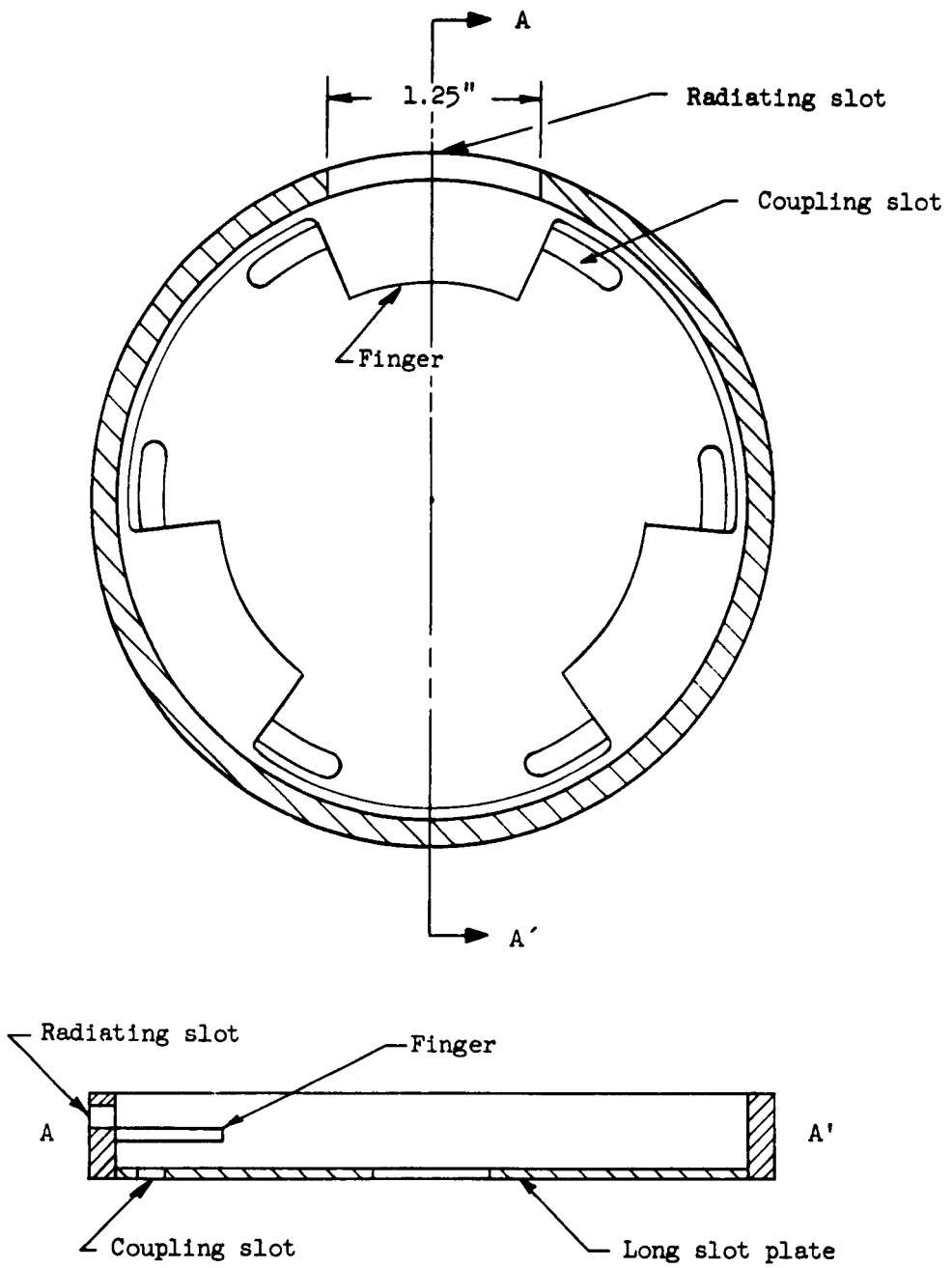

FIGURE 3. Location of radiating slot for maximum attenuation.

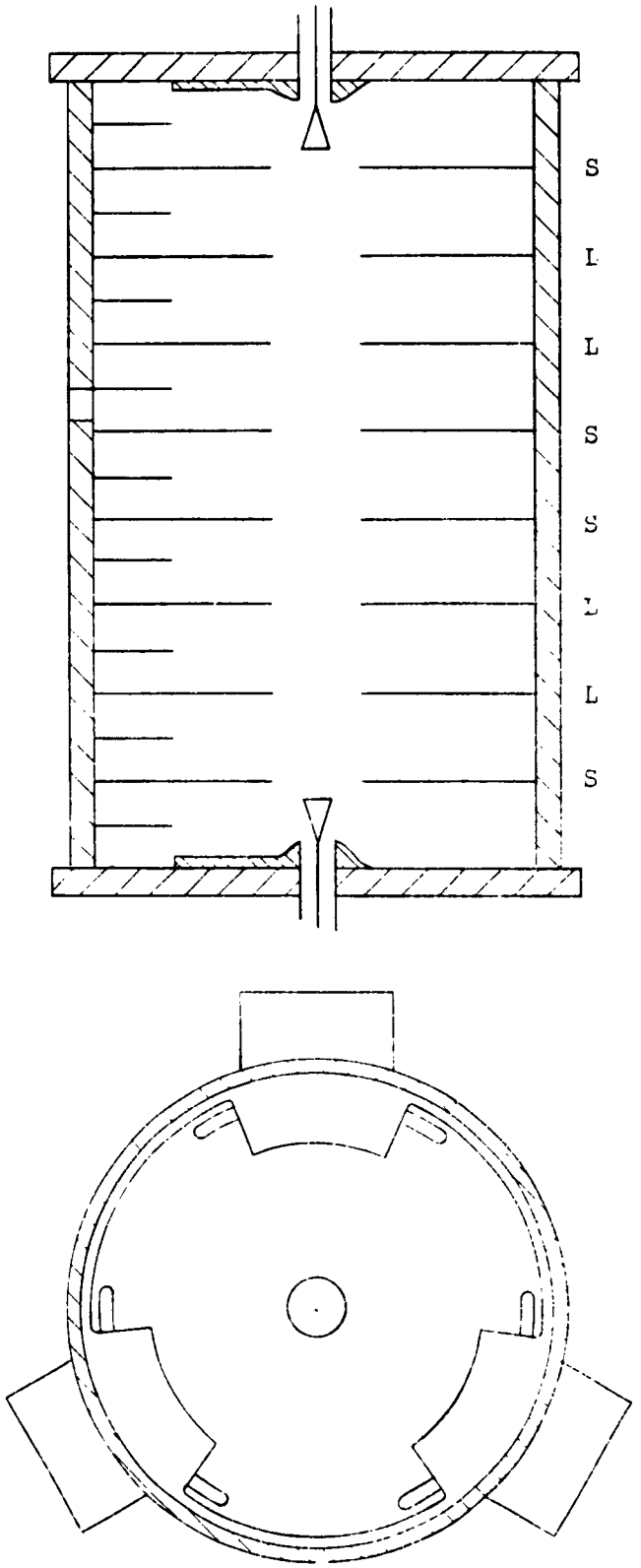

FIGURE 4. The location of lossy waveguides and position of "long" and "short" slot coupling apertures in the test structure.

which is cut into the wall), the nine-cavity test section was identically constructed as shown in Figure 4. This figure also shows the location of the lossy waveguides into which the slots radiate. The matching network associated with the input and output probes probably detunes the end cavities sufficiently to render the radiation from the wall slots in these cavities less effective than the others. Thus, the measured values of attenuation from the nine slots should be conservative.

The design of the lossy waveguide poses a problem since it is necessary for this component to present a resistance approximately equal to the radiation resistance of the slot if maximum attenuation is to be achieved. In addition, the loss must be of such magnitude that propagation from one slot to the next is negligible. This condition is necessary to prevent the power which is coupled out of one slot from being coupled back into the circuit through the next. Even though the phase is not proper, higher modes could be excited in the structure of such magnitude to enhance oscillations at frequencies other than those being suppressed.

The width of the lossless waveguide was chosen to be such that its cutoff frequency was slightly below that of the π mode of the upper passband. Thus, it adequately covered the radiating slots which are resonant slightly above the π mode of this passband. When the waveguide was placed over the slots, rf energy could easily be detected at each of its ends, which indicates that coupling is obtained from the slow-wave structure even though the propagation constants are not properly matched. The next step was to find a suitable material to make the guide sufficiently lossy to provide adequate attenuation to the slow-wave structure.

The initial tests were made with the slots radiating into free space and a lossy dielectric material known as Eccosorb. Both tests indicated that considerable attenuation could be obtained in the TM_{02} passband although the lossy dielectric material appeared to shift the resonant frequency of the radiating slots. This material is unsuitable for vacuum work and cannot be subjected to high temperatures so it is useful only to demonstrate feasibility of the attenuating scheme. The next test was made with the waveguide filled with Eccosorb. Attenuation values through the nine-cavity structure ranged from 20 db on up to possibly 30 db although the latter value was difficult to measure with the experimental setup used.

It was decided to approximate the waveguide filled with Eccosorb by replacing the Eccosorb with a lossy dielectric capable of withstanding high temperature. For this purpose, a porus, high alumina ceramic was impregnated with a aqueous sugar solution and the sugar was then carbonized by firing the ceramic in a hydrogen atmosphere. Since a guide filled with a material of such high relative dielectric constant (approximately nine) will have its cutoff frequency lowered by a factor of 3, only a portion of it was filled as indicated in Figure 5. Several measurements were made of attenuation through the nine-cavity structure with different width strips and some of the results are presented in Figure 6. Note that the attenuation is less when the strips are contiguous to the slots. This may be due to the fact that the guide height was reduced to obtain this condition and the dielectric fills relatively more of the guide, or it may be due to an impedance mismatch caused by moving the loss in the near-zone radiation field of the slot. Not enough data have been obtained as yet to verify either of these assumptions or to indicate other causes of this effect.

The important information contained in Figure 6 is that almost 2 db per cavity attenuation is obtained from one radiating slot in each cavity. As was mentioned previously, the slots at each end of the structure are probably not as effective due to the detuning of the end cavities by the probe matching network. It is not presently known why the peaks of attenuation occur in Figure 6, but it is suspected that some misalignment of the individual cavities may be causing internal reflections not noticeable at the input or output probes. This explanation seems plausible since the peak occurs even when the slots are shorted by aluminum foil and, hence, are effectively nonexistent.

One precaution must be observed in designing the lossy waveguide; the cutoff wavelength with the lossy material added must be above upper cutoff frequency of the amplification band to insure low attenuation therein. The problem is difficult theoretically but can be easily solved experimentally by measuring the guide wavelength as a function of frequency well above the cutoff frequency. The data is plotted in a manner similar

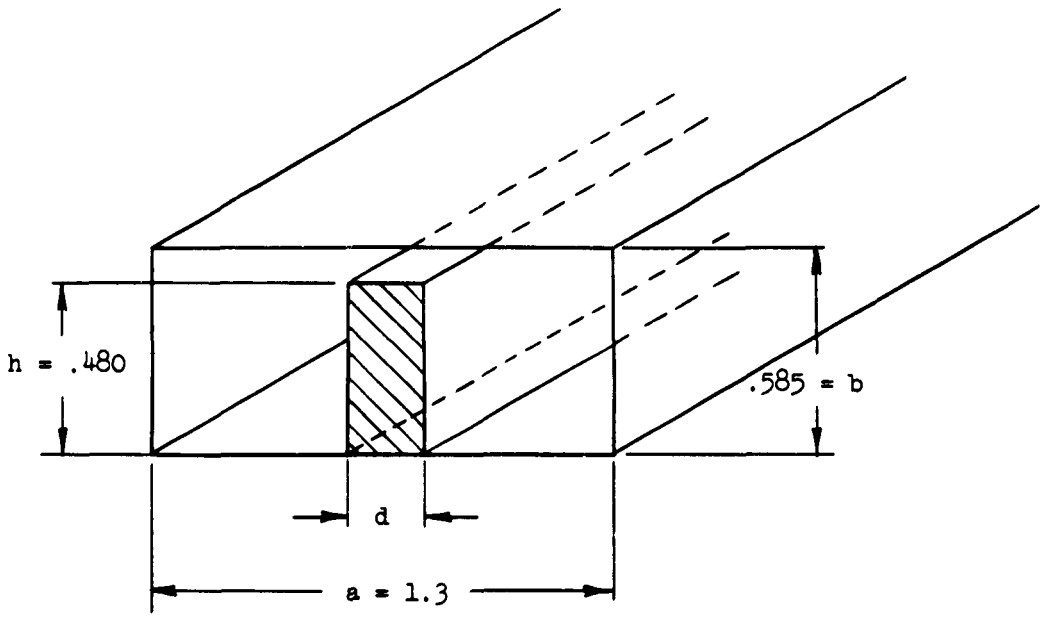

FIGURE 5. Location of lossy ceramic in waveguide.

to that of Vartanian[4] and his equations applied to determine the equivalent dielectric constant of the lossy material. It must be remembered that this is at best an approximate process because Vartanian's curves do not apply to a lossy medium nor for the case where the dielectric does not completely traverse the narrow dimension of the waveguide. Since a porous ceramic was impregnated with carbon for the loss material, the base material would be expected to have a lower equivalent dielectric constant than the lossy version. The two samples of identical size which were checked in the waveguide had equivalent dielectric constants of 2.6 and 3.8, respectively; the lower value is for the "lossless" ceramic. The computed cutoff frequencies of the waveguide are 3.8 and 3.1 kMc/s, respectively, for these two samples. Thus, the waveguide must be modified if it is to provide no loss in the fundamental passband.

It is easy to estimate the reduced value of the equivalent dielectric constant by assuming no fringing fields and only one waveguide mode. The subscripts 1 and 2 refer to the space above the dielectric and in the dielectric, respectively. In the case of the constant voltage between the broad waveguide faces, we have the equivalent dielectric constant reduced from that when the material completely traverses the guide by

$$\epsilon_2 \rightarrow \epsilon_2 \left(\frac{\ell_1}{\ell_2} + 1 \right) \frac{1}{\left(\frac{\epsilon_2}{\epsilon_1} \frac{\ell_1}{\ell_2} + 1 \right)} \quad ,$$

[4]P. H. Vartanian, W. P. Ayres, and A. L. Helgesson, "Propagation in Dielectric Slab Loaded Rectangular Waveguide," IRE Trans., *MTT-6*, 215-222 (April, 1958).

where l_1 = distance between the dielectric and the guide, and
l_2 = height of the dielectric.

For the sample measured, we have $\ell_1 \ll \ell_2$ and $\left(\frac{\epsilon_2}{\epsilon_1}\ \frac{\ell_1}{\ell_2}\right) \cong 1$,

so the equivalent dielectric constant is about half that of the material itself. This is in qualitative agreement with measured values since the ceramic is porous and should have a value of $\epsilon_2 < 9$. The above arguments are approximations at best and should only be used to obtain an estimate of the cutoff frequency of the loaded waveguide.

Modifications of the lossy waveguide are being made in an effort to raise its cutoff frequency to at least the upper cutoff frequency of the fundamental mode of the slow-wave structure. The attenuation in the upper (TM_{02}) passband must then be checked and the resistivity and/or dimensions adjusted to optimize this parameter. Finally, it must be determined that a relatively small amount of this attenuation is coupled into the operating region of the fundamental passband before construction of the amplifier can begin.

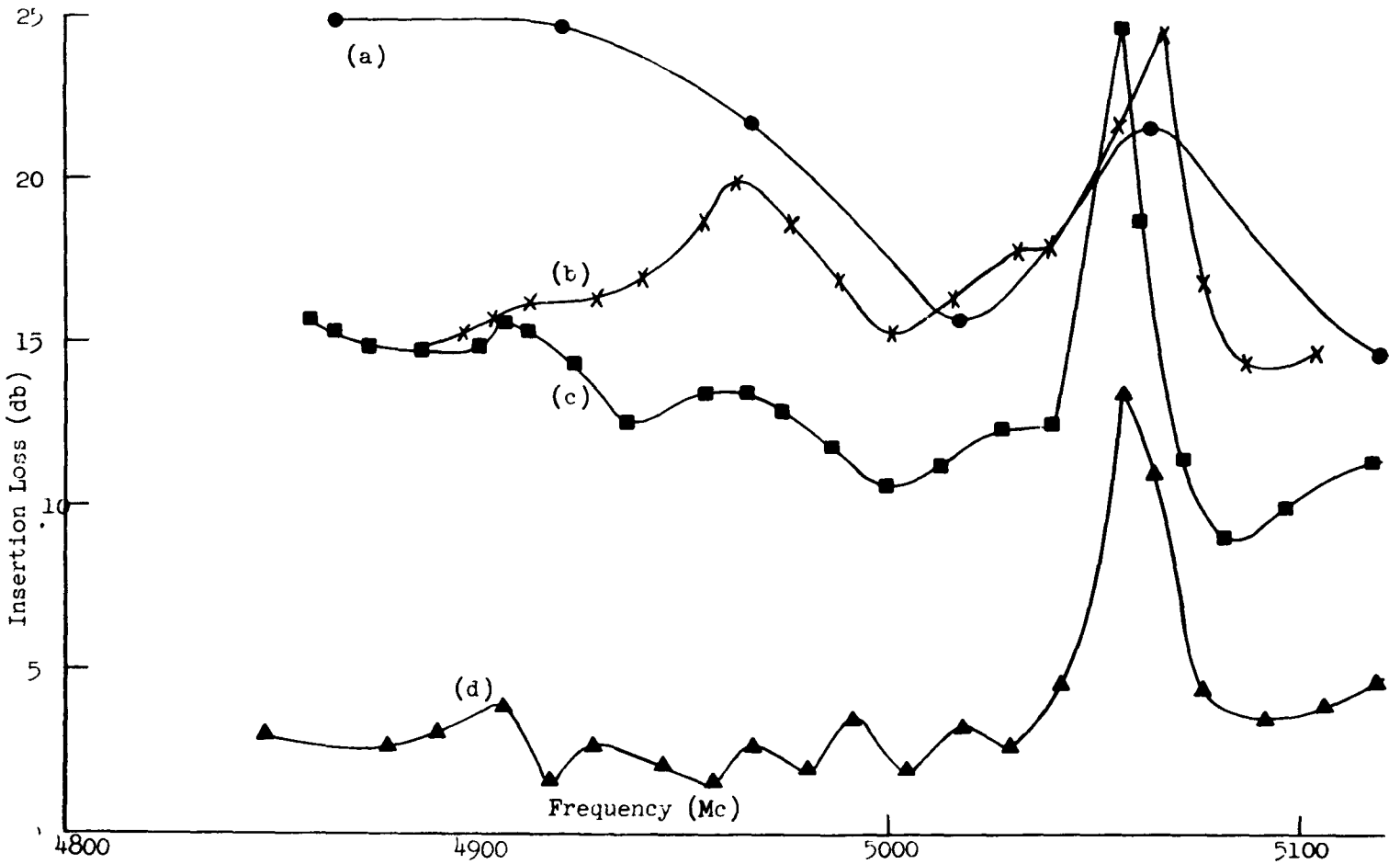

FIGURE 6. Measured attenuation through 9-cavity long-slot structure with lossy waveguide coupled through resonant slots. TM_{02} passband.

(a) $d/a \cong 0.1$, $h - b \cong .1$
(b) $d/a \cong 0.2$, $h - b \cong .1$
(c) $d/a \cong 0.2$, $h - b = 0$
(d) Slots covered with aluminum foil

II. TEN MEGAWATT CLOVERLEAF TWT

A. Introduction

The objective of this project was to develop a cloverleaf TWT with 10 megawatts peak power, a TWT with as high efficiency as possible and as much bandwidth that can be obtained in a cloverleaf circuit.

B. Discussion

An electron gun, which is adaptable to beam focusing of the convergent confined flow type, has been ordered. It will be used to replace the gun now in use which provides a Brillouin focused electron beam. Present plans are to make this modification and take measurements suitable for direct comparison with those previously taken on the amplifier. When these tests are complete the project will be terminated.

III. TAPERED CLOVERLEAF TWT

A. Introduction

The objectives of this project are to demonstrate that the pulse edge oscillation problem in high-power TWT amplifiers can be reduced or eliminated completely by the use of a tapered output section. It is to be understood that the other uniform sections would be designed with low enough gains so that pulse edge oscillations would not exist in the sections and be transmitted to the output by the modulated electron beam.

B. Discussion

A final report on a high-power TWT amplifier employing a tapered, cloverleaf circuit designed to suppress pulse-edge oscillations has been written. After this report has been completed and distributed, the project will be terminated. This report will be issued as a Technical Note titled "Studies of the Effect of Circuit Tapering on TWT Performance," by C. C. Lo. The abstract of this report follows:

"It is shown both theoretically and experimentally that by properly tapering the slow-wave structure of a pulsed, high-power, traveling-wave tube amplifier, one can eliminate pulse-edge oscillations and also improve the amplification characteristics. An approximate method of calculating the performance of the tapered-circuit amplifier from standard, small-signal analyses is presented and is validated by comparison to the experimental results. This method not only provides a convenient guide for the design of tapered-circuit traveling-wave tubes, but also provides a good physical understanding of the amplification mechanism in such a tube.

"The amplifier described in this paper had a relatively slight velocity taper in the amplification region and a larger taper in the region of pulse-edge oscillations. Thus, there was no expected or measured improvement in efficiency, but the pulse-edge oscillations were eliminated in the output section of the tube. This means that the section beyond the attenuator can be lengthened to increase the gain and maximize the efficiency without sacrificing stability. Other performance characteristics peculiar to tapered-circuit traveling-wave tubes are discussed in detail and methods of improving the performance of such tubes are suggested."

IV. CENTIPEDE TWT

A. Introduction

The centipede structure has given, to date, the most all-around satisfactory circuit performance for a high-power traveling-wave tube. The objectives of the present study are (1) to suppress the observed oscillations in the higher frequency loop passband and also the pulse-edge oscillations at the π-mode of the operating band without incorporating excessive attenuation in the frequency range of operating, and (2) to improve the overall circuit performance. The first objective is being pursued using two alternative approaches: coupling of the unwanted modes into a heavily attenuated external region or waveguide by means of resonant slots, and selective mode coupling of the undesired modes to an external lossless uniform guide. The techniques used here could be adapted to other types of circuits, such as the "cloverleaf" or the "long-slot." The study directed toward the second objective, *i.e.,* improved circuit performance, has a somewhat wider scope in that it also makes use of the existing knowledge of related structures and indicates the possibility of building new types of circuits.

B. Discussion

The current work is reported in three parts. Part 1 presents the investigation of coupling of undesired modes into an external attenuated region or into a waveguide which has the waveguide cutoff frequency above the operating frequency range of the tube. The improvement of overall circuit performance is also included in this section.

Part 2 has objectives similar to those of Part 1 and considers a similar method of coupling. The essential difference is that the external waveguide is coupled to the structure throughout the operating frequency range of the tube as well as the frequency ranges in which instabilities are observed. Attenuation of the undesired frequency ranges, with negligible attenuation in the operating band, is accomplished here by properly adjusting the phase and attenuation characteristics of the external circuit.

Part 3 shows the manner in which these coupled circuits can be evaluated when used on the electron stick. This procedure of measuring the amplitudes and phase of the growing wave along the structure should be most valuable in many basic circuit studies.

Part 1

The experimental work on this part of the project was recently completed, and a comprehensive report on it has been written. A draft of this report has been submitted for approval and should be completed and distributed in the near future. The report is "Study of Modes and Their Suppression in Broadband Periodic Structures for High Power TWT Amplifiers," by F. Ivanek. The abstract of this report is presented below:

"Methods of mode suppression which can prevent oscillations from building up in pulsed high-power TWT amplifiers were studied for a class of periodic structures. The approach consisted in the selective suppression of unwanted structure modes that were observed to give rise to oscillations, as opposed to the essentially nonselective approach which uses distributed loss, thus substantially deteriorating the amplifying properties of the tube.

"The prerequisite for the study of mode suppression methods is a thorough knowledge of the properties of the unwanted modes, and of the mode used for TWT amplification. A systematic investigation of mode properties was carried out by starting with a novel periodic structure which utilized combined disk loading. Its features are pertinent to the unified treatment developed for the more complicated actual high-power tube structures. The emphasis of this investigation was on the centipede structure which has given, to date, the most all-around satisfactory slow-wave structure performance for high-power TWT application. The experimental results demonstrated that a wide range of structure properties can be obtained by modify-

ing the geometry but there is no way of effectively changing, by modifications of the structure design alone, the inherently favorable conditions for the build-up of oscillations.

"A directional coupler scheme of energy transfer into attached smooth waveguide was studied in detail as a possible means of selective suppression of higher order backward-wave modes. These modes were observed to cause oscillations in the class of high-power TWT amplifiers under consideration. The results obtained from both coupled mode theory and the experimental investigation carried out on the centipede loop mode coupler demonstrated that, although the required tight coupling of complete energy transfer can be obtained by using resonant slots, this is inherently a frequency sensitive narrow-band scheme which is not capable of providing reliable mode suppression for the purpose of preventing oscillations.

"The study of the mode properties and of the mode coupling resulted in a leaky-wall scheme of selective mode suppression. Resonant slots are used in the cylindrical structure wall to leak out the energy of the unwanted mode into a lossy medium, for instance, a simple absorptive layer wrapped around the structure or a system of lossy rectangular waveguides. The latter have the advantage of providing, by virtue of their cutoff properties, effective protection against prohibitive effects of the leaky-wall scheme in the frequency range of amplification. This is what makes it possible to also achieve mode suppression at the upper limit of the TM_{01} cavity passband where band-edge oscillations were observed. The experimental results obtained under a variety of conditions show that the use of the leaky-wall scheme represents indeed the optimum solution to the problem of preventing oscillations which impose serious limitations on the optimization of the performance of high-power TWT amplifiers."

Part 2

The work on this part of the project during the reported period was directed toward the examination of the possibility of coupling an external waveguide to a periodic structure in order to eliminate the various types of oscillations that can occur when the periodic structure is excited by an electron beam. The waveguide is allowed to propagate over most or all of the operating frequency range of the periodic structure. A three-coupled-mode analysis of the interaction between the beam, periodic structure, and waveguide in a passband has been carried out.[1] It was found that the start-oscillation length for backward-wave oscillations near cutoff can be increased substantially (with relatively small accompanying loss in overall gain in the operating band) by adjusting the magnitude of coupling properly and by properly positioning the waveguide coupler. Also, a method of measuring the coupling between the periodic circuit and waveguide in a passband, as well as the question of the range of validity of the three-wave theory, was examined. A measure of the coupling through a slot in the periodic structure can be obtained by resonating the structure and measuring the difference in the Q obtained for zero and maximum coupling through the slot. The three-wave theory is valid in the regions $\beta L = \pi/8$ to $7\pi/8$, $9\pi/8$ to $15\pi/8$, etc., because in these regions the reflected circuit waves can be neglected.

In order to obtain the proper waveguide dispersion characteristic one must load the waveguide with dielectric. Moreover, it is desired to be able to vary the waveguide dispersion so that synchronism between the modes in the waveguide and periodic structure can be obtained at a number of frequencies around the π-point cutoff. This can be accomplished by partially filling the waveguide in its long dimension with dielectric and then splitting the dielectric slab symmetrically about the center of that long dimension. When the two dielectric slabs are moved symmetrically away from each other the dispersion of the waveguide will change continuously. The short dimension of the waveguide is filled completely so that the dominant mode in the dielectrically-loaded waveguide will be TE.

It was found that the combination of an X-band guide 2/3 filled with dielectric having $\epsilon' = 14$ gave the

[1]Quarterly Memorandum No. 2 for Contract AF 30(602)-2575, Microwave Laboratory Report No. 903, Stanford University (March 1962), pp. 9-21.

desired theoretical dispersion characteristic. A material having this dielectric constant and low loss is commercially available under the name of "Stycast."

In order to make cold-test measurements on the dielectric-loaded guide, a transition from air-filled S-band guide is needed. A split-taper transition was designed so as to give approximately constant cutoff frequency through the transition. If the waveguide is tapered linearly in all dimensions, this requires that the dielectric be tapered nonlinearly in the long dimensions of the waveguide. This nonlinear taper can be approximated by 3 linear types for ease of fabrication. The transition is currently being built.

All the theoretical analyses of the proposed oscillation suppression scheme that have been done so far have utilized coupled-mode theory. Coupled-mode theory, as it is usually formulated, is only applicable in a passband, *i.e.,* when all the modes are truly propagating. In this formulation, if a circuit is allowed to approach cutoff, non-meaningful singularities appear in the solutions. Therefore, a re-examination of the formulation of coupled-mode theory as applied to periodic structures was carried out and the results of that re-examination are presented below.

The small signal electronic equations for a one-dimensional beam that enters a longitudinal field at $z = 0$ and is weakly coupled to it are

$$\frac{da_f}{dz} = -j\beta_f a_f + \frac{E_c(z)}{4\sqrt{W}} \tag{1a}$$

$$\frac{da_s}{dz} = -j\beta_s a_s + \frac{E_c(z)}{4\sqrt{W}} \quad , \tag{1b}$$

where a_f and a_s are the amplitudes of the usual fast and slow space-charge waves with $\beta_{f,s} = \beta_e \mp \beta_q$ and E_c is the longitudinal electric circuit field. The beam impedance is $W = (2V_0\beta_q)/(I_0\beta_e)$ and a_f and a_s are defined so that

$$2(|a_f|^2 - |a_s|^2) = \tfrac{1}{2}\,\mathrm{Re}(U^*I) = \text{real kinetic power flow on the beam.} \tag{2}$$

In Eq. (2) U is the rf kinetic voltage and I is the total rf current. The longitudinal circuit field for a single mode on a periodic structure can be written in terms of the space-harmonics as follows:

$$E_c(z) = \sum_{n=-\infty}^{\infty} |a_n| \left[A_n^+(z) + A_n^-(z)\right] \tag{3}$$

To eliminate the infinite sum one makes use of the physical fact that the average interaction with the beam is determined by the space-harmonics to which the beam is nearly synchronized. Then one defines an equivalent transmission-line-like mode for the periodic structure whose magnitude of longitudinal field at all z (in the cold structure) is the same as that measured at a reflection plane in the periodic structure and from which one can compute the actual power flow on the structure. The propagation constants of the equivalent modes are those of the proper interacting space-harmonics. For a circuit such as the centipede, one would be interested in the fundamental and first backward space-harmonics. In other words, if the longitudinal electric

fields of the equivalent modes are called $\mathcal{E}^+$ and $\mathcal{E}^-$, $\mathcal{E}^+$ would vary as $e^{-\gamma\alpha}$ and $\mathcal{E}^-$ would vary as $e^{\gamma-1s}$ in the absence of a beam. The factor $(|a_n|)/(4\sqrt{W})$ measures the beam interaction with the n^{th} space-harmonic and, hence, this is the factor which determines the interaction with the equivalent modes. Equations (1) become:

$$\frac{da_f}{dz} = -j\beta_f a_f + \frac{|a_0|}{4\sqrt{W}}\,\mathcal{E}^+ + \frac{|a_1|}{4\sqrt{W}}\,\mathcal{E}^- \tag{4a}$$

$$\frac{da_s}{dz} = -j\beta_s a_s + \frac{|a_0|}{4\sqrt{W}}\,\mathcal{E}^+ + \frac{|a_1|}{4\sqrt{W}}\,\mathcal{E}^- \tag{4b}$$

The circuit equations are assumed to be of the form:

$$\frac{d\mathcal{E}^+}{dz} = -\gamma_0 \mathcal{E}^+ + c_1 a_f + c_2 a_s \tag{5a}$$

$$\frac{d\mathcal{E}^-}{dz} = \gamma_{-1}\,\mathcal{E}^- + c_3 a_f + c_4 a_s \tag{5b}$$

At this point, the procedure is to use the Chu Kinetic Power Theorem to determine relationships between the coupling constants appearing in Eqs. (5) (unknown) and those appearing in Eqs. (4) (known). With this information one can then determine the *type* of behavior that the system will exhibit, *i.e.*, growing or non-growing waves, etc. The Chu Kinetic Power Theorem for lossless systems can be written

$$\tfrac{1}{2}\,\mathrm{Re}\oint \left[\left(\vec{E}^* \times \vec{H}\right) + (U^* i)\,\hat{a}_z\right] \cdot \hat{n}\,ds = 0\,, \tag{6a}$$

or

$$\tfrac{1}{2}\,\mathrm{Re}\int_{s+} \left[\left(\vec{E}^* \times \vec{H}\right) + (U^* i)\,\hat{a}_z\right] \cdot \hat{n}\,ds = \text{constant}. \tag{6b}$$

By analogy with an ordinary waveguide, one has:

(a) in a passband:

$$\tfrac{1}{2}\,\mathrm{Re}\int_{s+} \left(\vec{E}^* \times \vec{H}\right) \cdot \hat{n}\,ds = 2G\left(|\mathcal{E}^+|^2 - |\mathcal{E}^-|^2\right) \tag{7a}$$

where $G>0$,

(b) at cutoff:

$$\tfrac{1}{2}\,\mathrm{Re}\int_{s^+}\left(\vec{E}^{\,*}\times\vec{H}\right)\cdot\hat{n}\,ds = 0 \tag{7b}$$

(c) in a stopband:

$$\tfrac{1}{2}\,\mathrm{Re}\int_{s^+}\left(\vec{E}^{\,*}\times\vec{H}\right)\cdot\hat{n}\,ds = \mathrm{Re}\left[-2j\beta\left(\varepsilon^{+}\varepsilon^{-*}-\varepsilon^{+*}\varepsilon^{-}\right)\right], \tag{7c}$$

where the sign of B depends on the type of mode. The factors G and B are admittance factors which determine the power flow for a given longitudinal, electric field (units = mko − m²). The singularities at cutoff arise because the circuit coupled-modes are usually defined in terms of these admittance factors, *i.e.*,

(a) in a passband:

$$A^{+} \triangleq \varepsilon^{+}\sqrt{G} \tag{8a}$$

$$A^{-} \triangleq \varepsilon^{-}\sqrt{G}\quad, \tag{8b}$$

so that the conservation theorem becomes

$$|A^{+}|^2 - |A^{-}|^2 + |a_f|^2 - |a_s|^2 = \text{constant}; \tag{9}$$

(b) in a stopband:

$$A^{+} \triangleq \varepsilon^{+}\sqrt{|B|} \tag{10a}$$

$$A^{-} \triangleq \varepsilon^{-}\sqrt{|B|}\quad, \tag{10b}$$

so that the conservation theorem becomes

$$\pm\, 2\,\mathrm{Im}\left(A^{+}A^{-*}\right) + |a_f|^2 - |a_s|^2 = \text{constant}; \tag{11}$$

where: top sign: $B>0$.

bottom sign: $B<0$.

By writing the coupled equations in terms of the new circuit coupled-modes and with the relationships between the coupling constants determined by Eqs. (9) and (11), one has:

(a) in a passband:

$$\frac{d}{dz}\begin{bmatrix} a_f \\ a_s \\ A^+ \\ A^- \end{bmatrix} = -j \begin{bmatrix} \beta_f & 0 & j\frac{|a_0|}{4\sqrt{WG}} & j\frac{|a_1|}{4\sqrt{WG}} \\ 0 & \beta_s & j\frac{|a_0|}{4\sqrt{WG}} & j\frac{|a_1|}{4\sqrt{WG}} \\ -j\frac{|a_0|}{4\sqrt{WG}} & j\frac{|a_0|}{4\sqrt{WG}} & \beta_0 & 0 \\ j\frac{|a_1|}{4\sqrt{WG}} & -j\frac{|a_1|}{4\sqrt{WG}} & 0 & 2\pi/L - \beta_0 \end{bmatrix} \begin{bmatrix} a_f \\ a_s \\ A^+ \\ A^- \end{bmatrix} \tag{12}$$

(b) in a stopband:

$$\frac{d}{dz}\begin{bmatrix} a_f \\ a_s \\ A^+ \\ A^- \end{bmatrix} = -j \begin{bmatrix} \beta_f & 0 & j\frac{|a_0|}{4\sqrt{W.|B|}} & j\frac{|a_1|}{4\sqrt{W.|B|}} \\ 0 & \beta_s & j\frac{|a_0|}{4\sqrt{W.|B|}} & j\frac{|a_1|}{4\sqrt{W.|B|}} \\ \pm\frac{|a_1|}{4\sqrt{W.|B|}} & \mp\frac{|a_1|}{4\sqrt{W.|B|}} & \beta_1 - j\alpha & 0 \\ \mp\frac{|a_0|}{4\sqrt{W.|B|}} & \pm\frac{|a_0|}{4\sqrt{W.|B|}} & 0 & \beta_1 + j\alpha \end{bmatrix} \begin{bmatrix} a_f \\ a_s \\ A^+ \\ A^- \end{bmatrix} \tag{13}$$

From Eqs. (12) and (13) it can be explicitly seen how letting G or B approach zero (cutoff) produces an apparent singularity.

In order to examine interaction at cutoff, one must presumably use Eqs. (4) and (5). Application of the conservation theorem

$$|a_f|^2 - |a_s|^2 = \text{constant} \tag{14}$$

gives

$$\frac{da_f}{dz} = -j\beta_f a_f \tag{15a}$$

$$\frac{da_s}{dz} = -j\beta_s a_s \tag{15b}$$

so that the space-charge waves are *completely decoupled* from the circuit. Solution of the circuit equations gives:

$$\mathcal{E}^+ = A\, e^{-j\beta_1 z} + \frac{c_1 a_f^o e^{-j\beta_f z}}{j(\beta_1 - \beta_f)} + \frac{c_2 a_s^o e^{-j\beta_s z}}{j(\beta_1 - \beta_s)} \tag{16a}$$

$$\mathcal{E}^- = B\, e^{-j\beta_1 z} - \frac{|a_0|}{|a_1|}\frac{c_1 a_f^o e^{-j\beta_f z}}{j(\beta_1 - \beta_f)} - \frac{|a_0|}{|a_1|}\frac{c_2 a_s^o e^{-j\beta_s z}}{j(\beta_1 - \beta_s)} . \tag{16b}$$

One sees that there will be oscillations if

$$\beta_1 = \beta_{f,s} \quad (a_{f,s}^o \neq 0) .$$

Physically, this means that the circuit fields form a naturally resonant configuration at cutoff and all that the beam does is excite the resonance. The appearance of poles is a result of not having included losses.

If one adds on an external waveguide, it is found that at cutoff the coupled-mode theory says that the waveguide does not load down the resonance but only serves as an additional means of exciting this resonance. This follows from the fact that the waveguide modes play a role in the coupled-mode equations similar to that played by the space-charge modes. This theory is obviously wrong. One says that there is no power flow on the circuit at cutoff and this is just what precludes the waveguide from loading down the resonance. Conservation of power says that if the waveguide were drawing power *from* the circuit there would have to be a finite power flow *on* the circuit. Hence, the assumption that the power flow on the circuit is given formally in terms of the unperturbed mode amplitudes breaks down. Therefore, in order to examine beam-circuit-waveguide interactions at cutoff, one must use a perturbation theory of high order than the first-order perturbation theory which has been called coupled-mode theory here. The possibility of using such a higher-order theory will be investigated.

An alternative approach to obtaining criteria for the suppression of cutoff oscillations is to use the monotron theory developed by Wessel-Berg.[2] The important parameters in this theory are the Q's of the system, which, of course, do take into account the perturbations due to all kinds of losses. Also, the loaded Q of the resonant, cutoff structure is an easily measured quantity. Thus, the monotron approach seems to have distinct advantages over the coupled-mode approach. An attempt will be made to relate these two methods.

Future work will be directed toward the experimental design of terminations for the dielectrically-loaded waveguide and the measurement of its dispersion characteristic. Also, the coupling to the dielectrically-loaded waveguide by a slot in the structure will be determined by measuring the Q of a resonated structure with and without the slot. It is yet to be determined how the loaded Q of the resonant cutoff structure varies with single-slot coupling and number of slots. Finally, the whole system will be experimentally evaluated under "hot" conditions on the "electron stick."

Part 3: Measurement of Fields Along the Centipede Slow-Wave Structure

A magnetic field probe has been designed and constructed to monitor the TM_{01} passband fields of the centipede structure. The probe consists of an 1/8 in. diameter loop attached mechanically to a remotely operated sliding carriage which moves longitudinally as close as possible to the slow-wave structure. The rf magnetic field inside the centipede sections is coupled through small slots to the probe. The probe and its mechanical linkages are designed to operate with the centipede structure mounted on the electron stick; all electrical and mechanical connections to the probe can be made through one waveguide size port at the bottom of the electron stick. Work is currently directed toward adjusting the probe for the proper sensitivity in order to measure the amplitude and phase of the growing wave in consecutive centipede sections while the entire setup, mounted on the electron stick, is operating as a TWT. It is expected that this method will be most useful in evaluating the effects of coupled waveguides and other basic circuit studies.

[2]T. Wessel-Berg, "A General Theory of Klystrons with Arbitrary, Extended Interaction Fields," Microwave Laboratory Report No. 376, Stanford University (March 1957).

V. ELECTRON STICK

A. Introduction

The electron stick has been developed to evaluate high-power tube circuits without the construction of a complete tube; it consists of an electron gun, collector, and a long glass tube shielded from the electron beam by a closely spaced tungsten helix. The helix prevents the charging of the glass and is essentially transparent to the rf developed by the circuits which are external to the glass vacuum envelope. Operating at a low duty cycle, nearly 100% beam transmission has been obtained at a peak power of 10 megawatts, 120 kv and 84 amperes. The objective is to adapt the electron stick to many of its possible uses, namely: to evaluate the the effectiveness of the externally coupled waveguides on the centipede circuit in order to eliminate backward wave oscillations; to test the dielectric loaded waveguide as a high-power traveling-wave tube; and to evaluate new circuits, the effects of tapering the circuit, and the effect on tube operation of changing many of the circuit and coupling characteristics. These operations may now be accomplished since the rf circuitry is outside the vacuum envelope.

B. Discussion

The new model of the electron stick has performed satisfactorily under dc tests at its designed operating level, 120 kv and 10 megawatts peak power. The movable focusing coils, the positioning mechanism for both the coils and the rf structures, and all the auxiliary equipment has been assembled and used during the dc tests. An assembly drawing is shown in Figure 1. A photograph of the setup as used is shown in Figure 2. The first structure to be mounted on the electron stick is a centipede structure, 15 sections long, with an input coupler and terminated in a sever. A traveling probe is mounted on the side of these 15 sections, coupled to each cavity by means of slots so that the amplitude and phase of the rf in the structure can be monitered under a variety of experimental conditions. This is discussed in more detail in the centipede section of this report, Section IV. Other experiments which are to be performed on the electron stick setup in the near future are the stub-supported meander line described in the "Extended Interaction Klystrons" section of this report, and also the "Nonperiodic Dielectric-Lined, High-Power TWT," which is described under this title in this report.

Backward wave oscillations have been observed when the electron stick is operated without external attenuation. These oscillations are attributed to the interaction of the electron beam with the $m = -1$ space harmonic of the helix which shields the glass from the electron beam. These oscillations vary from about 4.0 kMc to 4.6 kMc, increasing in frequency as the voltage increases. Attenuation, in the form of Eccosorb LS-22, prevents the oscillations when the 3/8 in. material is wrapped around the stick. The measured attenuation of this material is about three db/in. and at the peak operating voltage a gap (a length of exposed helix) of 1.5 in. can exist before the oscillations start. A number of methods have been evaluated to determine the means to prevent this mode from interfering with operation of the electron stick when used with different types of structures. Since these oscillations occur in the stop-band of the centipede structure and the structure will have internal kanthal loss, it is expected that little additional attenuation will be needed, particularly during the rf drive pulse which can extend throughout the beam pulse. An interesting observation has been made on the oscillations that occur in the interaction of the electron beam with the helix of the stick. At a given voltage and a given magnetic focusing field, oscillations are observed at a definite frequency. If all the dc magnetic fields are reversed, the frequency of oscillation changes by approximately 250 Mc, or approximately six percent. The amount of total beam rotation, obtained by varying the amount of flux through the cathode in a known manner, did not appreciably change the observed oscillation frequencies. Measurements of this type could prove to be very useful in verifying certain types of transverse waves that have been shown to exist on magnetically focused electron beams.

The electron stick with all of its associated mounting mechanism adapted for use with several circuits has been completed.

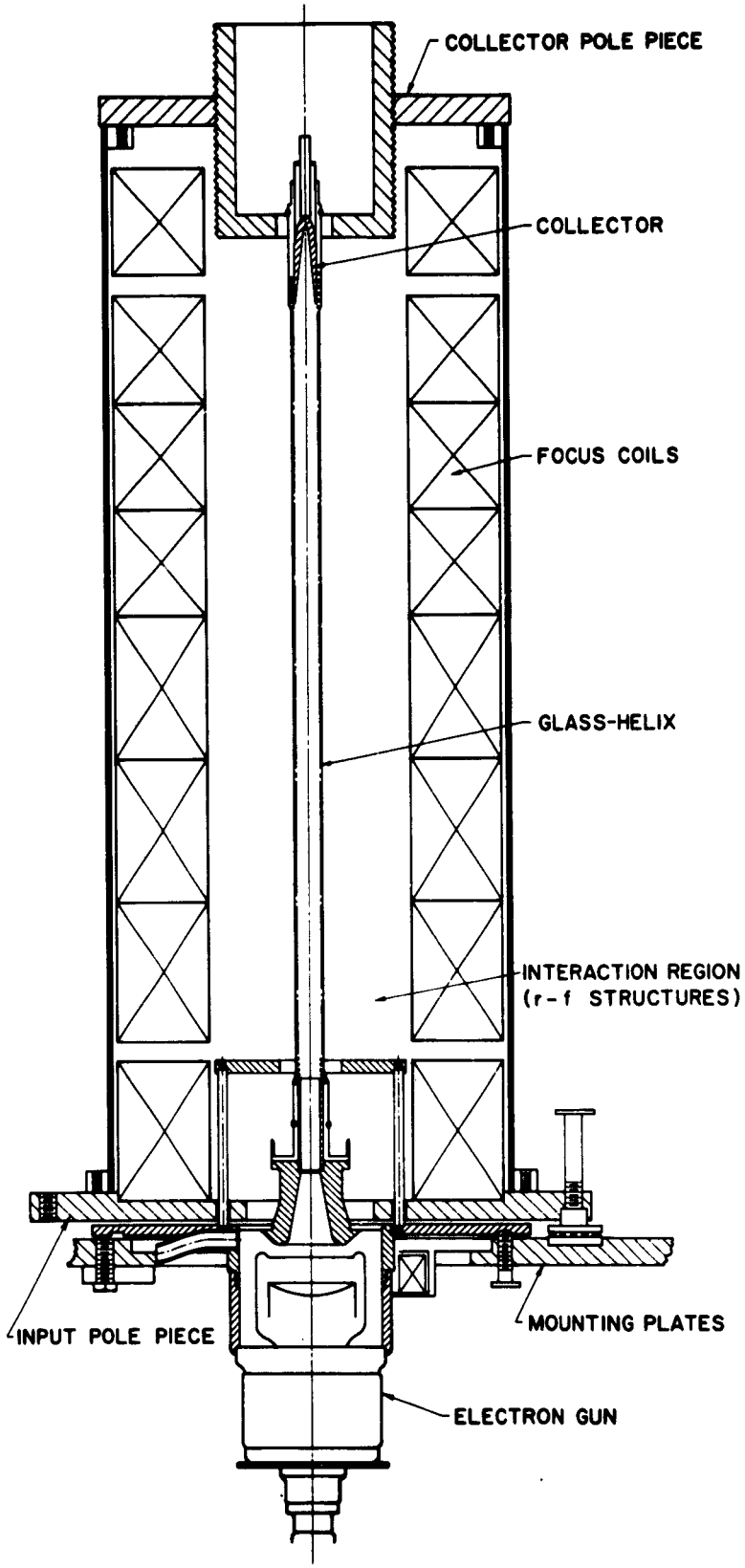

FIGURE 1. Assembly drawing of electron stick.

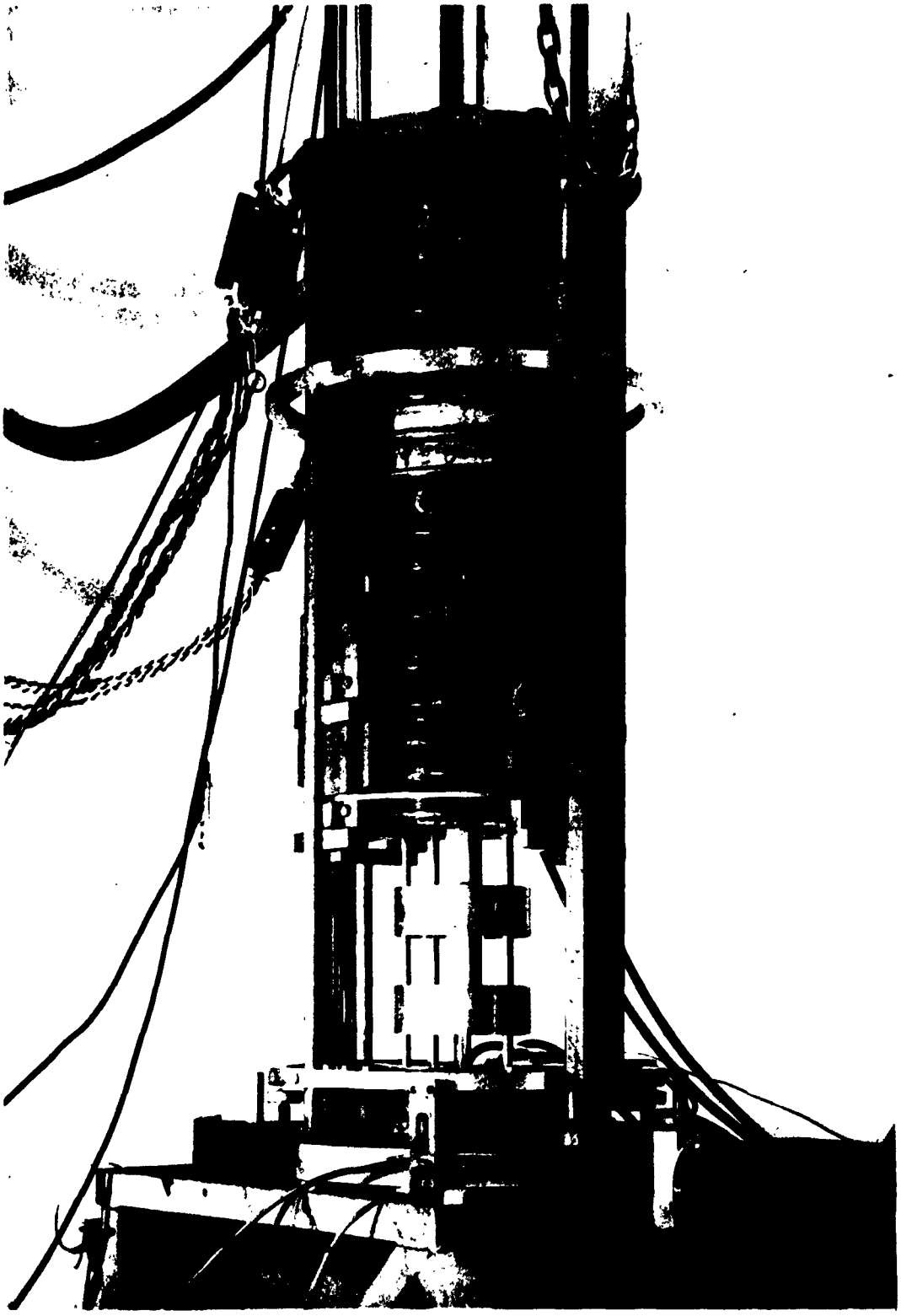

FIGURE 2. Photograph of electron stick mounted for test.

VI. HOLLOW BEAM ELECTRON GUNS

A. Introduction

This project is concerned with determining new methods for the design of high perveance and high convergence electron guns. The designer of these guns has always been limited in the past in his choice of gun designs to meet particular specifications, and considerable effort has been made over the years to make gun design methods more versatile. It is our purpose to find new methods which should increase this versatility.

B. Discussion

1. *Determination of Practical Cathode Shapes*

As mentioned in previous reports, the range of a solution to the equations of space-charge limited flow when the boundary conditions are given on the cathode is determined mainly by the position of the critical points in the complex plane of the cathode discussed in a technical note prepared under this contract.[1] No solution exists around such points, and it is important to seek cases where these singularities are either removed as far away as possible or they do not exist. We will now describe the work that has been done in the study of cathode shapes in which these singularities do not exist.

Such singularities only occur when the line element

$$ds^2 = dr^2 + (r\, d\, \theta)^2 \tag{1}$$

vanishes somewhere in the complex plane of the cathode.

In Eq. (1), the line element has been expressed in spherical polar coordinates (r, θ, ϕ) and is evaluated along a meridian (ϕ = const.) taken on the surface of the cathode. It is our purpose to use Eq. (1) as the generator of cathode surfaces $r(\theta)$ for which the line element cannot vanish.

Equation (1) can be written

$$\left(\frac{ds}{d\theta}\right)^2 = \left(\frac{dr}{d\theta}\right)^2 + r^2 \neq 0 \quad , \tag{2}$$

and the non-vanishing of Eq. (2) can be assured by writing

$$\left(\frac{dr}{d\theta}\right)^2 + r^2 = e^{f(\theta)} \quad . \tag{3}$$

The solutions to Eq. (3) for specific choices of $f(\theta)$ are then the cathode shapes $r(\theta)$ to be determined. For example, let $f(\theta) = 0$; then the solutions of Eq. (3) are $r = \pm 1$ and $r = \pm \cos(\theta + a)$, where α is constant. This example demonstrates that more than one solution can be expected, and it will always be necessary to exercise some caution in solving Eq. (3) so that all solutions are retained. We are specifically interested in solutions to Eq. (3) having the property that $(dr/d\theta)$ is zero when θ vanishes (this point is important in that it assures that the cathode will be smooth near the polar axis). This in turn requires that $f(\theta)$ be an even function.

[1] K. J. Harker, "Exact Solutions of the Equations of Space-Charge Limited Flow," Microwave Laboratory Report No. 858, Stanford University (October 1961).

The solution to Eq. (3) is written

$$r = a_0 + a^2\theta^2 + a_4\theta^4 + \ldots \quad , \tag{4}$$

where

$$f(\theta) = f_0 + f_2\theta^2 + f_4\theta^4 + \ldots \quad . \tag{5}$$

The coefficients a_0, a_2, a_4 are readily obtained by substitution in Eq. (3):

$$a_0^2 = e^{f_0} \tag{6a}$$

$$a_2 = (a_0/4)\left[-1 \pm \sqrt{1 + 4f_2}\right] \tag{6b}$$

and

$$a_4 = \frac{a_0}{2\left(-1 \pm \sqrt{1 + 4f_2}\right)}\left[(1/2)f_2^2 + f_4 - (1/8)\right.$$

$$\left. - (1/4)f_2 \pm (1/8)\sqrt{1 + 4f_2}\right] \quad , \text{ etc.} \tag{6c}$$

It is clear that these solutions are valid for complex values of θ, and are useful as a check on solutions obtained by numerical methods.

Numerical solutions to Eq. (3) were obtained for various values of the f_i in Eq. (5). In general, helical shapes which wound inward and outward were obtained. Two sketches of some typical shapes are shown in Figures 1 and 2. Possible useful portions of these shapes as cathode profiles would be the arcs between A and B.

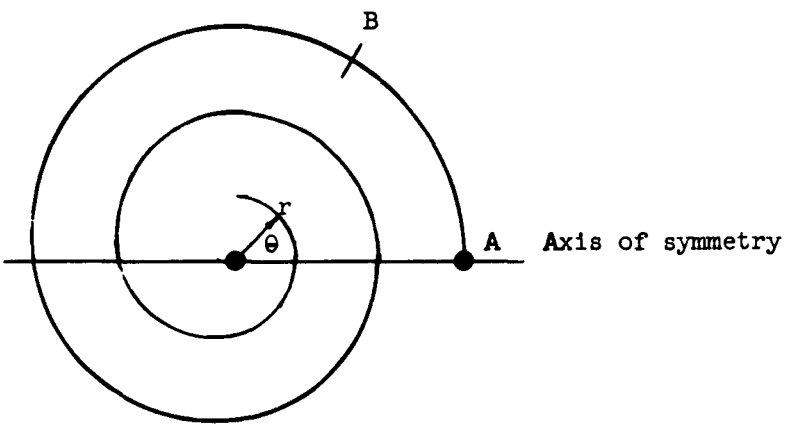

FIGURE 1. Generators of possible cathode shapes.

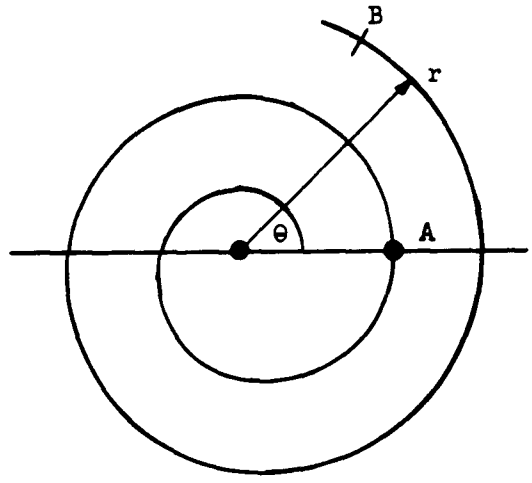

FIGURE 2. Generators of possible cathode shapes.

2. *Calculation of Analytic Continuation Required for Obtaining Electrode Shapes*

In previous reports we have discussed how a very general class of axially symmetric space charge limited flows may be calculated corresponding to a choice of cathode shape and cathode current density. It will be our purpose here to discuss how the electrodes required for forming and focusing these flows may be obtained. However, since the method for determining the electrode shapes cannot be properly understood without reference to the method for determining the flow itself, it will be necessary to repeat some of the latter subject matter.

Figure 3 shows the coordinate system in which the problem is to be solved. Cylindrical symmetry is assumed so that the problem can be studied in a meridian plane with the usual cylindrical coordinates, r and z. The pertinent equations describing the flow are the force equations,

$$\frac{dr}{dt} = v_r \tag{7}$$

and

$$\frac{dz}{dt} = v_z \quad ; \tag{8}$$

also

$$\frac{dv_r}{dt} = -\eta E_r \tag{9}$$

$$\frac{dv_z}{dt} = -\eta E_z \quad , \tag{10}$$

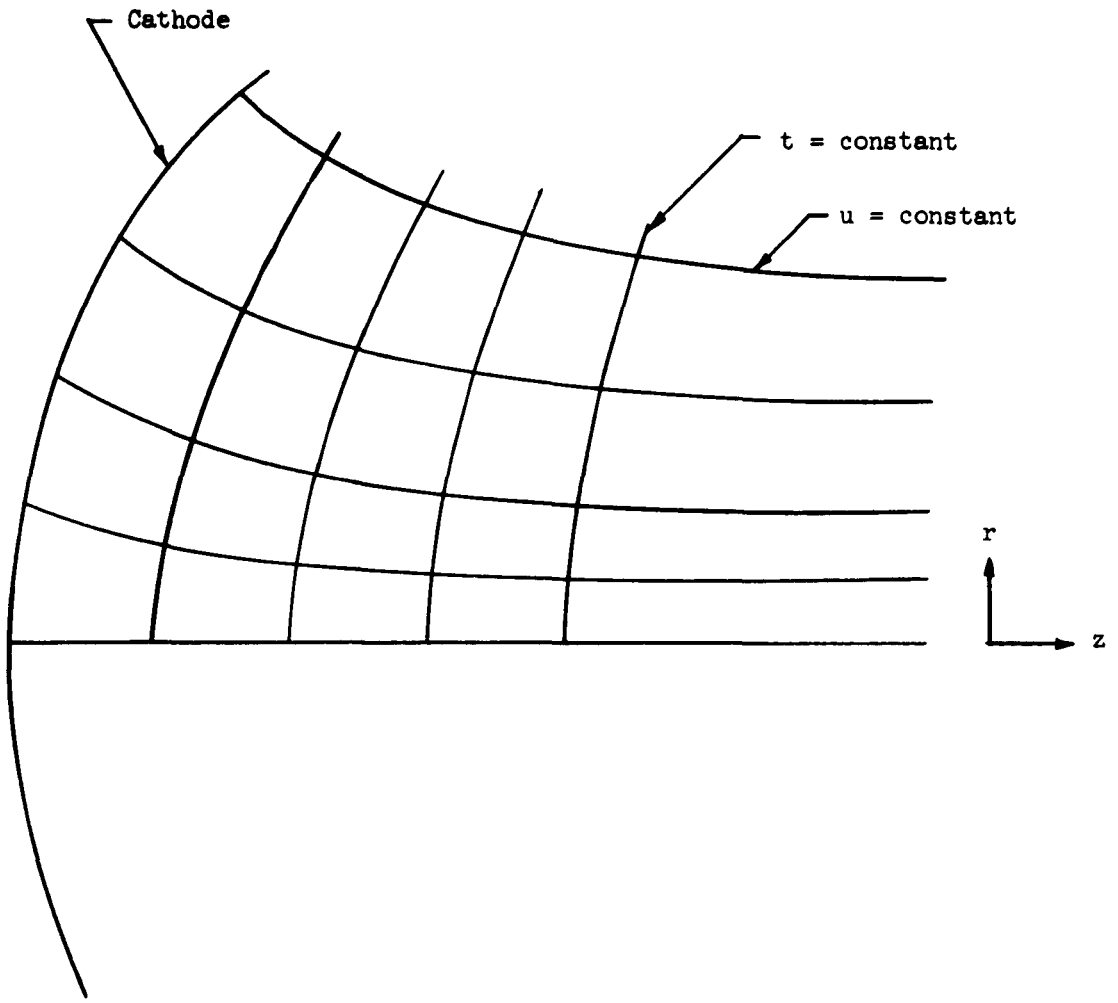

FIGURE 3. Co-ordinate system.

the field equations,

$$\frac{\partial E_r}{\partial r} + \frac{\partial E_z}{\partial z} + \frac{E_r}{r} = -\frac{\rho}{\epsilon_0} \tag{11}$$

$$\frac{\partial E_r}{\partial z} - \frac{\partial E_z}{\partial r} = 0 \quad , \tag{12}$$

and the equation of continuity. In these equations η is the absolute magnitude of the electron charge-to-mass

ratio, t is the transit time from the cathode, v_r and v_z are velocity components, E_r and E_z are the electric field, and ρ is the absolute magnitude of the charge density.

Letting u be some arbitrary function of arc length along the cathode, the initial conditions are the cathode shape given parametrically by the equations

$$r = r_0(u) \tag{13}$$

$$z = z_0(u) \tag{14}$$

and the cathode current density, $J_0(u)$.

It will be convenient to rewrite the field equations with u and t as independent variables. These coordinates are related to the cylindrical coordinates by the transformation

$$\frac{\partial}{\partial t} = v_r \frac{\partial}{\partial r} + v_z \frac{\partial}{\partial z} \tag{15}$$

and

$$\frac{\partial}{\partial u} = \alpha \frac{\partial}{\partial r} + \beta \frac{\partial}{\partial z} \quad , \tag{16}$$

where

$$\alpha = \frac{\partial r}{\partial u} \quad , \tag{17}$$

$$\beta = \frac{\partial z}{\partial u} \quad . \tag{18}$$

The inverse of this transformation may be found and substituted into Eqs. (11) and (12) to yield the equations

$$\frac{\partial E_r}{\partial t} = \mu \frac{\partial E_r}{\partial u} + \nu \frac{\partial E_z}{\partial u} + \frac{\beta}{r}\left(E_r v + \frac{\rho v r}{\epsilon_0}\right) \tag{19}$$

$$\frac{\partial E_z}{\partial t} = -\nu \frac{\partial E_r}{\partial u} + \mu \frac{\partial E_z}{\partial u} - \frac{\alpha}{r}\left(E_r v + \frac{\rho v r}{\epsilon_0}\right) \quad , \tag{20}$$

where

$$\sigma^2 = \alpha^2 + \beta^2 \tag{21}$$

$$\mu = (\alpha v_r + \beta v_z)/\sigma^2 \tag{22}$$

$$\nu = (\alpha v_z - \beta v_r)/\sigma^2 \tag{23}$$

We may eliminate ρ from the above two equations by using the principle of conservation of current. Referring to the slender filament of current in Figure 4 we may assert that

$$\sigma_0 J_0 r_0 = \left| \vec{J}r \times \frac{\partial \ell}{\partial u} \right| , \tag{24}$$

where σ_0 is the value of σ at the cathode and l and J are the displacement and current vectors, respectively. Noting that the components of $\partial l/\partial u$ are α and β and that

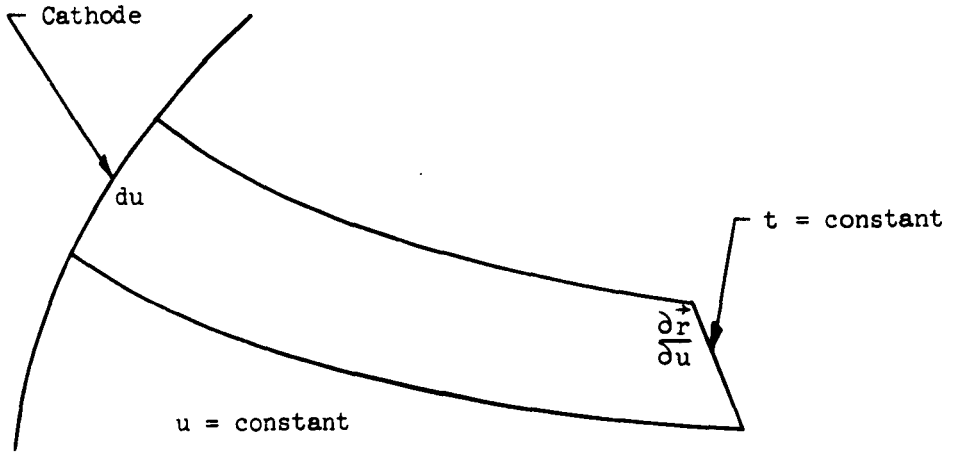

FIGURE 4. Thin current filament.

$$\vec{J} = \rho \vec{v} \tag{25}$$

where v is the velocity vector, we can reduce Eq. (24) to the form

$$\rho = \frac{J_0 r_0 \sigma_0}{r\,(\alpha v_z - \beta v_r)} \quad . \tag{26}$$

Substituting this into Eqs. (19) and (20) gives the equations

$$\frac{\partial E_r}{\partial t} = \mu \frac{\partial E_r}{\partial u} + \nu \frac{\partial E_z}{\partial u} + \frac{\beta}{r}\left[E_r \nu + \frac{J_0 r_0 \sigma_0}{\epsilon_0 \sigma^2}\right] \tag{27}$$

$$\frac{\partial E_z}{\partial t} = - \nu \frac{\partial E_r}{\partial u} + \mu \frac{\partial E_z}{\partial u} - \frac{\alpha}{r}\left[E_r \nu + \frac{J_0 r_0 \sigma_0}{\epsilon_0 \sigma^2}\right] \quad . \tag{28}$$

It will be necessary to define two additional dependent variables, γ and ϵ, by the relations

$$\gamma = \frac{\partial \alpha}{\partial t} \tag{29}$$

$$\epsilon = \frac{\partial \beta}{\partial t} \quad . \tag{30}$$

Differentiating with respect to t and substituting Eqs. (9), (10), (11), and (12), we obtain the additional equations

$$\frac{\partial \gamma}{\partial t} = - \eta \frac{\partial E_r}{\partial u} \tag{31}$$

$$\frac{\partial \epsilon}{\partial t} = - \eta \frac{\partial E_z}{\partial u} \quad . \tag{32}$$

Our equations may be put into more general form by normalizing. If length is measured in terms of some distance d, current density in terms of some current density k, electric fields in terms of the unit

$$\left[\frac{k^2 d}{2\eta\epsilon_0^2}\right]^{1/3} ,$$

velocities in terms of the unit

$$\left[\frac{2\ kd^2}{\epsilon_0}\right]^{1/3} ,$$

and transit time in terms of the unit

$$\left[\frac{2\ k}{\epsilon_0 d}\right]^{-1/3} ,$$

then Eqs. (7)–(10) and (27)–(32) reduce to the set

$$\frac{\partial r}{\partial t} = v_r \tag{33}$$

$$\frac{\partial z}{\partial t} = v_z \tag{34}$$

$$\frac{\partial v_r}{\partial t} = -\frac{E_r}{2} \tag{35}$$

$$\frac{\partial v_z}{\partial t} = -\frac{E_z}{2} \tag{36}$$

$$\frac{\partial \alpha}{\partial t} = \gamma \tag{37}$$

$$\frac{\partial \beta}{\partial t} = \epsilon \quad ; \tag{38}$$

also

$$\frac{\partial \gamma}{\partial t} = -\frac{1}{2}\frac{\partial E_r}{\partial u} \tag{39}$$

$$\frac{\partial \epsilon}{\partial t} = -\frac{1}{2}\frac{\partial E_z}{\partial u} \tag{40}$$

$$\frac{\partial E_r}{\partial t} = \mu \frac{\partial E_r}{\partial u} + \nu \frac{\partial E_z}{\partial u} + \beta P \tag{41}$$

$$\frac{\partial E_z}{\partial t} = -\nu \frac{\partial E_r}{\partial u} + \mu \frac{\partial E_z}{\partial u} - \alpha P \tag{42}$$

where

$$P = \frac{1}{r}\left[E_r \nu + \frac{J_0 r_0 \sigma_0}{\sigma^2}\right] \quad . \tag{43}$$

An initial value problem yields stable solutions only if the partial differential equations are hyperbolic. A system of quasi-linear equations is hyperbolic if it is possible to reduce them by a linear transformation into a new set of linearly independent equations equal in number to the original, each equation of which involves only one directional derivative.[2] It is also required that this directional derivative be real.[2]

We will now show how the above equations can be reduced to hyperbolic form. The reduction to equations involving only one directional derivative is fairly simple. Substitution of Eqs. (39) and (40) into Eqs. (41) and (42) leads to the following set of equations:

$$\frac{\partial E_r}{\partial t} = -2\mu \frac{\partial \gamma}{\partial t} - 2\nu \frac{\partial \epsilon}{\partial t} + \beta P \tag{44}$$

and

$$\frac{\partial E_z}{\partial t} = 2\nu \frac{\partial \gamma}{\partial t} - 2\mu \frac{\partial \epsilon}{\partial t} - \alpha P \quad . \tag{45}$$

Multiplying Eq. (42) by the imaginary number i and then adding and subtracting from Eq. (41) leads to the additional equations:

$$\left(\frac{\partial}{\partial t} - \mu \frac{\partial}{\partial u} + i\nu \frac{\partial}{\partial u}\right)(E_r + iE_z) = (\beta - i\alpha) P \tag{46}$$

$$\left(\frac{\partial}{\partial t} - \mu \frac{\partial}{\partial u} - i\nu \frac{\partial}{\partial u}\right)(E_r - iE_z) = (\beta + i\alpha) P \quad . \tag{47}$$

Equations [(33)–(38)] and [(44)–(47)] are a set in each equation of which only one directional derivative occurs.

The remaining requirement that these directional derivatives be real is satisfied by all of the equations except Eqs. [(46)–(47)], and it will be our purpose next to show how the directional derivative here may be made real also according to a novel method of Garabedian employing an analytic continuation into the complex domain.[3] Let us introduce the analytic continuation by replacing u by

[2]G. E. Forsythe and W. R. Wasow, *Finite-Difference Methods for Partial Differential Equations* (John Wiley and Sons, Inc., New York, 1960), pp. 383-385.

[3]P. R. Garabedian, Journal of Mathematics and Mechanics 9, 905 (1960).

$$u + i\bar{u} \tag{48}$$

and using the relation

$$\frac{\partial}{\partial u} = \frac{1}{i}\frac{\partial}{\partial \bar{u}} \tag{49}$$

which follows from it. If we define

$$\mu = \mu_r + i\mu_i \tag{50}$$

$$\nu = \nu_r + i\nu_i \tag{51}$$

such that the subscripted variables are real, then we can use Eq. (49) to reduce Eqs. (46) and (47) to the hyperbolic form

$$\left[\frac{\partial}{\partial t} - (\mu_r + \nu_i)\frac{\partial}{\partial u} - (\mu_i - \nu_r)\frac{\partial}{\partial \bar{u}}\right](E_r + iE_z) = (\beta - i\alpha)P \tag{52}$$

$$\left[\frac{\partial}{\partial t} - (\mu_r - \nu_i)\frac{\partial}{\partial u} - (\mu_i + \nu_r)\frac{\partial}{\partial \bar{u}}\right](E_r - iE_z) = (\beta + i\alpha)P \tag{53}$$

It is this step which is the essence of the analytic continuation.

By solving Eqs. (52)–(53) for $\partial E_r/\partial t$ and $\partial E_z/\partial t$, we obtain

$$\frac{\partial E_r}{\partial t} = \mu_r\frac{\partial E_r}{\partial u} + i\nu_i\frac{\partial E_z}{\partial u} + \mu_i\frac{\partial E_r}{\partial \bar{u}} - i\nu_r\frac{\partial E_z}{\partial \bar{u}} + \beta P \tag{54}$$

$$\frac{\partial E_z}{\partial t} = -i\nu_i\frac{\partial E_r}{\partial u} + \mu_r\frac{\partial E_z}{\partial u} + i\nu_r\frac{\partial E_r}{\partial \bar{u}} + \mu_i\frac{\partial E_z}{\partial \bar{u}} - \alpha P \quad . \tag{55}$$

Substituting these equations into Eqs. (44) and (45) and then solving for $\partial\gamma/\partial t$ and $\partial\epsilon/\partial t$ yields the additional equations

$$\frac{\partial \gamma}{\partial t} = -\frac{1}{2(\mu^2 + \nu^2)}\left\{(\mu\mu_r + i\nu\nu_i)\frac{\partial E_r}{\partial u} + (\mu_i\mu - i\nu_r\nu)\frac{\partial E_r}{\partial \bar{u}} - (\mu_r\nu - i\nu_i\mu)\frac{\partial E_z}{\partial u} - (\mu_i\nu + i\nu_r\mu)\frac{\partial E_z}{\partial \bar{u}}\right\} \tag{56}$$

$$\frac{\partial \epsilon}{\partial t} = -\frac{1}{2(\mu^2 + \nu^2)} \left\{ (\mu_r \nu - i\nu_i \mu) \frac{\partial E_r}{\partial u} + (\mu_i \nu + i\nu_r \mu) \frac{\partial E_r}{\partial \bar{u}} \right.$$

$$\left. + (\mu_r \mu + i\nu_i \nu) \frac{\partial E_z}{\partial u} + (\mu_i \mu - i\nu_r \nu) \frac{\partial E_z}{\partial \bar{u}} \right\} . \qquad (57)$$

Equations [(33)–(38)], and [(54)–(57)] form a set of differential equations which can be used for obtaining stable solutions to the space-charge flow equations. These equations may be solved by finite difference methods which have already been described in detail by Harker and Colburn.[4]

Figure 5 shows the domain of the calculation in schematic form. We now have three variables u, t, and u. The direction of flow coincides with increasing t. The data on the cathode is continued into the plane t = 0.

[4]K. J. Harker and D. S. Colburn, "Exact Solutions of the Equations of Space-Charge Limited Flow," Microwave Laboratory Report No. 858, Stanford University (October 1961).

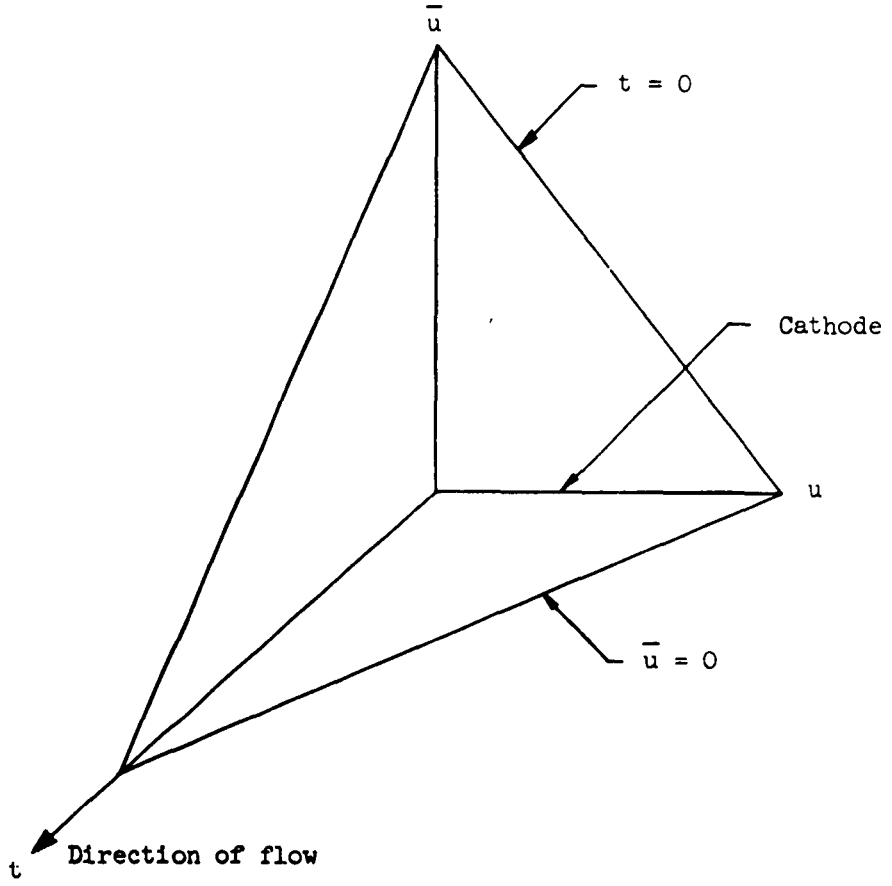

FIGURE 5. Domain of calculation.

One then starts integrating by finite difference methods away from the plane $t=0$, obtaining a solution which has no physical relevance except in the plane $u=0$. Here we obtain a valid solution which represents a physical flow.

The determination of the electrodes to focus these flows is complicated by the following fact. It can be shown that the determination of the electrode configuration depends upon knowing the values of the dependent variables as a function of the imaginary part, t, of the variable increasing along the direction of flow. However, the solution thus far obtained has only been found for the imaginary part, u, of the variable used to label trajectories. The problem at hand, then, is how to determine the solution as a function of t, and we shall now discuss this in detail.

Figure 6 shows in detail how we must proceed with our calculation in order to get these electrodes. At the beginning, the data along the cathode is continued analytically up into the u region, generating initial data on the surface $t=0$. One integrates forward in the t direction to get the solution in the (u, u, t) domain discussed previously. This is done up to some point $t=t_n$. We next assert that t be held constant at t_n. Let us assume that we have another set of equations in t, u, u. (The way in which these equations are obtained will be discussed shortly.) Using these equations, we integrate in the t direction in the t, u, u domain, holding t fixed. This is the domain between the plane $t=t_n$, $t=0$ and the plane through the point D in the figure. The integration proceeds until the point D is reached.

Let us assume that the beam edge along the line $u=ue$. Then along the line AB in Figure 6 we have the data required for determining the voltage and hence the electrodes exterior to the beam. This follows from the fact that we have now obtained the solution as a function of F along a line corresponding to the point at the beam edge located at $x=tn$ and $u=ue$. If $r_e(t)$ and $z_e(t)$ are the values of r and z along the line AB, we may define in the triangle ABC a set of conformal coordinates (t, w) defined by the transformation

$$r(\bar{t},\ w) = \frac{1}{2}\left\{r_e(\bar{t} + w) + r_e(\bar{t} - w) - i\, z_e(\bar{t} + w) + i\, z_e(\bar{t} - w)\right\} \tag{58}$$

$$z(\bar{t},\ w) = \frac{1}{2}\left\{r_e(\bar{t} + w) + z_e(\bar{t} - w) + i\, r_e(\bar{t} + w) - i\, r_e(\bar{t} - w)\right\} . \tag{59}$$

If we integrate outward in the triangle ABC with our standard method of analytic continuation for integrating Laplace's equation we will obtain along the line BC a set of voltages exterior to the beam. By repeating the process for various values of tn the complete solution for the voltage outside the beam is obtained.

We will now derive the set of hyperbolic equations in the variables u, u, and t. We may take Eqs. (33)–(38) and (44)–(47) as our starting point, and generalize our previous work by replacing t by $t + it$ and u by $u + iu$. It follows immediately from the theory of complex variables that

$$\frac{\partial}{\partial t} = \frac{1}{i}\frac{\partial}{\partial t} \tag{60}$$

$$\frac{\partial}{\partial u} = \frac{1}{i}\frac{\partial}{\partial \bar{u}} \quad . \tag{61}$$

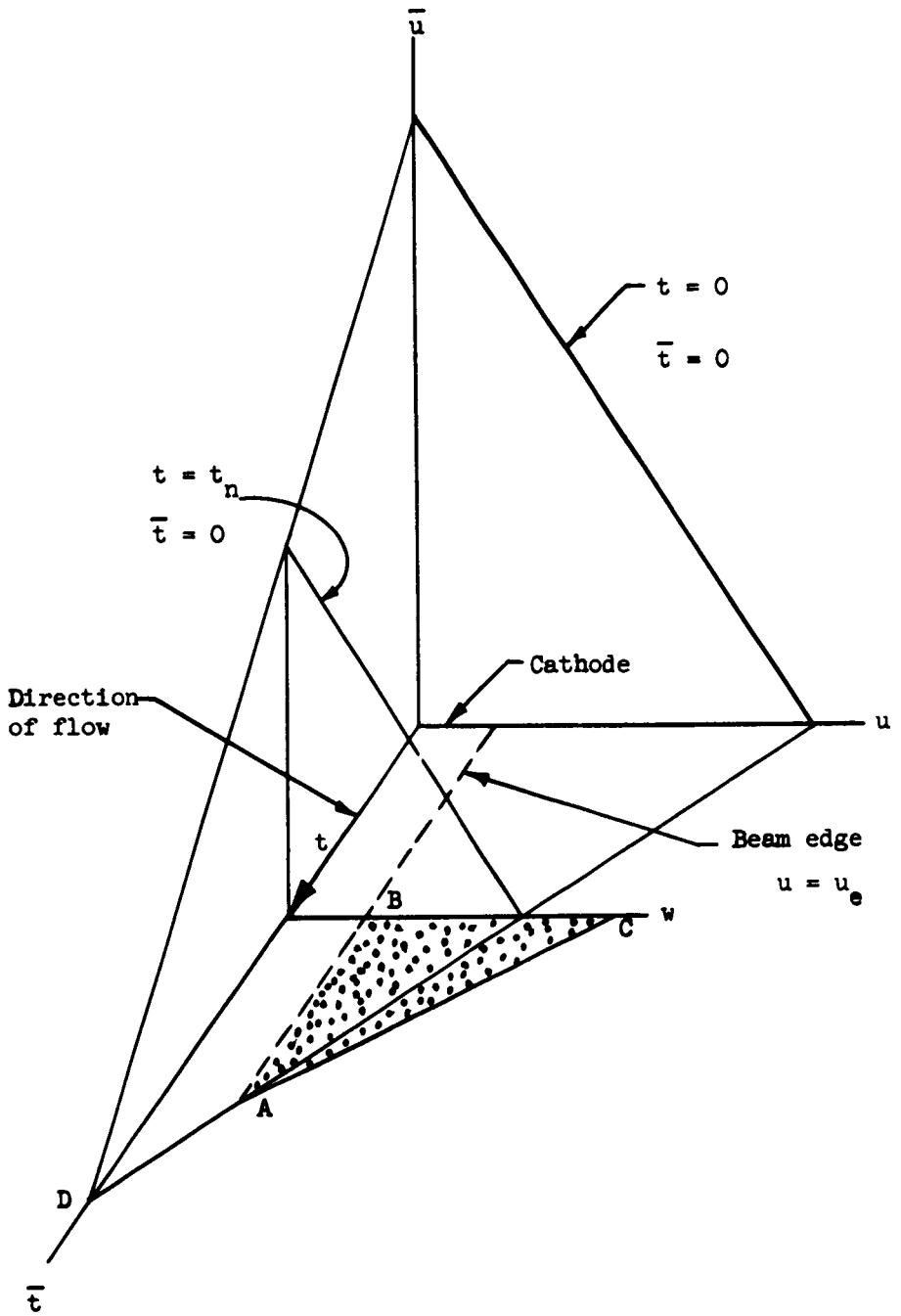

FIGURE 6. Method of electrode calculation.

Substituting Eq. (60) into Eqs. (33)–(38) yields the equations

$$\frac{\partial r}{\partial \bar{t}} = iv_r \tag{62}$$

$$\frac{\partial z}{\partial \bar{t}} = iv_z \tag{63}$$

$$\frac{\partial v_r}{\partial \bar{t}} = -\frac{iE_r}{2} \quad , \tag{64}$$

and

$$\frac{\partial v_z}{\partial \bar{t}} = -\frac{iE_z}{2} \tag{65}$$

$$\frac{\partial \alpha}{\partial \bar{t}} = i\gamma \tag{66}$$

$$\frac{\partial \beta}{\partial \bar{t}} = i\epsilon \tag{67}$$

Substituting Eq. (60) into Eqs. (44)–(45) yields

$$\frac{\partial E_r}{\partial \bar{t}} = -2\mu \frac{\partial \gamma}{\partial \bar{t}} - 2\nu \frac{\partial \epsilon}{\partial \bar{t}} + i\beta P \tag{68}$$

$$\frac{\partial E_z}{\partial \bar{t}} = 2\nu \frac{\partial \gamma}{\partial \bar{t}} - 2\mu \frac{\partial \epsilon}{\partial \bar{t}} - i\alpha P \quad . \tag{69}$$

Substitution of Eqs. (50)–(51) and (60)–(61) reduces Eqs. (46)–(47) to the form

$$\left[\frac{\partial}{\partial \bar{t}} + (\mu_i - \nu_r)\frac{\partial}{\partial u} - (\mu_r + \nu_i)\frac{\partial}{\partial \bar{u}}\right](E_r + iE_z) = i(\beta - i\alpha)P \tag{70}$$

$$\left[\frac{\partial}{\partial \bar{t}} + (\mu_i + \nu_r)\frac{\partial}{\partial u} - (\mu_r - \nu_i)\frac{\partial}{\partial \bar{u}}\right](E_r - iE_z) = i(\beta + i\alpha)P \quad . \tag{71}$$

Solving Eqs. (68)–(71) for the partial derivatives with respect to t yields finally the relations

$$\frac{\partial E_r}{\partial \bar{t}} = -\mu_i \frac{\partial E_r}{\partial u} + \mu_r \frac{\partial E_r}{\partial \bar{u}} + i\nu_r \frac{\partial E_z}{\partial u} + i\nu_i \frac{\partial E_z}{\partial \bar{u}} + i\beta P \tag{72}$$

$$\frac{\partial E_z}{\partial \bar{t}} = -i\nu_r \frac{\partial E_r}{\partial u} - i\nu_i \frac{\partial E_r}{\partial \bar{u}} - \mu_i \frac{\partial E_z}{\partial u} + \mu_r \frac{\partial E_z}{\partial \bar{u}} - i\alpha P \tag{73}$$

and

$$\frac{\partial \gamma}{\partial \bar{t}} = \frac{1}{2(u^2 + v^2)} \left\{ (\mu_i \mu - i\nu_r \nu) \frac{\partial E_r}{\partial u} - (\mu\mu_r + i\nu\nu_i) \frac{\partial E_r}{\partial \bar{u}} \right.$$
$$\left. - (\mu_i \nu + i\nu_r \mu) \frac{\partial E_z}{\partial u} + (\mu_r \nu - i\nu_i \mu) \frac{\partial E_z}{\partial \bar{u}} \right\} \tag{74}$$

$$\frac{\partial \epsilon}{\partial \bar{t}} = \frac{1}{2(u^2 + v^2)} \left\{ (\mu_i \nu + i\nu_r \mu) \frac{\partial E_r}{\partial u} - (\mu_r \nu - i\nu_i \mu) \frac{\partial E_r}{\partial \bar{u}} \right.$$
$$\left. + (\mu_i \mu - i\nu_r \nu) \frac{\partial E_z}{\partial u} - (\mu\mu_r + i\nu_i \nu) \frac{\partial E_z}{\partial \bar{u}} \right\} \tag{75}$$

Eqs. (62)–(67) and (72)–(75) comprise the complete set of hyperbolic equations required in the (u, u, t) domain. They can be solved by finite difference methods to yield the analytic continuation in t required for the application of our standard electrode determination program.

3. *High Precision Methods of Calculation*

A detailed study was made of high precision methods (*i.e.*, carrying many significant figures) for gun design. This was studied as an alternative to the method of analytic continuation.

The two equations of gun design Laplace's and Poisson's, are elliptic and thereby unstable for numerical solution by finite difference methods when the boundary conditions are given on an open boundary. However we were able to show that in the case of the simple two-dimensional Laplace equation with analytic boundary conditions that the solution converged both theoretically and by studies on a digital computer. In practice this means that more and more significant figures must be carried along as the mesh size is decreased in order that the roundoff error be kept small in comparison with the magnitude of the solution itself.

Unfortunately, it was not possible to extend the theory beyond the case of the two-dimensional Laplace

equation because of the increased mathematical complexities. However, studies were made on a digital computer of other elliptic equations which again verified the principle that the solution converges as long as sufficient significant figures are carried.

Complete details of this phase of the work are found in Microwave Laboratory Report No. 923.[5]

[5]K. J. Harker and J. Llacer, "Conditions for the Solubility of an Elliptic Difference Equation as an Initial Value Problem," Microwave Laboratory Report No. 923, (June 1962), submitted for publication to the Quarterly of Applied Mathematics.

VII. EXTENDED-INTERACTION KLYSTRONS

A. Introduction

A principal objective of this project is to evaluate the stub-supported meander (SSM) line and related planar circuits as interaction structures in high-power S-band klystrons, with cavities consisting of resonant sections of slow-wave structure. Extended-interaction klystrons, in general, give greater efficiency and gain-bandwidth product than conventional single-gap klystrons.[1] Planar circuits, in particular, have good beam interaction impedance even at high beam velocities; impedance at the circuit is nearly independent of phase velocity. In conjunction with sheet beams, planar circuits also lead to more efficient beam-circuit interaction because more electric field becomes accessible to the beam.

The past year's work has been concerned mainly with improving the theoretical prediction of basic circuit characteristics, and with exploring, by theory and experiment, possible improvement of these characteristics by modifications of the circuit geometry.

B. Discussion

1. *Basic Circuit Characteristics*

a. *The Single-deck SSM Line*

Theoretical analysis of the SSM line has been based throughout on the assumption that TEM waves propagate along the metal bars forming the circuit. The characteristic admittances of such waves have been derived by Fletcher,[2] assuming a constant electric field in the space between the bars. Fletcher's theory, however, gave consistently high predictions of interaction impedance. Butcher[3] has derived a characteristic admittance for thin tapes in an open array, allowing for nonconstant fields as well as edge singularities. While it leads to more difficult computations, Butcher's model does seem to represent a wide-spaced circuit such as the SSM line much more closely then does Fletcher's model. For simplicity, the Butcher admittance used was that corresponding to the case: tape width = gap width. Even with this approximation it was then possible to predict the Pierce impedance of the fundamental space harmonic within less than a factor of two. However, due to the extreme idealization of circuit geometry which it implies, this approximation cannot predict the effect of modifications in the circuit geometry. Dashenkov[4] has computed the characteristic admittances of circular conductors in coupled parallel arrays, with results that are accurate for reasonably wide inter-conductor spacings (*i.e.*, conductor radius/spacing <0.3). To apply the Dashenkov formulation, the rectangular bars of the SSM line were represented by an equivalent circular cross section. Results were found to duplicate closely those of the Butcher approximation, with the added advantage of being based on the exact geometry of the circuit concerned.

Figure 1 gives a comparison of dispersion as predicted by the three different methods, together with measured data, for a single-deck SSM line with dimensions as shown. The particular geometry of this circuit is that of a particular stub-supported ring-bar circuit[5] flattened into the plane of the stubs. The quantity α used in Figure 1 is an important geometrical parameter of the SSM line:

$$\alpha \equiv \frac{\ell_2}{\ell_1 + \ell_2} \equiv \frac{\text{midsection}}{\text{total width}}$$

---

[1] M. Chodorow, T. Wessel-Berg, Trans. PGED, *ED-8*, No. 1, 44-55 (January 1961).

[2] R. C. Fletcher, Proc. IRE *40*, 951-958 (August 1952).

[3] P. N. Butcher, Proc. IEE *104*, 177-187 (March 1957).

[4] V. M. Dashenkov, Radiotekhnika i Elektronika 6, No. 4, 584-592 (1961).

[5] W. R. Ayers, Microwave Laboratory Report No. 554, Stanford University (December 1958), p. 41.

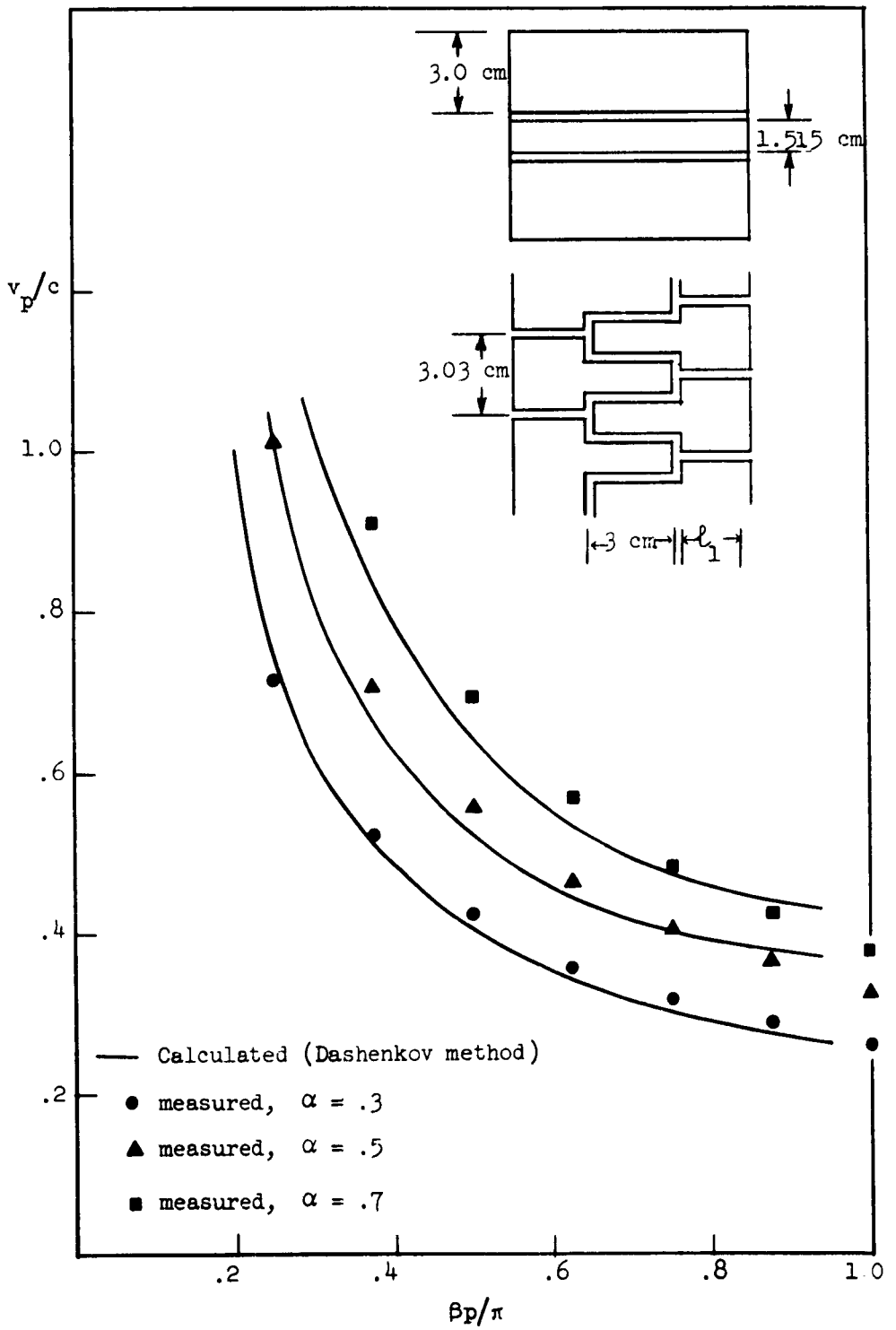

FIGURE 1. Single-deck SSM line: dispersion

Due to the longitudinal connecting links, the electrically effective width of the midsection can be expected to differ somewhat from the geometrical mean width. Best consistency was obtained when it was assumed that the longitudinal connecting links effectively increase the mean length of the midsection by 0.25 cm, or 1/6 the mean length of the link. From Figure 1 it is clear that dispersion increases as, with increasing α, the geometry of the circuit approaches that of a simple ladder.

Figure 2 gives the R_{sh}/Q per resonant wavelength for the same circuit, as measured, and as predicted by the Dashenkov theory. The R_{sh}/Q per wavelength is a parameter relevant to klystron application; it is simply related to the Pierce impedance by[6]

$$\frac{R_{sh}}{Q} = 2\pi \frac{V_g}{V_p} K_0$$

Referring to Figure 2, it is seen that the theory generally predicts the measured value of R_{sh}/Q within less than a factor of two. The calculated R_{sh}/Q is higher than measured because the theory did not allow for the energy stored in the fringing fields near the longitudinal connecting links. The droop of the measured $\alpha = 0.8$ curve at small phase-shift angles could be due to a rapid increase in this energy as the distance between these links and the cavity sidewalls becomes very small compared to the periodic spacing.

Figure 3 illustrates the merit of Dashenkov's method and, for the circuit in question, Butcher's over Fletcher's method. The discrepancy between measured and predicted R_{sh}/Q is seen to be reduced more than two-fold.

It should be noted that R_{sh}/Q is measured here by a perturbation technique in a region grazing the structure; elsewhere, it decreases exponentially away from the circuit.

The general increase of R_{sh}/Q (measured on the axis) with α is a direct consequence of a higher proportion of total energy being stored in the center region. It is a particular advantage of the SSM line that most of this energy is being carried by the even harmonics, including the forward fundamental. This situation is evident from purely theoretical calculations of stored energy vs. α (Figure 4). As a plausibility argument, one might also consider the SSM line as an interdigital circuit in which the odd space harmonics of E_z field (having odd variation in the direction of the bars, normal to the z axis) are "shorted out" by the longitudinal connecting links of the SSM line. By way of contrast, the simple interdigital line, as Fletcher has shown,[2] always stores equal amounts of energy in the even and odd space harmonics. This explains why the SSM line generally has a higher interaction impedance than the interdigital line.

b. *The Double-deck SSM Line*

The double-deck version of the SSM line consists of two planar SSM structures of the type described, spaced parallel to one another within a rectangular metal enclosure (Figure 5). Only the symmetrical (in-phase) mode has been studied. Behavior of a double-deck circuit cannot, in general, be obtained by superposition of two single-deck lines because of coupling between the decks depending on the electrical distance between them. However, the properties of the double-deck circuit are again closely predicted by the Dashenkov theory (Figures 5 and 6).

As a matter of incidental interest, scaled results from the double-deck SSM line are plotted together with data from the "centipede" TWT circuit[7] (Figure 7). It can be seen that the dispersion and Pierce gain parameter of the two circuits are quite close. One should note, however, that in *klystron* (as opposed to TWT) applications, dispersion is of limited importance because bandwidth is obtained with high R_{sh}/Q rather than with low dispersion.

[6]T. Wessel-Berg, T. R. No. 32, Norwegian Defense Research Establishment, Bergen, Norway (Sept. 1960).
[7]M. Chodorow, A. F. Pearce, D. K. Winslow, Microwave Laboratory Report No. 695, Stanford University (May 1960).

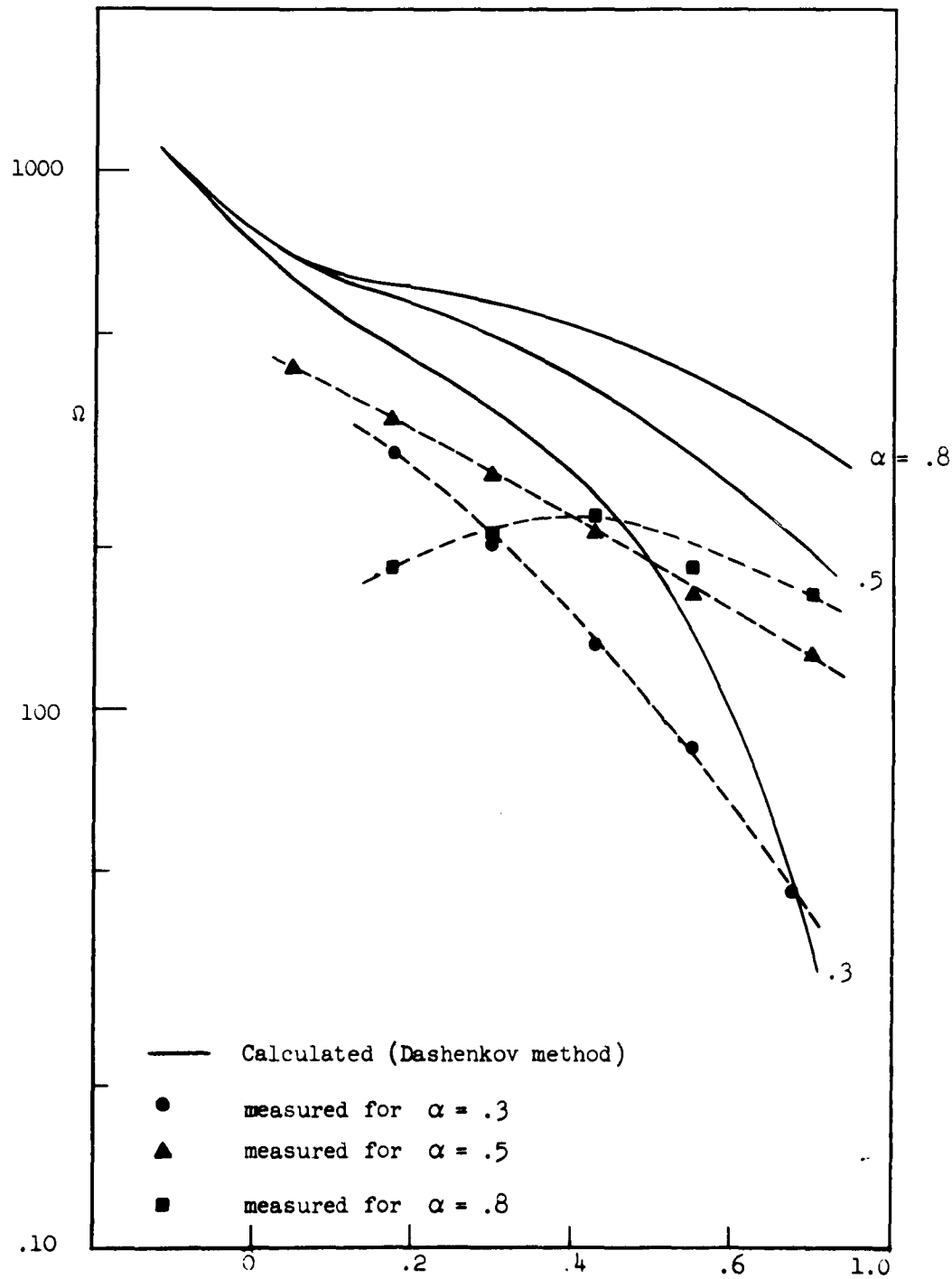

FIGURE 2. Single-deck SSM line: R.., Q per λ, grazing the center line.

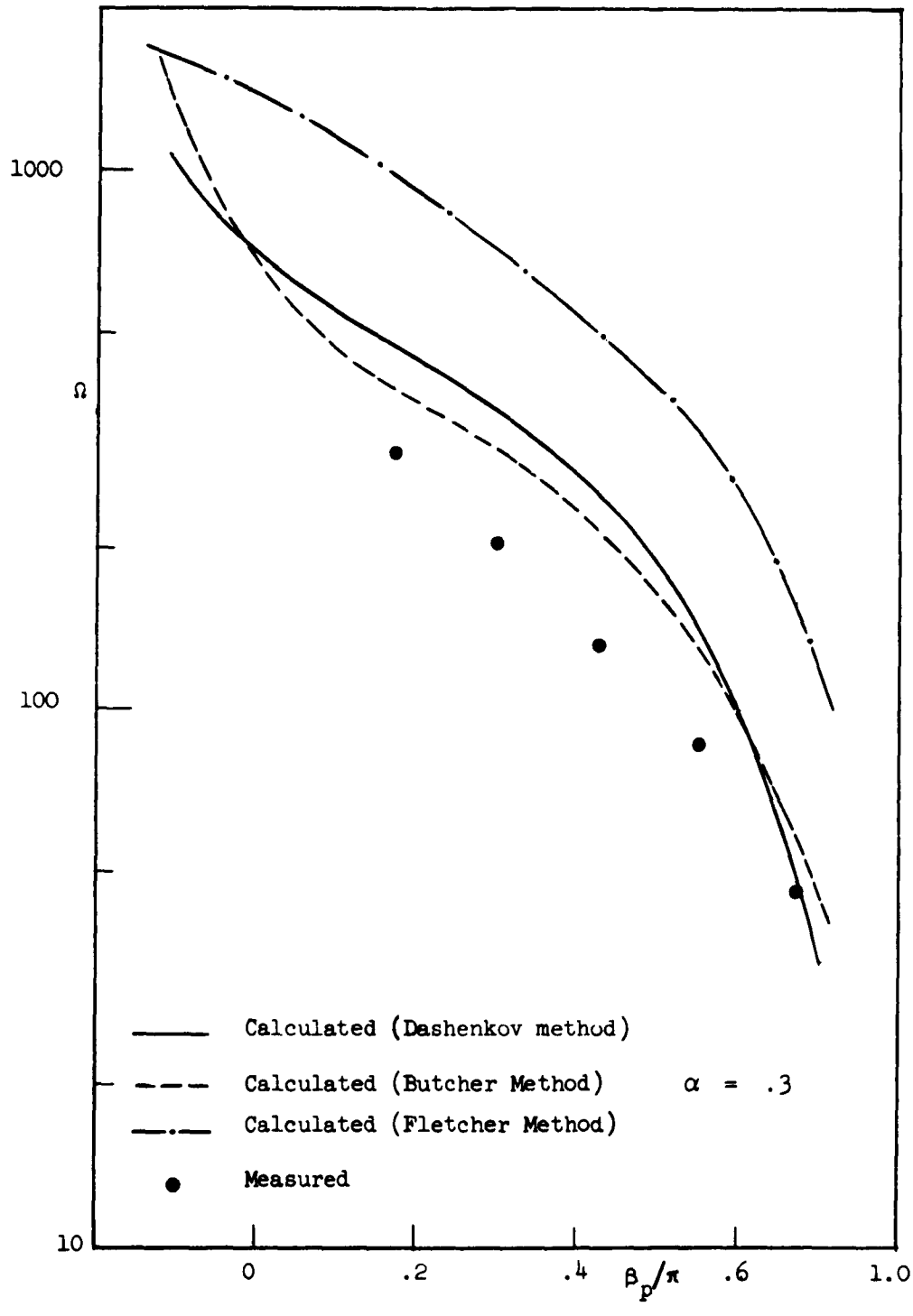

FIGURE 3. Single-deck SSM line: R_{sh}/Q per λ, grazing the center line.

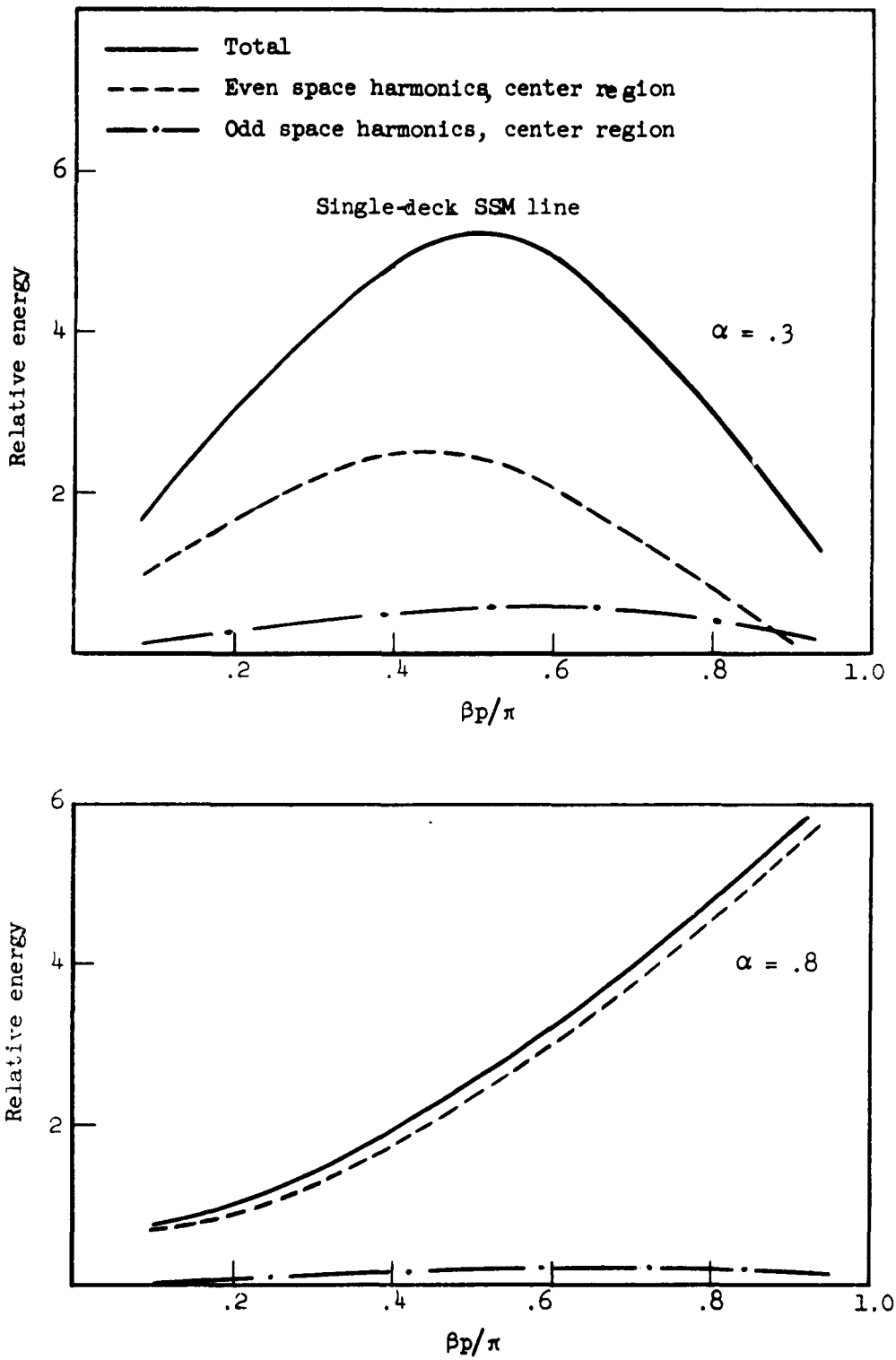

FIGURE 4. Distribution of stored energy (Dashenkov theory) among space harmonics.

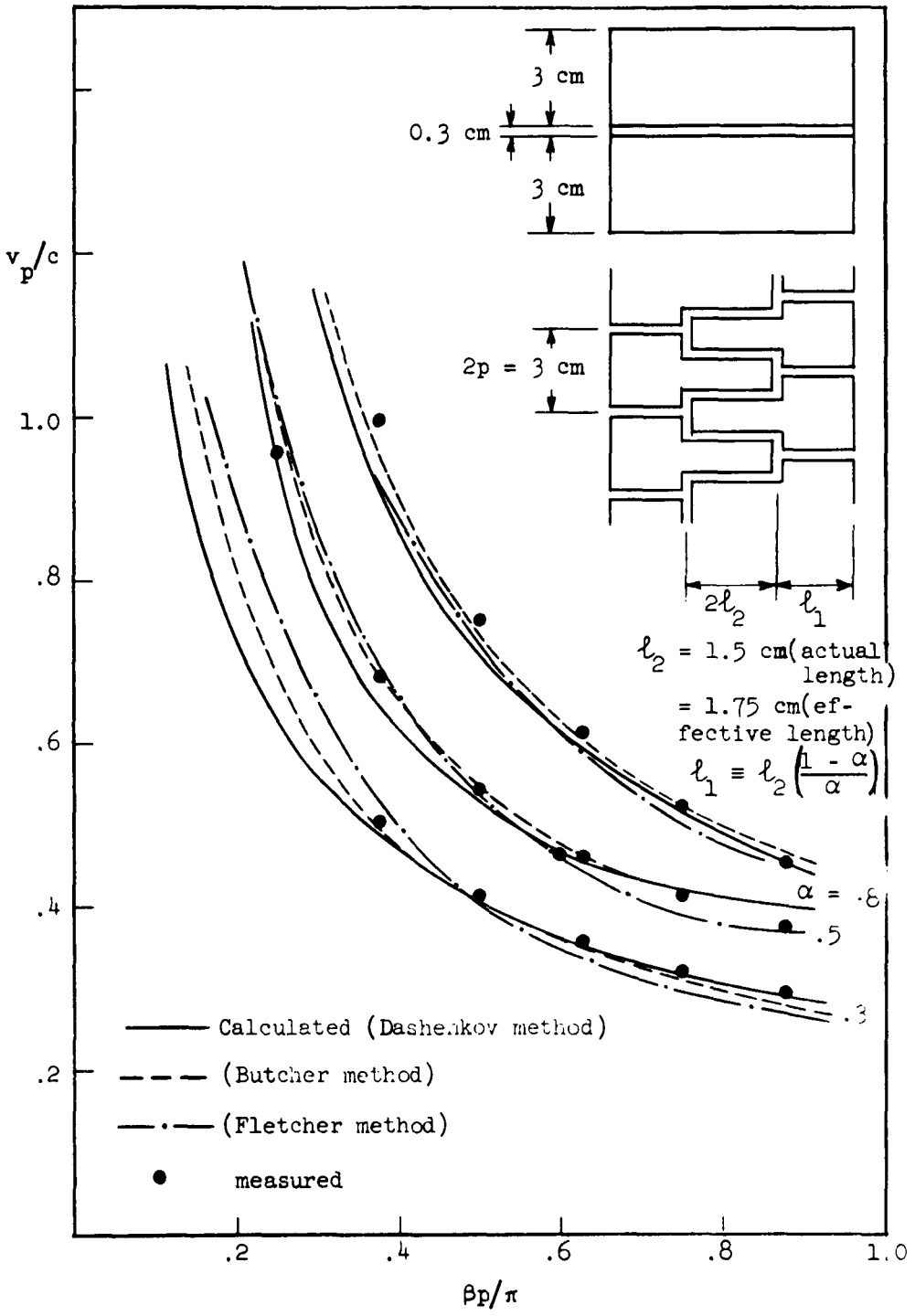

FIGURE 5. Double-deck SSM line: dispersion.

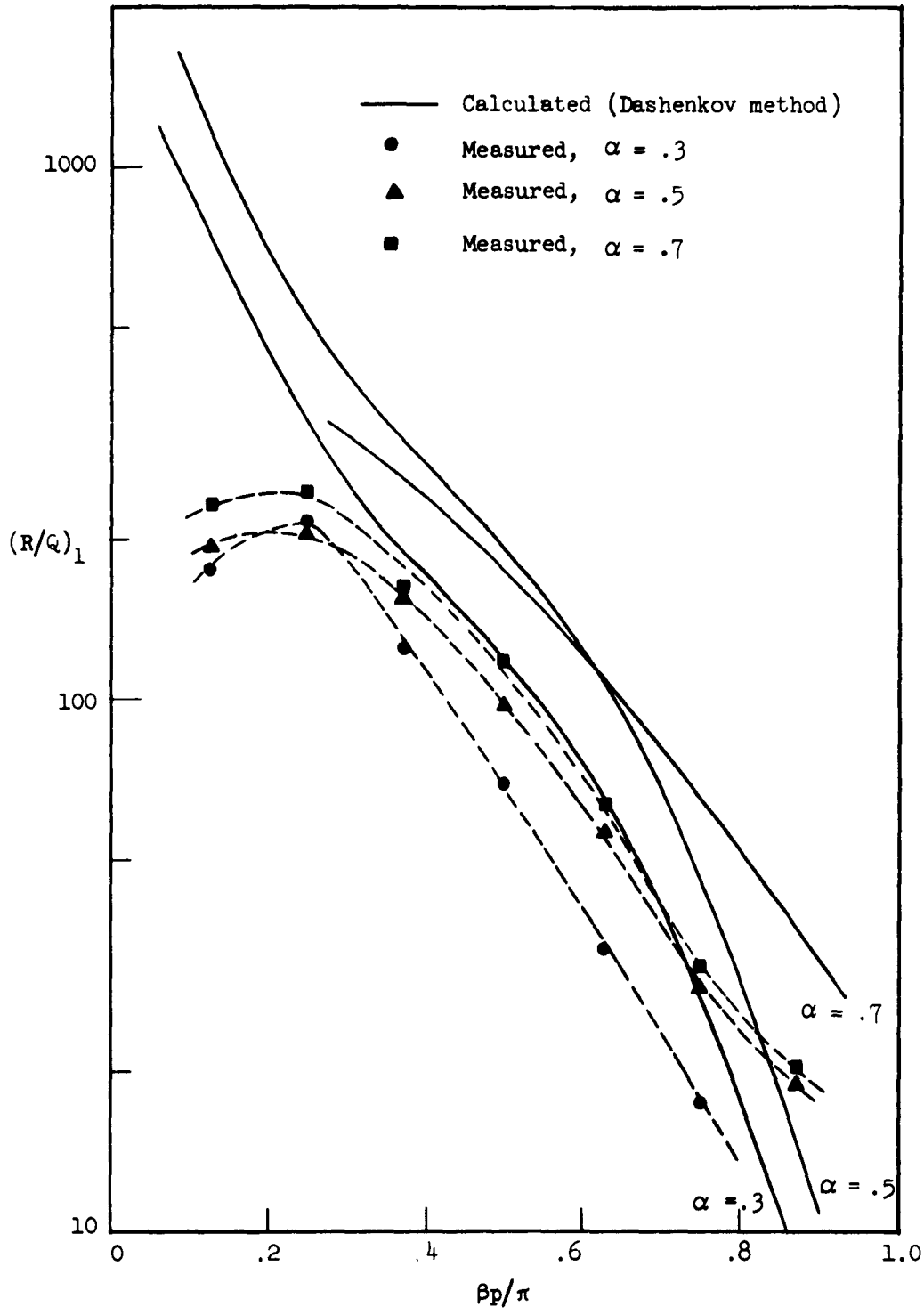

FIGURE 6. Double-deck SSM line: R_{sh}/Q per λ, on axis.

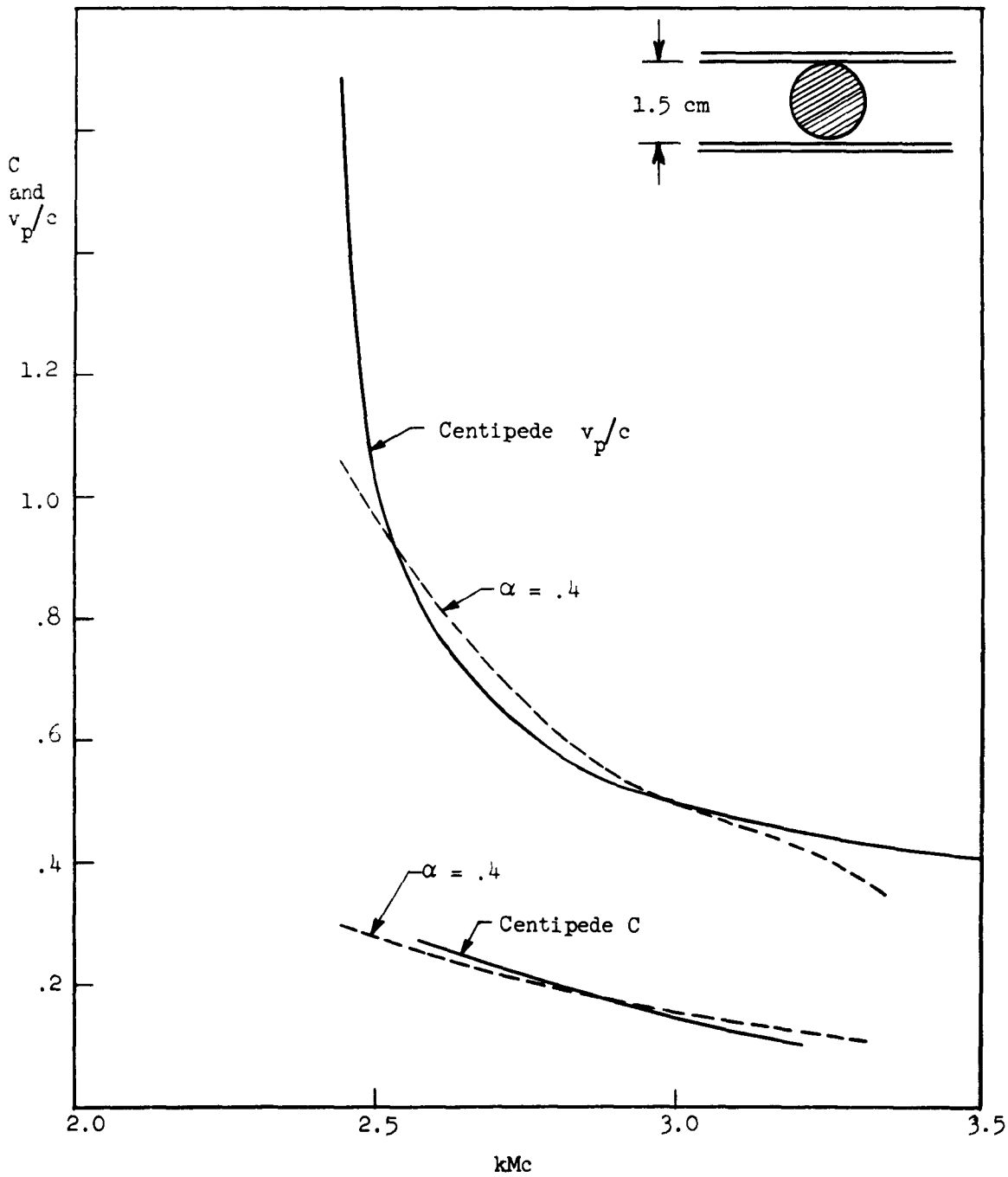

FIGURE 7. Comparison of TWT parameters of double-deck SSM line and "centipede" structure $\alpha = .4, .5$ with 120 kv, 68 amp beam (K_0 measured on axis).

2. *Circuit Modifications*

To control the properties of the SSM line, various degrees of capacitive loading were tried, such as adding ridges and/or reducing the height of the cavity sidewalls. It has been found, however, that such modifications are of doubtful value since they inevitably result in a large increase in stored energy away from the beam and loss of interaction impedance. For example, decreasing the height of the sidewall from 2p to p/2 (p is the separation between adjacent bars in the center region) decreased the Pierce impedance on the axis by more than a factor of two while decreasing the dispersion only slightly. The best circuit configuration appears to be the simple rectangular enclosure where the cavity sidewalls have a height of at least 2p, for maximum impedance, and with the α value as high as can be tolerated dispersion-wise.

A theoretical study was made of a circuit which could be considered as an SSM line with the supporting stubs turned inward to give a crankshaft-like appearance. The calculated dispersion characteristic of this circuit (Figure 8) does not suggest a modified SSM line, however, but rather a hybrid between an interdigital circuit and a simple meander line. The calculated interaction impedance was of the same order as that of the SSM line. This circuit was not investigated further.

In klystron applications where a resonant section of slow-wave structure is to be used for beam interaction, it may become necessary to suppress adjacent modes or orders of resonance. Due to the simple field configuration of planar circuits, selective attenuation of modes appears to be particularly straightforward. Simplified measurements of Q_0 were made to detect the effect of thin transverse slots in the sidewall of a double-deck SSM cavity. The slots were placed so as to interrupt the z-directed wall currents of certain modes, and they were bridged on the outside with 400-ohm/square resistance card. Typical data are tabulated below. The large attenuation of modes other than those for which $\beta_{0p} = 2\pi/8$ and $\beta_{0p} = 6\pi/8$ is evident. Since operation of an extended-interaction cavity at a low phase shift per period (such as $2\pi/8$) is desirable to achieve the R_{sh}/Q, this method of attenuation applies directly.

TABLE I

β_{0p}	$\pi/8$	$2\pi/8$	$3\pi/8$	$4\pi/8$	$5\pi/8$	$6\pi/8$	$7\pi/8$
Q_0 (unattenuated)	580	560	540	780	760	590	580
Q_0 (attenuated)	250	420	160	90	180	590	150

Approximate effect on Q_0 of resonant modes of 8 sections of double-deck SSM line with $\alpha = .6$ of resistance-loaded transverse slots in cavity sidewall set for minimum effect on the modes for which $\beta_{0p} = 2\pi/8$ and $\beta_{0p} = 6\pi/8$.

For planar circuits in general, it can be shown that the R_{sh}/Q per wavelength at the circuit is essentially insensitive to velocity scaling. A theoretical prediction to this effect was confirmed by measurements on two planar circuits of the Ash type[8] (see Figure 9). The circuit velocity was scaled by a factor of two while R_{sh}/Q remained constant within ten percent, including measurement error. This feature is desirable because it allows one to optimize circuit velocity for a given beam independently of impedance considerations. Ash circuits,

[8]E. A. Ash, A. C. Studd, Trans. IRE, *ED-8*, 294-301 (July 1961).

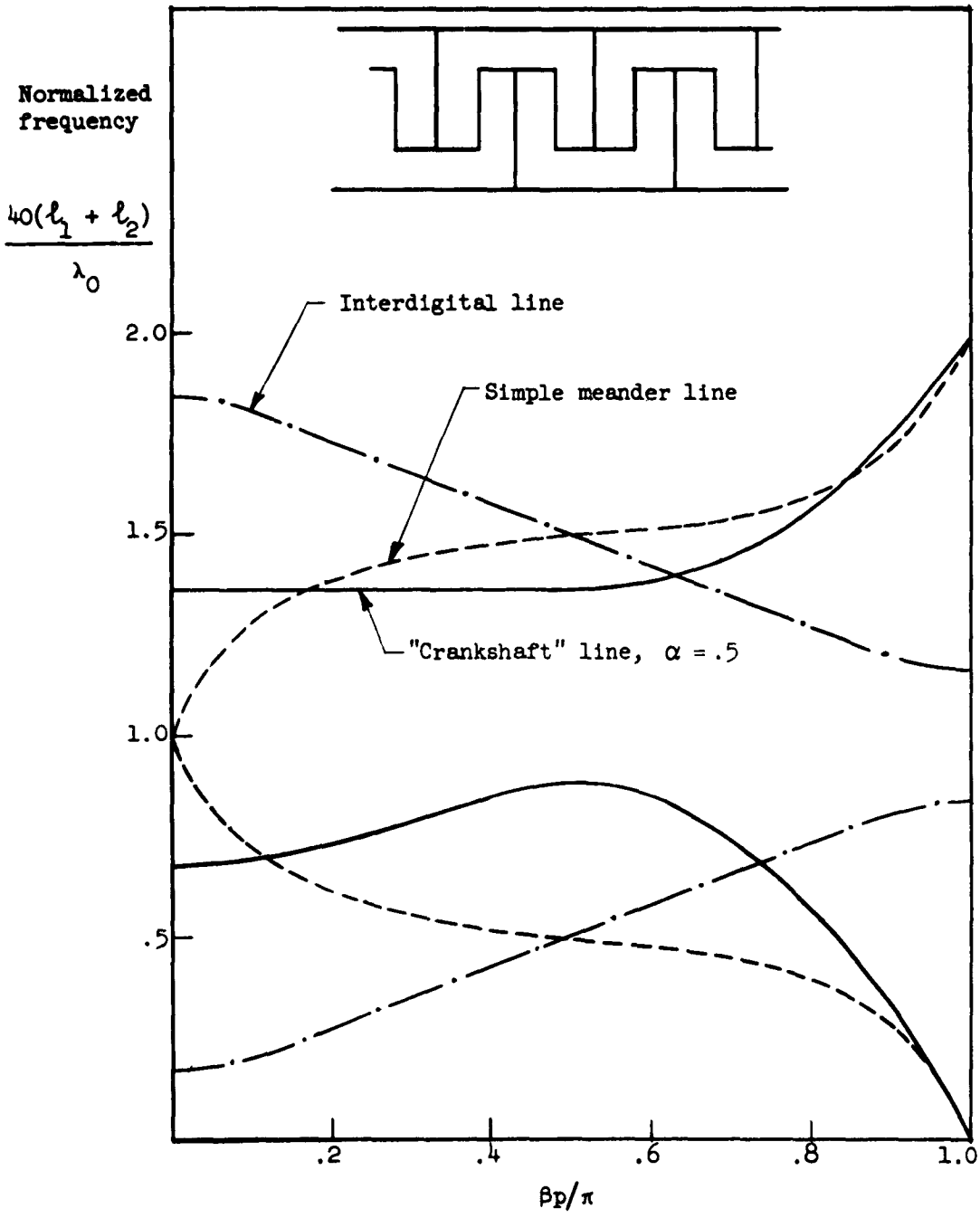

FIGURE 8. Dispersion (Fletcher theory).

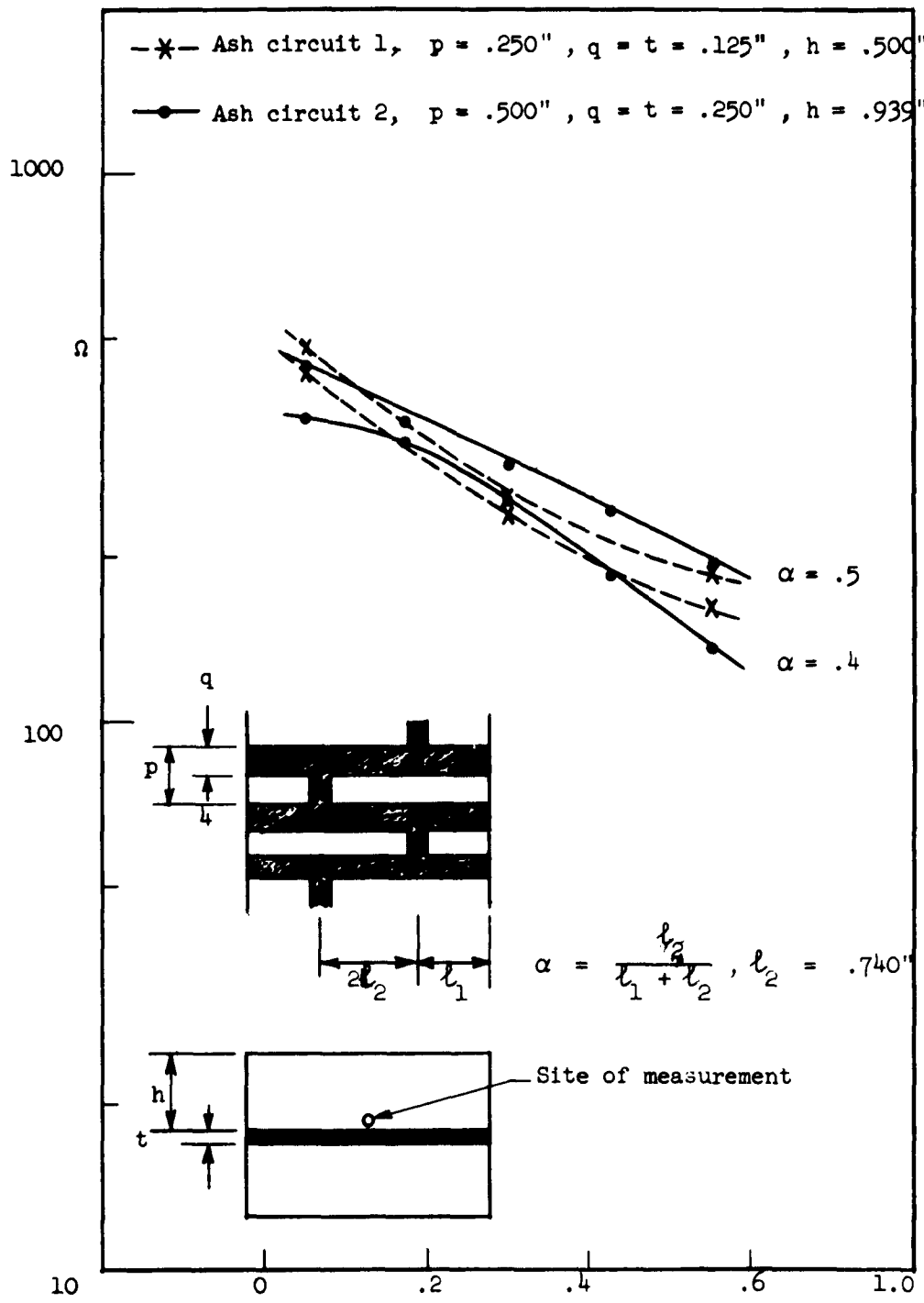

FIGURE 9. R_{sh}/Q per resonant wavelength, at the circuit.

rather than SSM lines, were used in this experiment because manufacture of the former is somewhat simpler while the two structures are almost indistinguishable electrically.

3. *Immediate Objectives*

With the "cold" properties of the chosen class of circuits sufficiently under control, an immediate objective is the building of a four-cavity extended-interaction klystron. The experimental tube is to consist of unevacuated cavities assembled around the "electron stick" (see Section V). The conveniences of hot-testing with the "electron stick" are bought at the price of mismating the planar circuit with a cylindrical beam located somewhat distantly from the circuit, so that the test results would have to be extrapolated to the more favorable sheet-beam situation as a first phase of hot-testing, conventional re-entrant cavities (parts for which are readily available) might be used as input and intermediate stages. Thus, only the output cavity would initially be of the extended-interaction type, with more extended-interaction cavities to be added once the behavior of the more important output cavity alone is well established.

VIII. NONPERIODIC DIELECTRIC-LINED HIGH-POWER TWT

A. Introduction

A principal aim of this project is to complete the preliminaries preparatory to construction of an S-band TWT whose rf structure is simply a homogeneous beryllium-oxide (beryllia) tube (0.75 in. ID x 2 in. OD) bonded to an outer copper shell. Calculated to give interaction between the TM°_{01} waveguide mode (near its cutoff) and an (approximately 80 kilovolt electron beam, this design is predicted to yield gain and bandwidth performance comparable to that of existing periodic TWT's employing the same electron optics. A fine tungsten (0.010 in. wire) helix of small pitch (50 T.P.I.) would be partially imbedded in the inner bore of the ceramic to remove static charge while being essentially transparent to the rf fields of the desired mode.[1]

This approach was originally proposed as a radical solution to the problem of spurious oscillations due to the π-modes and backward space-harmonic waves associated with structure periodicity in conventional TWT's. However, our approach is seen to be equally valuable in providing an exceptionally high peak- and average-power capacity due to the high thermal conductivity of solid beryllia with liner and outer case intimately bonded thereto. In addition, instability provoking extra passbands of the circuit (only TM_{0n} modes in the present instance) are comfortably more remote.

B. Discussion

A hollow beryllia cylinder in the required length and tolerances, though procurable, has been priced quite high and there might be a personnel hazard in handling or further processing it. In addition, development of the best method for bonding to the tungsten helix would also be costly, though straightforward.[2] For these reasons, it was decided to proceed as far as possible without using beryllia itself. For example, in addition to the cold tests made earlier (see previous annual report), it is planned to hot test at low duty cycle with the Electron Stick, which has the helix liner (see Section V) and an external circuit of metal and Stycast plastic. Due to the time required to set up the Electron Sticks to be run by a number of researchers and to satisfy prior commitments for their use, testing of the dielectric TWT is not feasible before the end of 1962.

One set of tests could be made in conjunction with the distributed interaction klystron project (see Section VII); *i.e.*, a resonated section of dielectric line could be used as an output cavity on a beam prebunched to saturation by any convenient means, such as a trio of tunable conventional klystron cavities. This arrangement would be by far the simplest constructionally, and most of the TWT parameters could be deduced.

An alternative, simplified test procedure could use just that part of the S-band TWT between the input coupler and the first sever, with gain measured by probing a nonpropagating longitudinal slot. This scheme requires only a low-power input coupler of not especially good performance. The termination could consist of splicing in material of the same dielectric constant and increasing loss.

C. Future Work

A millimeter-wave version of the nonperiodic dielectric tube has been considered. Workers at the University of Illinois agree that tunnels in *inorganic* dielectrics do need a semiconductor film (such as a residue of aquadag that has been applied and wiped off) to be penetrated by electron beams as slow as 100 Kv (assuming

---

[1]M. Chodorow and D. K. Winslow, "The Electron Stick—a Tool for Evaluating High Power Traveling-wave Tube Circuits," Microwave Laboratory Report No. 717, Stanford University (May 1960).

[2]Although there is evidence that such a helix can itself generate backward-wave oscillations, it is now felt that these oscillations are weak and unlikely to occur when the electron beam is bunched by several kilowatts of input power in the TM_{01} mode. A margin of safety should also be provided by iron-plating the helix so as to affect neither its dc and thermal properties nor its negligible perturbation of the TM_{01} mode. Substitutes for the helix, such as the semiconductor films, were considered but were set aside as undependable.

the tunnel is too small to contain a fine-pitch helix). Further plans will be made after some S-band data are on hand.

A potential substitute for beryllia (at any wavelength) is boron nitride, provided it is of the anisotropic pyrolitically-deposited form having good thermal conductivity in at least one direction. This product was only recently announced, with few details given, and may not yet be commercially available or capable of being fabricated in the shape required with the best thermal conductivity in the radial direction. *If* anisotropy of dielectric constant also exists, it might permit a higher interaction impedance for a given phase velocity reduction factor.[3] However, it is feared that with the material oriented for best heat removal, the anisotropy of dielectric constant might be just opposite to that giving improvement in impedance.

---

[3]R. B. R. Shersby-Harvie, et al., "A Theoretical and Experimental Investigation of Linear Electron Accelerators," Proc. IEE *104B*, 273-292 (May 1957).

IX. FAST WAVE TUBES

A. Objective

The coherent interaction between a fast cyclotron wave associated with a rotational electron beam and an electromagnetic field has been investigated theoretically and experimentally at 10 cm wavelength,[1] and an S-band tube has been operated successfully. The object of this project has been to investigate the feasibility of generating microwave power at millimeter wavelength range by the same principle. A 1 to 2 mm wavelength tube has been built and tested.

B. Background: The 1-2 mm Wavelength Oscillator

This project was originated under an NSF grant in 1960. By 1962, much of the work had been done. This background is described below. During mid-1962, this project was transferred to the present contract. The work done since that time is described in Part C below.

The 1-2 mm wavelength oscillator (Figure 1) was scaled down from the S-band tube. It consists basically of three major parts, namely, a hollow electron beam, an unloaded rectangular waveguide (0.040 in. x 0.027 in.) of 2 mm cutoff wavelength for the TE_{10} mode, and a 50 to 100 kilogauss aircore solenoid. The electron is rotating at the cyclotron frequency ($\omega_c = e/m B_0$). This cyclotron motion is produced by the dc excited radial magnetic field near the annular anode and the fringing field of the main solenoid. This radial field controls the transmitted current and the fraction of electron energy in rotational motion. The signal is coupled out by a 45 bend at the entrance of the interaction waveguide.

1. *Design of 100 Kilogauss Magnet**

The solenoid was designed to generate a uniform magnetic field 1 cm long of 50 to 100 kilogauss for 1 millisecond constant in time and space to $\pm$ 1%. In addition, a suitable control and pulsing circuit was needed. The latter goal was accomplished with conventional techniques. The interesting part of the problem lay in the design of the magnet coil and pulse-forming network (PFN).

The most promising type of magnet for this application appeared to be a modified Bitter coil as developed by Furth and others.[2-5] This coil is made up of individual split copper disks with Mylar insulation, which has the advantages of strong mechanical strength, efficient cooling, and no longitudinal slippage of turns. Thus it is capable of generating very high magnetic fields. However, it also has some peculiarities due to skin effects since the current flows primarily on the inside surface of the disk conductors to a depth limited by the rate of penetration of magnetic field into the metal. This means that the magnetic field spreads out from the bore of the coil during the pulse. Thus for a constant current pulse, the field strength decreases.

More important than the change in magnetic field is the changing impedance during a pulse. This makes it difficult to get a flat-top pulse with conventional PFN. A constant voltage network with a tapered impedance seemed unattractive due to its lack of flexibility. A constant impedance, separately switched, tapered voltage, parallel network was also rejected as being too complicated.

An optimally flat five-stage PFN was selected of the type described by Perry[6] for which he presents

---

[1]K. K. Chow, "The Cyclotron Resonance Oscillator," Microwave Laboratory Report No. 800, Stanford University (1961).

*The assistance of D. Cummings, from the University of California, for his consulting in the design of the pulser for the magnet supply is gratefully acknowledged.

[2]F. Bitter, Rev. Sci. Instr. 7, 482 (1936).

[3]H. P. Furth and R. W. Waniek, Rev. Sci. Instr. 27, 195 (1956).

[4]H. P. Furth, M. A. Larvine and R. W. Waniek, Rev. Sci. Instr. 28, 949 (1957).

[5]D. H. Birdshall and H. P. Furth, Rev. Sci. Instr. 30, 600 (1959).

[6]A. D. Perry, IRE Convention Record, Part 3 (1959).

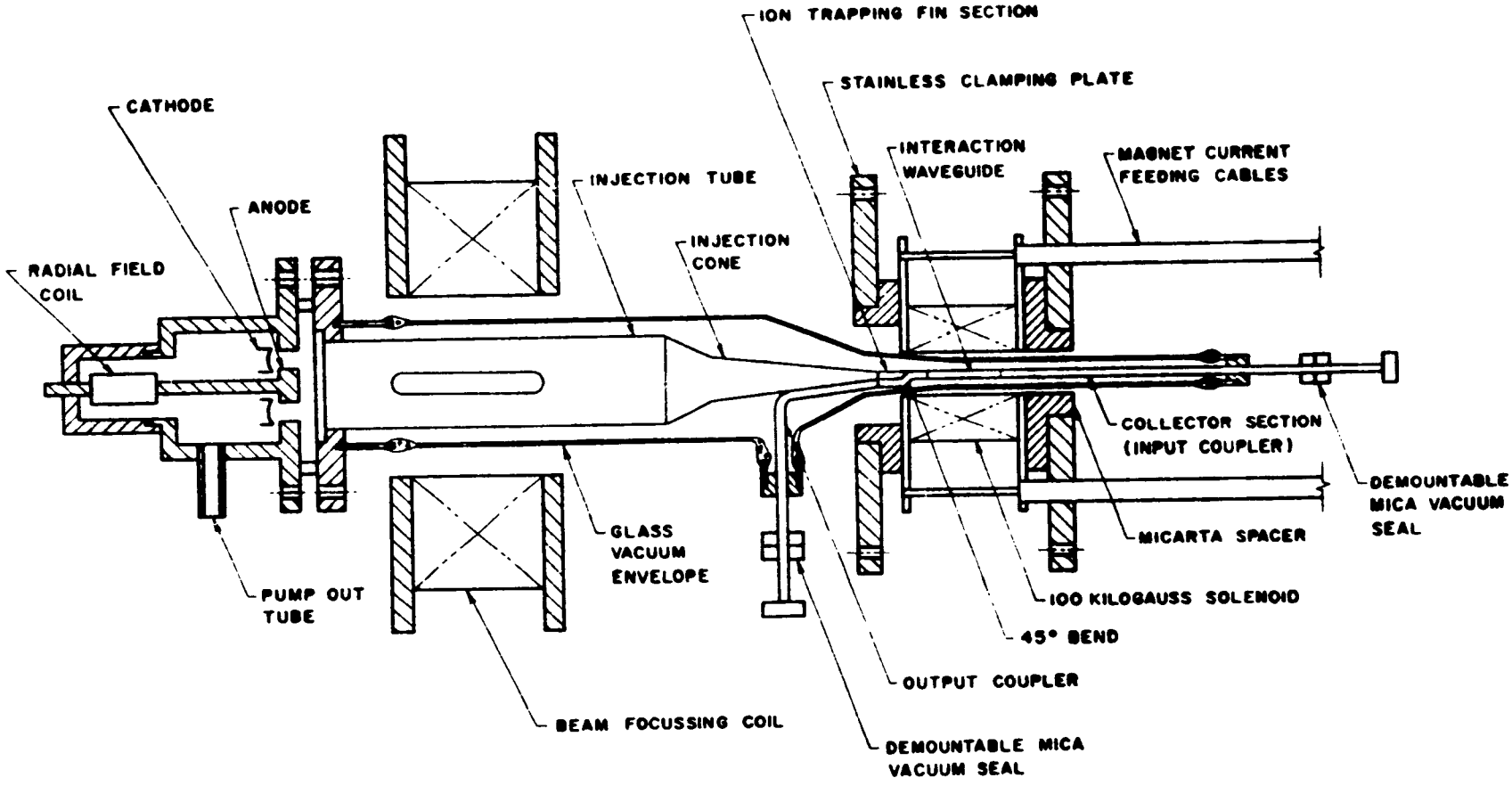

FIGURE 1. Assembled view of the 1-mm wavelength cycloton resonance oscillator

detailed trimming procedures. The approach was to make the normal impedance of the PFN the same as the resistance of the coil at the beginning of the flat top portion of the pulse. Resistance was then added to the inductance in each section so that the sum of the resistances carrying current, as the pulse progressed down the line, was equal to the loss of resistance in the coil up to that time. Thus each stage in turn would see the same impedance.

The field strength on the axis of a uniformly spaced coil with a spacing factor λ and a geometric factor G will be

$$H = \frac{2\pi}{10} i_0 \lambda \log_e \left(\alpha^2 \frac{[1 + (\beta + K_x)^2]^{\frac{1}{2}} + (\beta + K_x)}{[\alpha^2 + (\beta + K_x)^2]^{\frac{1}{2}} + (\beta + K_x)} \right.$$

$$\left. \times \frac{[1 + (\beta - K_x)^2]^{\frac{1}{2}} + (\beta - K_x)}{[\alpha^2 + (\beta - K_x)^2]^{\frac{1}{2}} + (\beta - K_x)} \right) \text{ gauss} , \qquad (1)$$

where i_0 is the current density, λ is the spacing factor defined as the ratio of the conductor volume to the total volume, α is the ratio of the outer radius to the inner radius $= a_2/a_1$, β is the ratio of the length of the coil to the inner diameter of the coil $= b/a_1$, and K_x is the distance from the center of the coil to the point where H is measured, normalized to the inner radius of the coil $= x/a_1$ (see sketch below).

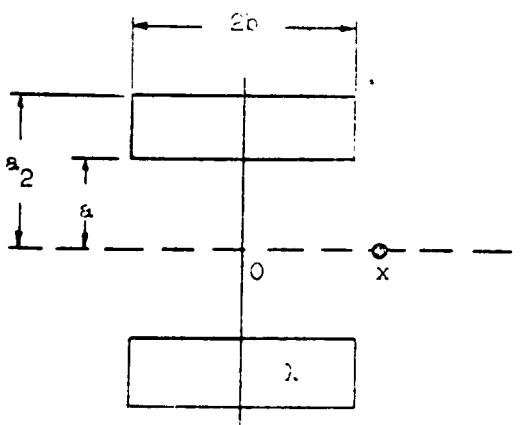

Then we have

$$G = \log_e\left(\alpha^2 \frac{\left[1 + (\beta + K_x)^2\right]^{\frac{1}{2}} + (\beta + K_x)}{\left[\alpha^2 + (\beta + K_x)^2\right]^{\frac{1}{2}} + (\beta + K_x)} \times \frac{\left[1 + (\beta - K_x)^2\right]^{\frac{1}{2}} + (\beta - K_x)}{\left[\alpha^2 + (\beta - K_x)^2\right]^{\frac{1}{2}} + (\beta - K_x)}\right) \tag{2}$$

A uniform field can be achieved by adding additional sections of coil at the sides with higher coil densities. A five-section coil was designed, and the field strength on the axis is given by

$$H = \frac{2\pi}{10} i_0 \left[\lambda_1 G_1 + \lambda_2 G_2 + \lambda_3 G_3\right] , \tag{3}$$

where G_1 is given by Eq. (2), and

$$G_2 = \log_e\left(\frac{\left[1 + (K_2 - \beta_2 + K_x)^2\right]^{\frac{1}{2}} + (K_2 - \beta_2 + K_x)}{\left[\alpha^2 + (K_2 - \beta_2 + K_x)^2\right]^{\frac{1}{2}} + (K_2 - \beta_2 + K_x)} \times \frac{\left[1 + (K_2 - \beta_2 - K_x)^2\right]^{\frac{1}{2}} + (K_2 - \beta_2 - K_x)}{\left[\alpha^2 + (K_2 - \beta_2 - K_x)^2\right]^{\frac{1}{2}} + (K_2 - \beta_2 - K_x)} \tag{4}$$

$$\times \frac{\left[1 + (K_2 + \beta_2 + K_x)^2\right]^{\frac{1}{2}} + (K_2 + \beta_2 + K_x)}{\left[\alpha^2 + (K_2 + \beta_2 + K_x)^2\right]^{\frac{1}{2}} + (K_2 + \beta_2 + K_x)} \times \frac{\left[1 + (K_2 + \beta_2 - K_x)^2\right]^{\frac{1}{2}} + (K_2 + \beta_2 - K_x)}{\left[\alpha^2 + (K_2 + \beta_2 - K_x)^2\right]^{\frac{1}{2}} + (K_2 + \beta_2 - K_x)}\right)$$

Here, G_3 is given by the same expression as Eq. (4) except that every subscript is changed from 2 to 3, and K_2, K_3 is the normalized distance from the center of each sectional coil to the center of the coil (L_2/a_1, L_3/a_1), $\beta_2 = b_2/a$, $\beta_3 = b_3/a_1$ (as shown in sketch):

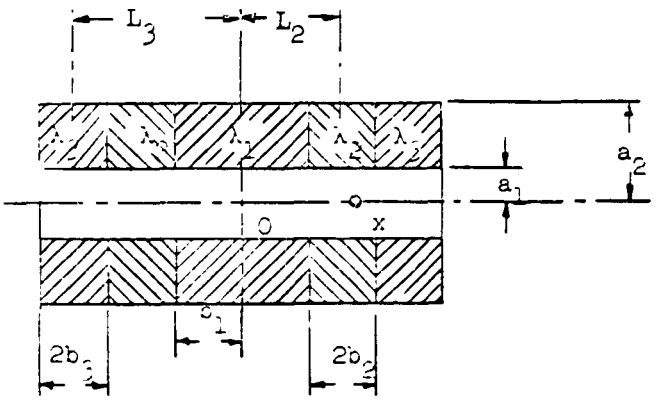

By suitable choice of λ's and G's, and by using a desk calculator, spatial variations can be minimized to $\pm$ 1%. The final parameters of the coil are summarized as in Table I.

TABLE I

Parameters of the 10^5 Gauss Solenoid

Total Length L (in.)	Outer Rad. a_2	Inner Rad. a_1	b_1	b_2	b_3	λ_1	λ_2	λ_3	Uniformity 1%
1.500	.750	.250	.288	.105	.125	.625	.667	.8	.500 in.

The physical dimensions of the coil are given in Table II.

TABLE II

Dimensions of the 10^5 Gauss Solenoid

	Center Coil		First Side Coil		Second Side Coil	
Copper Disk Thickness (in.)	No. of Disks	Spacer Thickness	No. of Disks	Spacer Thickness	No. of Disks	Spacer Thickness
0.020	18	0.012	14	0.010	20	0.005

The field strength in the uniform region was computed and was given by

$$H = 13.14\, I_0 \quad , \tag{5}$$

where I_0 is the total current fed to the solenoid. Equation (5) was then checked at low current levels. The measured field strength related to the current by

$$H = 13.1\, I_0 \ , \qquad (6)$$

which agreed very well with the calculated value.

Measurements were made of the change of magnetic field and instantaneous resistance as a function of time during constant-current, low-level pulses. The change in the magnetic field was found to be small throughout the pulse. The resistance decreased by more than a factor of 10 in the first 0.2 msec and a factor of 2 thereafter.

A five-stage PFN was designed using the solenoid as the load. The first inductor in the PFN was the combined inductance of the coil, leads and ignition switch. The capacitor value was picked to make the line impedance equal to the sum of the resistances (0.040 ohms) measured and computed for the coil, ignition and leads after about 0.25 msec (the expected rise time). The PFN inductor was then wound out of wire small enough to make a first order correction for the resistance change in the coil. These requirements gave a low but acceptable voltage level for the PFN voltage and the ignition switch (600 v).

The design pulse length was 1.25 msec. But, due to the high initial resistance, the rise time was twice longer than expected and the flat portion was about 1.0 msec. However, the design of first order correction was effective since only one day of trimming was required to get the desired flatness. Figure 2 shows the pulse shape and the field distribution on the axis.

2. *Electron Gun and the Beam Tester*

The idea of converging an electron beam by an axially increasing magnetic field has been suggested by many investigators.[7,8,9] This scheme is especially useful for high density electron beam applications in millimeter-wave tubes and transverse-wave tubes. A detailed treatment of the electron trajectories in a nonuniform magnetic field has been given by Dunn and Holaday.[10]

If the magnetic field is axially symmetric and the electric field is zero (in the drift region), the electron entering such a field will preserve its angular momentum:

$$P_\theta = \gamma^2 \dot{\theta} - \eta \gamma A_\theta = \text{const.} \ ,$$

where $\eta = |e|/m$ and A_θ is the vector potential of the magnetic field. It is possible to define a potential function U such that

$$U = \frac{1}{2\eta\gamma^2} (P_\theta + \eta\gamma A_\theta)^2 = \frac{\gamma^2 \dot{\theta}^2}{2\eta} \ .$$

Then the equation of motion will reduce to

$$\ddot{r} + \eta(\partial U/\partial r) = 0$$

$$\ddot{z} + \eta(\partial U/\partial z) = 0 \ .$$

[7] J. R. Pierce, *Theory and Design of Electron Beams*, D. Van Nostrand Co., Inc., New York, 1954, p. 164.

[8] O. Heil (unpublished).

[9] J. F. Gittins, Services Electronics Res. Labs. Tech. J. 5, 119-126 (1955).

[10] D. A. Dunn and R. E. Holaday, J. Appl. Phys. 32, 1612-1620 (1961).

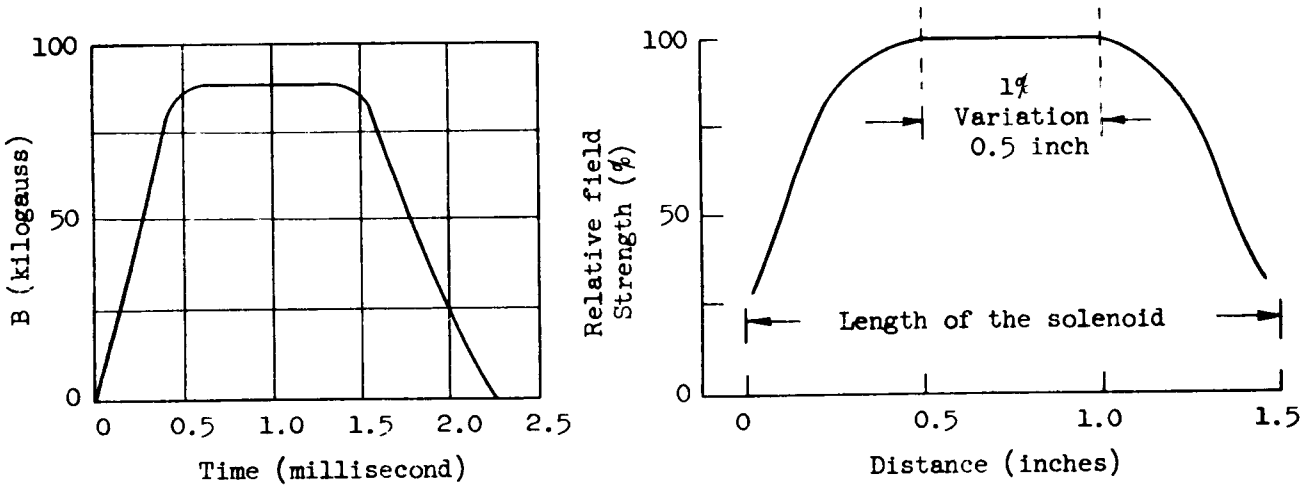

FIGURE 2. Pulse shape and field distribution on the axis.

The total energy will be given by

$$\frac{1}{2}(\gamma^2 + \dot{z}^2) + \eta U = \eta U_0 \ ,$$

where U_0 is a constant which corresponds to the initial energy of the electron at $t = 0$ and U is the potential corresponding to the θ energy. It is obvious that when $U = U_0$, the electron has no radial and axial motion and all the energy is in the spinning motion.

It is the critical injection condition. It can be shown[10] that the trajectory of an electron injected to a slow, axially increasing magnetic field is a helical path about a flux line; the angular frequency of rotation is the "local" cyclotron frequency.

The electron gun used in the S-band tube was modified and used to produce a small intense hollow beam for the 1 mm wavelength oscillator. A glass tube of 1-1/4 in. diameter tapered to 0.050 in. diameter, with thin, transparent metallic coating, was used for the beam transmission test. The experiment showed that with careful alignment of the solenoid and the tube, and careful adjustment of the tranverse field and focusing field, an optimum collector current of 160 ma was obtained which was controllable by the transverse field at the annular anode.

C. Present Status

The work from the time this project was transferred to this present contract up to the time of this report, 31 October 1962, is described below.

1. *The RF Circuit*

For cyclotron resonance interaction, a smooth transmission circuit is needed. Unloaded rectangular waveguides have been selected for S-band tubes with markable success, as they permit the use of the necessary bends in the circuit without problems. Therefore, unloaded rectangular waveguides are chosen for 1 mm wave tubes.

The home-made rectangular waveguide has an inner dimension of 0.040 in. x 0.027 in., with a cutoff wavelength $\lambda_c = 2.03$ mm for the TE_{10} mode. This dimension of the waveguide permitted enough transmission current without too serious a mode interference.[11] (The next higher order mode is TE_{01}.)

2. *Experimentation*

The assembled view of the experimental tube is shown in Figure 1. The glass envelope and the mica windows complete the vacuum system. The electron beam is condensed by the fringing magnetic field and injected into the interaction waveguide through the injection tube and the injection cone. The waveguide system consists of a 45° bend, an interaction guide 1 in. long, a collector section and an output coupler. The fins are essentially an rf short so that the backward wave propagates through the 45° bend with little reflection.

Preliminary tests show that a collector current as high as 120 ma with a beam diameter less than 0.020 in. at 4 kv beam voltage has passed through the interaction waveguide with almost no interception. The transmitted current can be controlled by the radial field. As yet no clear indication of oscillation has been obtained. The present effort has been to improve the electron optics, to stabilize the anode pulse and to add adequate cooling for the magnet.

[11] K. K. Chow, Microwave Laboratory Report No. 937, Stanford University (July 1962).

X. ELECTRON BEAM INTERACTION WITH A CESIUM PLASMA

A. Objectives

The objectives of this project are to carry out a detailed theoretical and experimental study of the interaction between an electron stream and a plasma. The study includes methods of exciting the interaction. Diagnostic techniques necessary for the experimental work are also being studied.

The experimental work utilizes a plasma produced by the thermal ionization of cesium. The cesium plasma is of relatively low temperature (2300°K), has a high percentage of ionization, is free of many of the oscillations present in discharge plasmas, and allows a well-formed electron beam to pass through it without hitting neutral atoms.

B. Review

This project has only recently come under Contract AF 30(602)-2575. This report, since it is the first report on the project while under this contract, includes a brief review of some of the work which was done on the project before it came under this contract. A brief summary of the nomenclature and abbreviations is also included.

When an electron beam passes through a plasma it is possible to get an interaction between beam and plasma which results in large rf gain. A field theory was developed which took account of the finite size of the beam and plasma and of the magnetic field. Some very successful cesium tubes were built which allowed very detailed comparison between experiment and theory. The gain of the tubes was studied as a function of the various system parameters; *i.e.*, ω, ω_{p}, ω_{c}, I_{0} and V_{0} (see nomenclature and abbreviations on the following page). The theory was found to be in excellent agreement with experimental results for $\omega < \omega_{p0}$ plasma gain of as much as 15 db/cm at S-band being obtained. Overall tube gains of 25 db for a 2 cm plasma section were not unusual. For $\omega_{p} < \omega < (\omega_{p}^{2} + \omega_{c}^{2})^{1/2}$, the theory was only in qualitative agreement with the experimental results.

Nomenclature and Abbreviations

ω = (rf frequency) x 2π

ω_{p} = (plasma frequency) x 2π

ω_{p0} = ω_{p} on axis

ω_{c} = $e\beta/m$ = (cyclotron frequency) x 2π

n = electron density

α = parameter of parabolaticity

a = radius of plasma column

E_{z} = longitudinal electric field

E_{r} = radial electric field

β = propagation constant

ϵ_{zz} = $1 - \omega_{p}^{2}/\omega^{2}$ longitudinal relative dielectric constant of plasma (parallel to magnetic field)

ϵ_{rr} = $1 - \omega_{p}^{2}/\omega^{2} - \omega_{c}^{2})$ radial relative dielectric constant of plasma (perpendicular to magnetic field)

β_1 = propagation constant of a cold mode

v_0 = $\sqrt{(2V_0e)}/m$ beam velocity

β_e = ω/v_0

V_0 = beam voltage

I_0 = dc beam current

ω_{p0} = (plasma frequency of beam) x 2π

F = ω/ω_{p0}

FC = ω_c/ω_{p0}

One reason for the differences between theory and experiment is that the radial density distribution of the plasma is not uniform as is assumed in the theory. As there are strong rf fields in the plasma far from the beam in the frequency range $\omega_p < \omega < (\omega_p^2 + \omega_c^2)^{1/2}$, good quantitative gain predictions are difficult to make. Another more fundamental difficulty that occurs arises from a consideration of the interaction of the beam with the backward waves which can propagate along the plasma in the frequency range $\omega_p < \omega < (\omega_p^2 + \omega_c^2)^{1/2}$. The field theory results do not provide enough physical insight to determine whether calculated growth constants in the direction of travel of the beam correspond to forward wave gain or backward wave attenuation. Other approaches giving more physical insight into the problem are now being considered (see this section, Part C, Present Status).

All of the gain experiments had been done using a beam which had been rf modulated by a helix before entering the plasma. After the gain measurements of the final cesium tube with helices were completed, the fields outside the tube were investigated. Weak rf fields were detected outside the tube in the frequency range $\omega_p < \omega < (\omega_p^2 + \omega_c^2)^{1/2}$. The existence of these fields outside the plasma encouraged the possibility of coupling directly to the beam via the plasma. A new cesium tube and a waveguide system were built for an experiment to couple directly to the plasma. A small amount of coupling from the waveguides through the plasma was observed. The large gain obtained in earlier experiments, where the coupling was directly to the beam, was not observed. This, we feel, is due to the extremely weak coupling obtained in the experiment.

Diagnostic techniques using the transmission characteristics of a plasma were studied both theoretically and experimentally. Experimental results were obtained which were consistent qualitatively with a simplified theory which assumes a plasma of uniform electron density over its cross section.

C. Present Status

As mentioned in Part B, above, the field theory of the plasma-beam interaction does not give much physical insight into the actual gain mechanism of the interaction. We have been examining the problem by considering the special case of the plasma and beam filling the drift tube. For this case the dispersion relation may be expressed in the form

$$(\beta^2 - \beta_1^2)(\beta - \beta_e)^2 = -\frac{\beta_{pb}^2 \beta^2}{1 - \omega_p^2/\omega^2}$$

From this dispersion relation a four-wave solution may be obtained and the relevant propagation constants found. By using the boundary conditions at each end we can find the amplitudes and phases of the beam current, beam velocity and longitudinal electric field for each wave. Using a computer program, numerical

results were obtained for four different types of boundary conditions. The results are being checked and analyzed.

We have developed the propagation theory for a plasma column with a nonuniform density variation over its cross section. This theory has been evaluated on the computer for a plasma column with a parabolic density variation; *i.e.*, $n = n_0[1 - \alpha(r^2/a^2)]$, where "a" is the radius of the plasma column. When this work is completed, we hope to be able to put our diagnostic techniques on a firmer theoretical basis. Moreover, with a knowledge of the field variations within such a plasma, we would then expect to be in a better position to design a strong coupling system.

Our propagation theory predicts that all cutoffs of the passbands of the "cold" plasma modes, except that at zero frequency, are determined solely by the plasma density at the edge of the plasma column. On the other hand, the slope of the ω-β characteristic near zero frequency depends on the average density, or ω_p^2, over the cross-section of the plasma column.

It is well known that for a plasma column of uniform density in free space or filling a drift tube, the upper cutoff of the backward wave passband occurs at $\epsilon_{rr} = 0$. For a nonuniform plasma column, ϵ_{rr} is a function of radius. In this case, as is shown in the following derivation, the cutoff occurs when $\epsilon_{rr} = 0$ at the *edge* of the plasma column. The differential equation satisfied by E_z (in the quasi-static approximation) with no beam present is

$$\frac{1}{r}\frac{d}{dr}\left(r\epsilon_{rr}\frac{dE_z}{dr}\right) - \beta^2 \epsilon_{zz} E_z = 0 \quad . \tag{1}$$

Let us define a new parameter r_0 to be the radius at which $\epsilon_{rr} = 0$. Then ϵ_{rr} is negative or positive according to whether r is less than or greater than r_0 (assuming the plasma density decreases with radius). We may examine the behavior of E_z near r_0 by expanding ϵ_{rr} about r_0 in a Taylor series, letting $\delta = r - r_0$ and solving Eq. (1) for small δ. Thus, we have

$$\epsilon_{rr}(\delta) \approx \delta\left(\left.\frac{d\epsilon_{rr}}{dr}\right|_{r_0}\right) \quad , \tag{2}$$

and ϵ_{zz} is a slowly varying function of δ and may be treated as a constant. Equation (1) then becomes

$$\frac{d}{d\delta}\left(\delta\frac{dE_z}{d\delta}\right) - \beta^2 \frac{\epsilon_{zz}}{\left(\left.\frac{d\epsilon_{rr}}{dr}\right|_{r_0}\right)} E_z = 0 \quad , \tag{1a}$$

and has the solution

$$E_z = AI_0\left(\beta\sqrt{\frac{\epsilon_{zz}}{\left(\left.\frac{d\epsilon_{rr}}{dr}\right|_{r_0}\right)}}\,\delta^{\frac{1}{2}}\right) \quad , \tag{3}$$

where I_0 is the modified Bessel function finite for zero argument. The quantity under the radical is positive; hence for $r > r_0$, E_z varies either as an I_0 or J_0 Bessel function depending on whether ζ is real or imaginary. For later comparison and physical interpretation, it will be helpful to write Eq. (3) in the form

$$E_z = AI_0\left(\beta\sqrt{\frac{\epsilon_{zz}}{\epsilon_{rr}}}\, c\right) . \tag{3a}$$

Outside the plasma column we have

$$E_z = CK_0(\beta r) , \tag{4}$$

where K_0 is the modified Bessel function of the second kind. The boundary conditions at the plasma edge require that

$$\left.\frac{\epsilon_{rr}\left(\frac{dE_z}{dr}\right)}{E_z}\right|_{a-0} = \left.\frac{\left(\frac{dE_z}{dr}\right)}{E_z}\right|_{a+0} . \tag{5}$$

From this boundary condition we obtain the dispersion relation

$$\frac{1}{2}\sqrt{\epsilon_{zz}\cdot\epsilon_{rr}(a)}\;\frac{I_1\left[\beta\sqrt{\frac{\epsilon_{zz}}{\epsilon_{rr}(a)}}\,(a-r_0)\right]}{I_0\left[\beta\sqrt{\frac{\epsilon_{zz}}{\epsilon_{rr}(a)}}\,(a-r_0)\right]} = -\frac{K_1(\beta a)}{K_0(\beta a)} . \tag{6}$$

For real argument, I_1/I_0 and K_1/K_0 are always positive. Hence the dispersion relation cannot be satisfied for real ζ, and the plasma wave is cut off when $\epsilon_{rr} = 0$ just inside the edge of the plasma column. When $r_0 > a$, in which case r_0 is no longer a physical radius but is still a useful parameter, a dispersion relation is obtained which has a solution for real ζ. The proof is then complete that cutoff occurs exactly when $\epsilon_{rr} = 0$ at the plasma edge (*i.e.*, $\epsilon_{rr}(a) = 0$).

We now wish to prove that for $\omega_c < \omega_p(a)$, the lower end of the backward wave passband is at the frequency for which $\epsilon_{zz} = 0$ at the plasma edge. The procedure used to solve for E_z and to derive the dispersion relation is outlined according to the following steps.

Step 1: Solve Eq. (1) near $r = 0$ to obtain the result

$$E_z(0 < r \ll r_0) \simeq E_z(0)\; I_0\left(\beta\sqrt{\frac{\epsilon_{zz}}{\epsilon_{rr}}}\, r\right) . \tag{7}$$

Step 2: Solve Eq. (1) using the WKB method, which is valid at points far from r_0 (r_0 is now the turning point where $\epsilon_{zz} = 0$). This WKB solution has the form

$$E_z \simeq \frac{A_\pm}{\left[r^2(\epsilon_{zz} \cdot \epsilon_{rr})\right]^{1/4}} e^{\pm \beta \int^r \sqrt{\frac{\epsilon_{zz}}{\epsilon_{rr}}}\, dr} \quad . \tag{8}$$

Match the WKB solution to Eq. (7) to evaluate A_+ and A_-.

Step 3: Obtain the turning point solution about r_0 from Eq. (1) in terms of ζ. Match this to the WKB solution. All of the constants of integration are now evaluated. The solution for E_z near the plasma edge is

$$\frac{E_z(r_0 < r < a)}{E_z(0)} = \frac{1}{3}\sqrt{\frac{2}{r_0}}\, \zeta^{\frac{1}{2}} \left[J_{\pm\frac{1}{3}}\left(\frac{2}{3}\beta\sqrt{-\frac{\epsilon_{zz}}{\epsilon_{rr}}}\,\zeta\right) + J_{\mp\frac{1}{3}}\left(\frac{2}{3}\beta\sqrt{-\frac{\epsilon_{zz}}{\epsilon_{rr}}}\,\zeta\right)\right] \quad . \tag{9}$$

When the argument in Eq. (9) is written as

$$\frac{2}{3}\beta\sqrt{\frac{\left(\frac{d\epsilon_{zz}}{dr}\Big|_{r_0}\right)}{-\epsilon_{rr}}}\,\zeta^{\frac{3}{2}} \quad ,$$

the expression for E_z may be recognized as a constant times the Airy function of negative argument, *i.e.,*

$$\Lambda(-y) = \frac{1}{3}\sqrt{\pi|y|}\left\{ J_{\frac{1}{3}}\left(\frac{2}{3}|y|^{\frac{3}{2}}\right) + J_{-\frac{1}{3}}\left(\frac{2}{3}|y|^{\frac{3}{2}}\right) \right. \quad ,$$

where $y<0$. The Airy function is tabulated and may be used for numerical evaluation of E_z or of the dispersion relation. The dispersion relation obtained by applying the boundary condition [Eq. (5)] may be expressed in several different forms. One useful form is

$$\sqrt{-\epsilon_{rr} \cdot \epsilon_{zz}(a)}\, \frac{\left[J_{-\frac{2}{3}}\left(\frac{2}{3}\beta\sqrt{-\frac{\epsilon_{zz}}{\epsilon_{rr}}}\,(a - r_0)\right) - J_{\frac{2}{3}}\left(\frac{2}{3}\beta\sqrt{-\frac{\epsilon_{zz}}{\epsilon_{rr}}}\,(a - r_0)\right)\right]}{\left[J_{\frac{1}{3}}\left(\frac{2}{3}\beta\sqrt{-\frac{\epsilon_{zz}}{\epsilon_{rr}}}\,(a - r_0)\right) + J_{-\frac{1}{3}}\left(\frac{2}{3}\beta\sqrt{-\frac{\epsilon_{zz}}{\epsilon_{rr}}}\,(a - r_0)\right)\right]} = 1 \quad . \tag{10}$$

A convenient way to interpret the dispersion relation, however, is to define and plot a function

$$F(x) = x^{\frac{1}{3}} \left[J_{\frac{1}{3}}(x) + J_{-\frac{1}{3}}(x) \right] , \tag{11}$$

where

$$x = \frac{2}{3} \beta \sqrt{\frac{\left(\frac{\partial \epsilon_{zz}}{\partial r} \Big|_{r_0} \right)}{-\epsilon_{rr}}} \delta^{\frac{3}{2}} = \frac{2}{3} \beta \sqrt{\frac{\epsilon_{zz}}{-\epsilon_{rr}}} \delta . \tag{12}$$

The dispersion relation then may be written as

$$\sqrt{-\epsilon_{rr} \cdot \epsilon_{zz}(x_z)} \frac{F'(x_a)}{F(x_a)} = 1 , \tag{13}$$

where, of course,

$$x_a = \frac{2}{3} \beta \sqrt{\frac{\epsilon_{zz}(a)}{-\epsilon_{rr}}} (a - r_0) .$$

A crude plot of $F(x)$ is shown on Figure 1. The dispersion relation may be satisfied for real β when $F(x_a)$ and $F'(x_a)$ have the same sign. Thus a solution to Eq. (13) *may* exist when $0 < x_a < 0.687$, and a solution *does* exist when $2.38 < x_a < 3.80$, since in this latter region $F'(x_a)/F(x_a)$ can take on all values between infinity and zero. The solution in this latter range goes to the well-known solution for the uniform plasma in the limit as the plasma taper goes to zero.

From the examples given in this report and from the results of our computer programs, several general conclusions may be drawn concerning the behavior of the electric field in the backward wave passband. One significant physical feature is that in a plasma region where ϵ_{zz} and ϵ_{rr} are of the same sign, E_z varies radially like an exponential function, whereas if ϵ_{zz} and ϵ_{rr} are of opposite sign, E_z varies radially as an oscillating function; this result will be seen directly from Eq. (8). Another significant feature is that E_z changes sign just inside the edge of the plasma column (with the possible exception to Eq. (13) when $0 < x_a < 0.687$). This "field reversal" phenomenon also occurs with the uniform plasma column in free space and is a consequence of the fact that ϵ_{rr} changes sign at the edge of the plasma.

"Field reversal" occurs very close to the plasma edge, and in effect means that the electric fields behave very much as though the plasma were filling a metal drift tube. That is, for a plasma filling a drift tube, E_z must go to zero at the plasma edge, whereas for a plasma column in free space E_z goes to zero just inside the edge. The fields in the body of the plasma are essentially the same in both cases. Thus in theoretical work concerning the backward wave passband, we may neglect the presence of dielectrics or of a free space region just outside

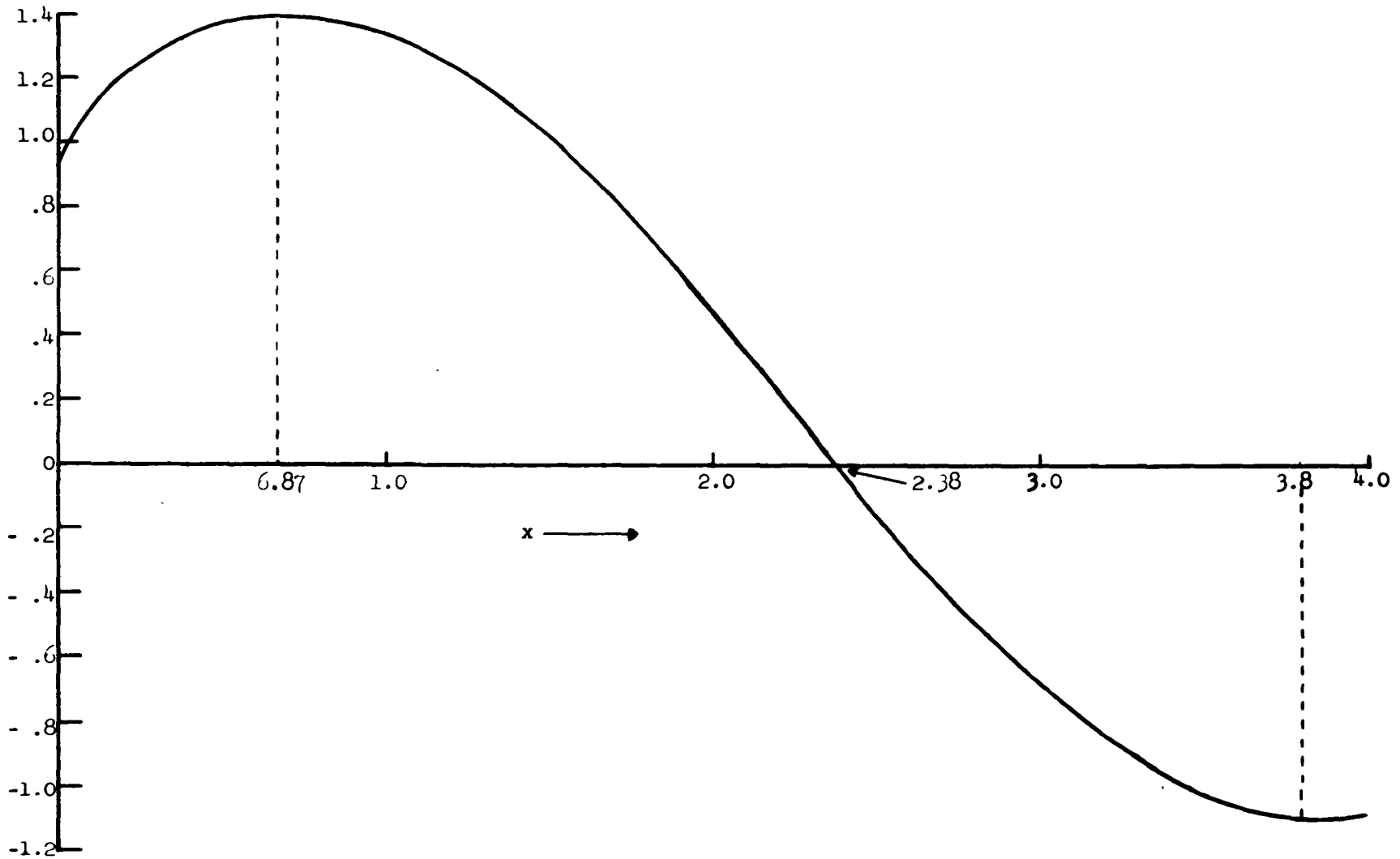

FIGURE 1. Sketch of $F(x)=x^{1/3}\,[J_{1/3}(x) + J_{-1/3}(x)]$

the plasma column and solve the problem of a plasma filling a drift tube, the change in calculated propagation between the different cases being negligible. This simplifies the application of the theory immensely. We have tested this hypothesis numerically on the computer, both with the beam present and without the beam present and find that it is indeed a very good and useful approximation (see Figure 2).

Some other results of our propagation theory will be given here without proof, the proofs being similar to the examples already given:

1. For $\omega_c < \omega_p(a)$, the forward wave passband is in the range $0 < \omega < [\omega_c^2 + \omega_p^2(a)]/2$ for a plasma column in free space. For a plasma filling a drift tube, the forward wave passband is in the range $0 < \omega < \omega_c$, (*i.e.*, $\beta \to \infty$ as $\varepsilon_{rr} \to \infty$).
2. For $\omega_c > \omega_p(a)$, the lower end of the backward wave passband is at $\omega = \omega_c$ (*i.e.*, $|\varepsilon_{rr}| = \infty$), whether the plasma is in a drift tube or in free space.
3. For $\omega_c > \omega_p(a)$, the forward wave passband covers the range $0 < \omega < \omega_p(a)$, whether the plasma is in a drift tube or in free space.

In general, insofar as the cutoffs and asymptotes of the $\omega - \beta$ diagram are concerned, they are the same as for the uniform plasma if we replace $\omega_{p\,\text{uniform}}$ by $\omega_p(a)$. The electric field variations, however, and the $\omega - \beta$ characteristics between endpoints are quite different from the uniform case and depend upon more than mere edge effects. Some curves of E_z are shown in Figures 3 and 4. Note that the examples in Figure 4 do indeed behave as predicted in Eq. (9).

An experiment has been set up to test our propagation theory. A schematic of the experiment is shown in Figure 5. A mercury discharge plasma tube and a cesium discharge plasma tube will be used in the experiment. The long plasma tube is inside a slotted drift tube centered in the magnetic field of a long solenoid. A traveling probe assembly has been built with the crystal detector and tuning stub an integral part of the assembly and very close to the probe. The probe extends into the space between the drift tube and the glass tube in order to detect the electric field outside the glass. An rf signal is launched into the plasma from the collector end of the tube and a small rf signal from the same source is fed into the probe assembly just before the crystal. The plasma is modulated with a 1000 cps sinusoidal signal applied to the auxiliary anode of the tube. Maxima and minima are detected along the length of the plasma column, the minima being a wavelength of the propagating mode apart. Thus we expect to experimentally obtain detailed $\omega - \beta$ diagrams which we can compare to theoretical curves in order to check our theory and to learn something about the plasma profile.

the plasma column and solve the problem of a plasma filling a drift tube, the change in calculated propagation between the different cases being negligible. This simplifies the application of the theory immensely. We have tested this hypothesis numerically on the computer, both with the beam present and without the beam present and find that it is indeed a very good and useful approximation (see Figure 2).

Some other results of our propagation theory will be given here without proof, the proofs being similar to the examples already given:

1. For $\omega_c < \omega_p(a)$, the forward wave passband is in the range $0 < \omega < [\omega_c^2 + \omega_p^2(a)]/2$ for a plasma column in free space. For a plasma filling a drift tube, the forward wave passband is in the range $0 < \omega < \omega_c$, (*i.e.*, $\beta \to \infty$ as $\varepsilon_{rr} \to \infty$).
2. For $\omega_c > \omega_p(a)$, the lower end of the backward wave passband is at $\omega = \omega_c$ (*i.e.*, $|\varepsilon_{rr}| = \infty$), whether the plasma is in a drift tube or in free space.
3. For $\omega_c > \omega_p(a)$, the forward wave passband covers the range $0 < \omega < \omega_p(a)$, whether the plasma is in a drift tube or in free space.

In general, insofar as the cutoffs and asymptotes of the $\omega - \beta$ diagram are concerned, they are the same as for the uniform plasma if we replace $\omega_{p\,\text{uniform}}$ by $\omega_p(a)$. The electric field variations, however, and the $\omega - \beta$ characteristics between endpoints are quite different from the uniform case and depend upon more than mere edge effects. Some curves of E_z are shown in Figures 3 and 4. Note that the examples in Figure 4 do indeed behave as predicted in Eq. (9).

An experiment has been set up to test our propagation theory. A schematic of the experiment is shown in Figure 5. A mercury discharge plasma tube and a cesium discharge plasma tube will be used in the experiment. The long plasma tube is inside a slotted drift tube centered in the magnetic field of a long solenoid. A traveling probe assembly has been built with the crystal detector and tuning stub an integral part of the assembly and very close to the probe. The probe extends into the space between the drift tube and the glass tube in order to detect the electric field outside the glass. An rf signal is launched into the plasma from the collector end of the tube and a small rf signal from the same source is fed into the probe assembly just before the crystal. The plasma is modulated with a 1000 cps sinusoidal signal applied to the auxiliary anode of the tube. Maxima and minima are detected along the length of the plasma column, the minima being a wavelength of the propagating mode apart. Thus we expect to experimentally obtain detailed $\omega - \beta$ diagrams which we can compare to theoretical curves in order to check our theory and to learn something about the plasma profile.

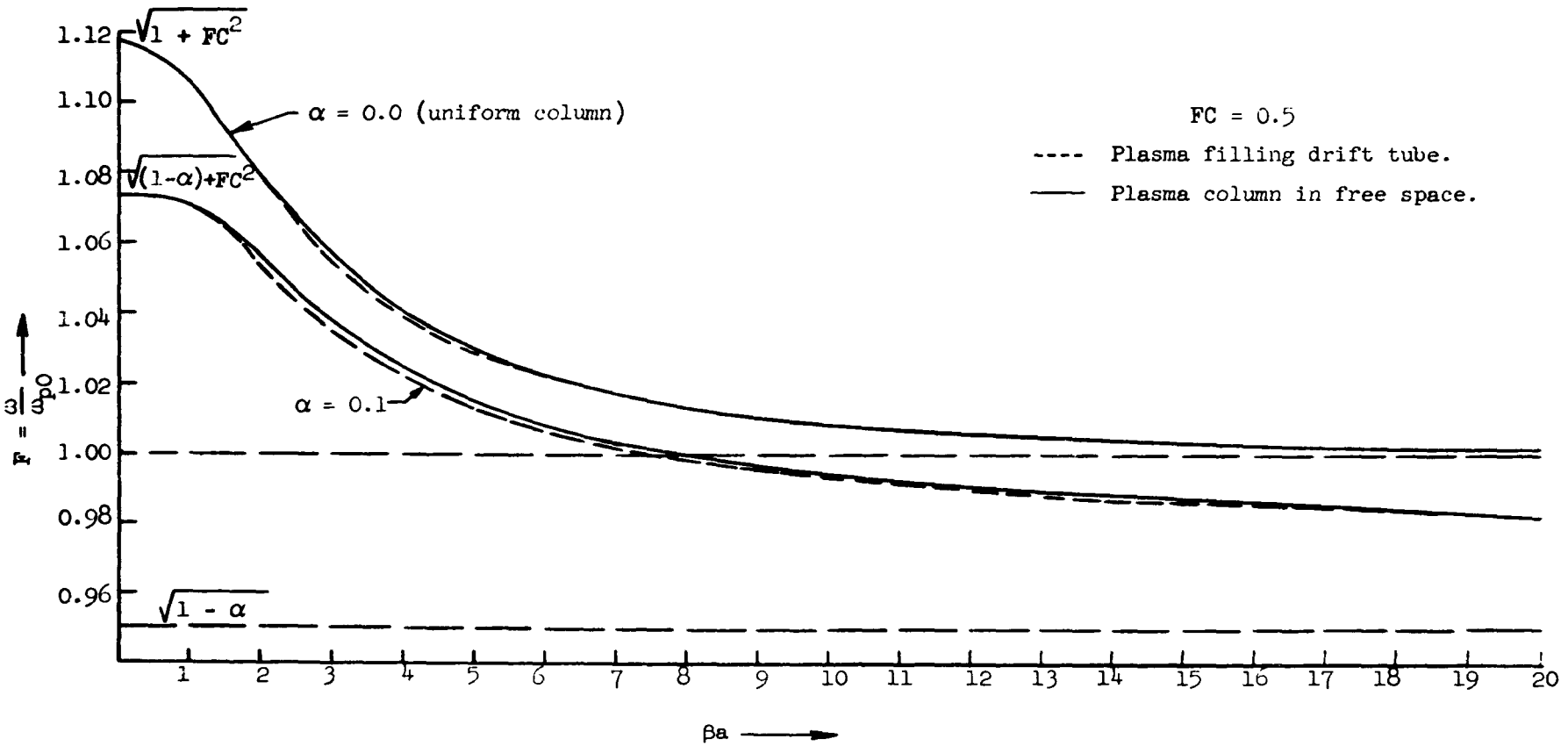

FIGURE 2. Backward wave phase characteristics of plasma column with radial parabolic density variation.

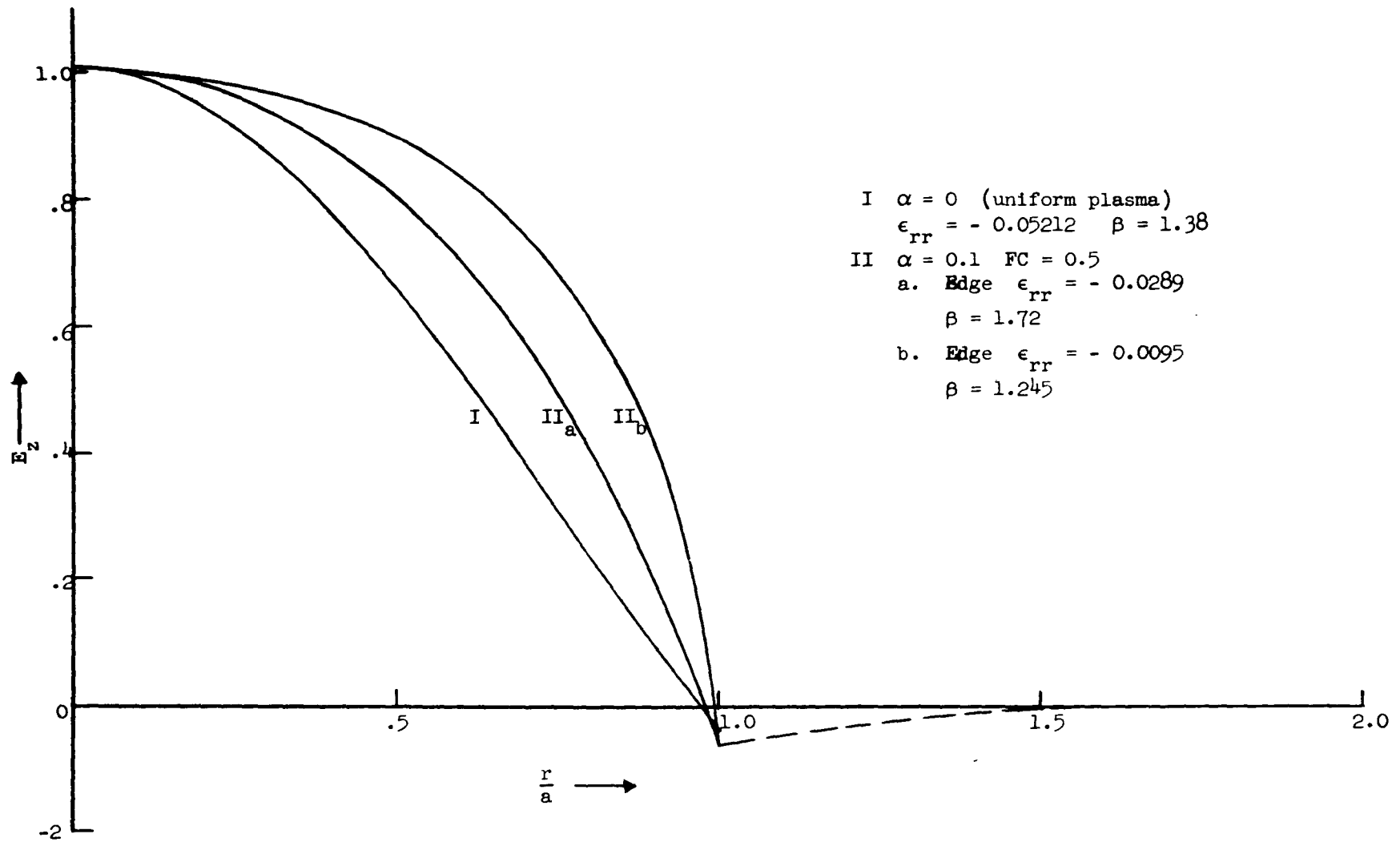

FIGURE 3. Behavior of E_z inside a plasma column of nonuniform cross section as ϵ_{rr} goes to zero at plasma edge. (No turning point inside plasma column.)

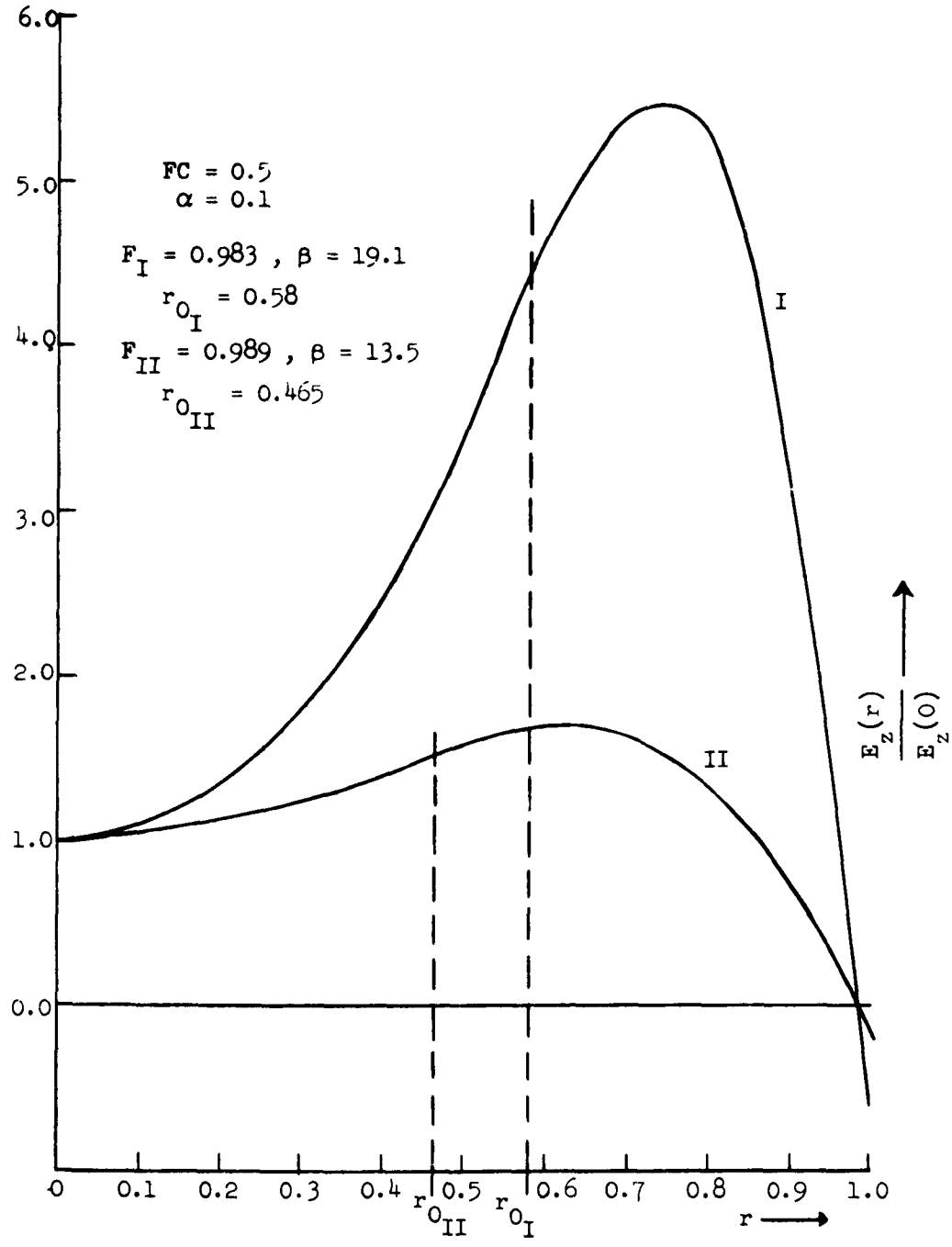

FIGURE 4. Plasma column in free space. Behavior of E_z in backward wave passband as ϵ_{rr} goes to zero at plasma edge. (Turning point is inside plasma column.)

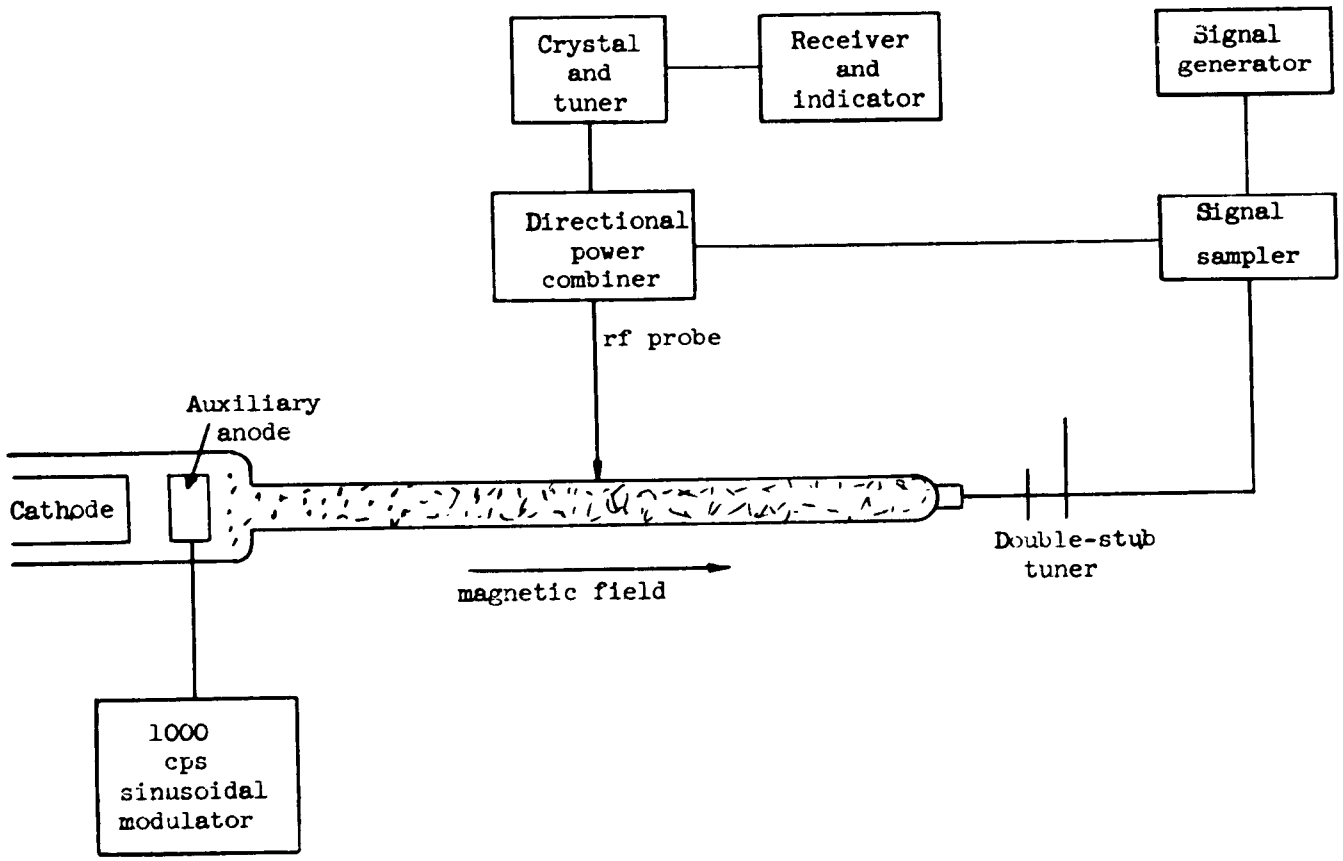

FIGURE 5. Schematic diagram of experiment to measure phase characteristics of a plasma. Tube is in a slotted drift tube centered in a long solenoid.

XI. Transverse Wave Devices

A. Introduction

The objective of this project is to study a possible approach to broadband high-powered amplifiers which involves interaction between an electron beam and a circuit in the presence of an axial dc magnetic field. This amplification mechanism depends on interaction between the transverse motion of an electron in a magnetic field with transverse electric fields. Examples of such interaction are the Adler low-noise tube using quadrupole amplifiers, and the so-called fast wave tubes where the electron beam is interacting with an ordinary fast electromagnetic wave in an unloaded waveguide. In the first case, this type of interaction was used for low-noise amplifiers; in the second case, for very high frequency amplifiers. There are many possible variations of this kind of interaction, however, which would be appropriate to any frequency range and not merely for low-noise.

B. Background

This project has been in a formative stage for several months and this is the first regular report on the work done to date.

During the course of these past few months the work has been essentially theoretical and is now nearing a point where experimental work can begin. The theoretical work has not been written out in a complete discussion. However, there have been four papers presented on the theoretical work, as well as one technical note, and collectively they present the work done to date. They are:

1. *Two papers presented at the Conference on Electron Tube Research, University of Minnesota, June 1962.*

   (a) T. Wessel-Berg, "A Thick Beam Analysis of Transverse-Wave Propagation on Brillouin Beams," also prepared as an Internal Memorandum, Microwave Laboratory Report No. 938.

The abstract follows:

"This paper presents a general analysis of transverse-wave propagation on Brillouin beams in a drift tube under relativistic conditions, including the effect of the rf magnetic field. The latter point is essential in obtaining correct results for waves having infinite or near infinite phase velocity.

"The waves are obtained by separation of Maxwell's equations in the form $\exp j(\omega t - \beta z - m\theta)$ where the transverse or θ-varying modes are obtained by setting $m = \pm 1, \pm 2, \ldots$ In general, there are four independent solutions for each m. Two of these are characterized by having an inside field pattern and beam ripple which result in no fields external to the beam; these waves can therefore not interact with external circuit modes. Of the remaining two waves, one can be characterized as a cyclotron wave, and the other as a synchronous or quasi-synchronous wave. The waves are positive or negative polarized according to the sign of m.

"In particular, setting $m = \pm 1$, one obtains the ordinary cyclotron waves and synchronous waves. Curves are presented showing the propagation factors as functions of beam and drift tube diameter, and beam velocity. For very small beam diameter they reduce to the values obtained from the filamentary beam model.

"The analysis shows, moreover, that the details of transverse electron motion and displacements do not correspond to the simple picture obtained from the filamentary beam model. In particular, this applies to the "synchronous" waves, which are not simple displacement waves, but have transverse velocity components as well. This implies that the details of the interaction between a circuit and the transverse beam waves in certain respects differ from that obtained using the filamentary beam model.

"In conclusion, the paper discusses higher order transverse modes obtained for $|m| > 1$ and suggests some simple amplifying schemes based on these."

(b) T. Wessel-Berg and K. Blotekjaer, "DC-pumped Transverse-Wave Amplifiers Using Synchronous Waves."

The abstract follows:

"This paper describes two experimental dc pumped amplifiers based on transverse synchronous waves. The first amplifier is based on a pumping scheme involving active coupling of the fast cyclotron wave and the slow synchronous wave in a periodic magnetostatic field of rotational symmetry. The second amplifier makes use of the two synchronous waves which are coupled actively in a straight electrostatic quadrupole field. The input and output couplers are of the Cuccia type, with magnetic field reversals between the couplers and the pump for conversion from cyclotron to synchronous waves.

"This paper presents experimental results for gain and bandwidth for both tubes."

2. *Two papers presented at the International Congress of Microwave Tubes, The Hague, Netherlands, September, 1962.*

(a) T. Wessel-Berg and K. Blotekjaer, "Minimum Noise Temperature of Transverse-Wave DC-pumped Electron Beam Amplifiers." (M. L. Report 948.)

The abstract follows:

"This paper is concerned with a general analysis of noise properties in dc-pumped amplifiers involving transverse electron beam waves. The analysis deals with the fundamental noise excitation processes at the cathode and the subsequent noise transformation taking place in the region between the cathode and the amplifying section. The approach is based on a noise-matrix description and is analogous to the work done by Haus and Robinson for longitudinal space-charge wave amplifiers.

"It is shown that any nonparametric amplifier involving either the cyclotron waves or the synchronous waves has the same theoretical minimum noise temperature, which is determined by the physical conditions at the cathode. The noise temperature can be reduced to an arbitrarily small value by increasing the magnetic field at the cathode or by reducing the cathode diameter. In the former case, the noise reduction is due to the fact that the rf power carried by transverse beam waves generally is proportional to ω/ω_c. In the latter case, the reduction is caused by noise cancellation due to correlated noise components. It is shown that this latter effect depends only on the smallest dimension of the cathode. Therefore, a thin flat beam can have extremely low minimum noise temperature and at the same time carry sufficient beam current.

"The minimum noise temperature for any of these beam configurations can be realized by inserting a suitable noise transformer between the cathode and the amplifier. In general, structures with electric and magnetic fields having rotational symmetry, such as used in normal electron guns, can perform the required transformation. Some specific examples of noise transformers are discussed.

"The paper further deals with a comparison of the present theory with the idea of noise reduction by letting the beam expand due to electric lenses or its own space-charge. The idea that the intrinsic transverse noise temperature is reduced inversely proportional to the beam cross section is shown to be basically incorrect. Provided nonlinear effects are neglected, the results appear to explain the failure of beam cooling experiments based on beam expansion."

(b) T. Wessel-Berg, "A Thick Beam Analysis of Transverse-Wave Propagation on Electron Beams." (M. L. Report No. 978.)

The abstract follows:

"The paper presents results from a theoretical analysis of transverse wave propagation on electron beams of finite diameter and dc space-charge between zero and full Brillouin value. The waves are obtained by separation of Maxwell's equations in the form exp $j(\omega t - m\phi - \beta z)$ where m is an integer specifying the

number of full cycles around the circumference. The amount of dc space charge in the beam is a very important parameter as far as propagation characteristics of higher order modes are concerned.

"For each value of m, four independent wave solutions are obtained. In particular, the number of fundamental transverse waves, obtained by setting $m = \pm 1$, is eight, rather than the four predicted from the filamentary beam theory.

"The paper discusses dispersion and energy relations, and points out possible applications of some of the waves in amplifiers using nonperiodic circuits."

3. *Technical Note.*

(a) T. Wessel-Berg, "Electronic Interaction Theory for Transverse-Wave Couplers," Microwave Laboratory Report No. 922, Stanford University, (July, 1962).

The abstract follows:

"This report is concerned with a general theoretical anaylsis of the interaction between transverse waves propagating on a filamentary electron beam and electromagnetic circuits. The class of circuits considered is that for which the transverse electric and magnetic fields are symmetric with respect to the z-axis. Aside from this restriction on the symmetry properties, the analysis is quite general in the sense that the transverse electric and magnetic field components are arbitrary functions of axial distance. Therefore, the analysis is valid for a variety of circuit configurations, ranging from simple coupler circuits, serving the purpose of coupling rf power in and out of the beam in rf and dc-pumped devices, to transverse traveling-wave tubes and multicavity klystrons.

"The transverse field components in pump circuits used for parametric pumping and dc pumping of transverse waves are all antisymmetric with respect to the z-axis and are therefore excluded from the present analysis.

"The material contained in this report deals almost exclusively with the electronic part of the interaction, that is, how the transverse beam waves are affected by a specified electromagnetic circuit field. The merit of this approach is that it preserves generality, and leads to results which hold regardless of the details of the circuit configuration. Specifically, the analysis leads to the establishment of criteria for selective coupling to one or several transverse waves, expressed in terms of coupling integrals;—it deals with power relations and discusses various methods of calculating the exchange of power between the beam waves and transverse circuit fields;—it proves conclusively that the established term of the kinetic power conservation theorem is correct under the most general circumstances;—and finally, the analysis deals with the question of whether or not the transverse waves are monoenergetic. It is shown that the waves generally are not monoenergetic, but carry a second-harmonic longitudinal modulation representing a spread in energy which under certain circumstances is comparable to the rf energy carried by the waves. The energy spread depends on the details of the circuit field used for launching the wave, and is identically zero only for circularly polarized fields."

C. Present Status

1. *Thick Beam Analysis of Transverse Waves*

During the report period significant progress has been made in establishing a theory for transverse wave propagation on electron beams of finite diameter. The analysis is not yet fully completed in all the details as far as dispersion diagrams, etc., are concerned. However, some apparently significant results are available. These can be summarized as follows:

The filamentary beam model is inadequate in several respects. First, it does not properly describe the details of the electron motions inside a beam of finite thickness. In particular, it does not predict velocity

spread across the beam cross section. The thick beam analysis, including the effect of beam space charge, shows considerable velocity spread, a result which is significant for possible applications of transverse waves in high-efficiency devices based on depressed collector schemes.

Second, the filamentary theory does not predict all the transverse waves that can exist on a beam of finite space charge. The presence of space charge introduces a splitting of modes. The total number of transverse waves is therefore eight, rather than the four predicted from the filamentary theory.

Third, the filamentary theory does not predict higher order transverse waves having more than one full variation around the circumference. Some of these higher order modes appear to have very interesting properties. Specifically, the higher order waves can have infinite or near infinite phase velocities and still carry negative energy, making possible electron beam amplifiers using nonperiodic circuits. This obvously may be of importance in millimeter wave applications.

The work is now progressing to finish the details of the calculations and to evaluate the various possible new interaction schemes which have resulted from the analysis.

2. *Experimental Work*

Since the main emphasis has been on establishing a more adequate theory for transverse wave propagation, very little experimental work has been done. Preliminary work has been started on the design of a dc pumped synchronous wave amplifier using exclusively nonperiodic structures and two magnetic field reversals. The tube will employ a 10 kV Brillouin beam of perveance unity, operating in the S-band with bandwidth of approximately 10 percent. The theoretical efficiency is of the order of 50 percent.

Rome Air Development Center, Griffiss AF Base, N. Y. Rpt. No. RADC-TDR-62-618. MULTI-MEGAWATT BROADBAND MICROWAVE TUBES AND RELATED STUDIES. First Annual Rpt., 1 Sept 61–31 Oct. 62, 87 pp. incl. ills.

Unclassified Report

This report describes theoretical and experimental investigations of microwave tubes. The general objectives of the contract were to develop tubes capable of at least 10 megawatts of peak power, average power approaching 50 kilowatts, bandwidths approaching 30 percent, gains of 35 db, and efficiencies of 40 percent and to conduct theoretical and experimental investigations of other related microwave devices.

1. Electron Tubes
2. Electron Guns
3. Electron Multipliers

I. RADC Project 5573, Task 557303

II. Contract AF30(602)-2575

III. Microwave Laboratory, W.W. Hansen Laboratories of Physics, Stanford Univ., Stanford, Calif.

IV. In ASTIA Collection

Rome Air Development Center, Griffiss AF Base, N. Y. Rpt. No. RADC-TDR-62-618. MULTI-MEGAWATT BROADBAND MICROWAVE TUBES AND RELATED STUDIES. First Annual Rpt., 1 Sept 61–31 Oct. 62, 87 pp. incl. ills.

Unclassified Report

This report describes theoretical and experimental investigations of microwave tubes. The general objectives of the contract were to develop tubes capable of at least 10 megawatts of peak power, average power approaching 50 kilowatts, bandwidths approaching 30 percent, gains of 35 db, and efficiencies of 40 percent and to conduct theoretical and experimental investigations of other related microwave devices.

1. Electron Tubes
2. Electron Guns
3. Electron Multipliers

I. RADC Project 5573, Task 557303

II. Contract AF30(602)-2575

III. Microwave Laboratory, W.W. Hansen Laboratories of Physics, Stanford Univ., Stanford, Calif.

IV. In ASTIA Collection

Rome Air Development Center, Griffiss AF Base, N. Y. Rpt. No. RADC-TDR-62-618. MULTI-MEGAWATT BROADBAND MICROWAVE TUBES AND RELATED STUDIES. First Annual Rpt., 1 Sept 61–31 Oct. 62, 87 pp. incl. ills.

Unclassified Report

This report describes theoretical and experimental investigations of microwave tubes. The general objectives of the contract were to develop tubes capable of at least 10 megawatts of peak power, average power approaching 50 kilowatts, bandwidths approaching 30 percent, gains of 35 db, and efficiencies of 40 percent and to conduct theoretical and experimental investigations of other related microwave devices.

1. Electron Tubes
2. Electron Guns
3. Electron Multipliers

I. RADC Project 5573, Task 557303

II. Contract AF30(602)-2575

III. Microwave Laboratory, W.W. Hansen Laboratories of Physics, Stanford Univ., Stanford, Calif.

IV. In ASTIA Collection

Rome Air Development Center, Griffiss AF Base, N. Y. Rpt. No. RADC-TDR-62-618. MULTI-MEGAWATT BROADBAND MICROWAVE TUBES AND RELATED STUDIES. First Annual Rpt., 1 Sept 61–31 Oct. 62, 87 pp. incl. ills.

Unclassified Report

This report describes theoretical and experimental investigations of microwave tubes. The general objectives of the contract were to develop tubes capable of at least 10 megawatts of peak power, average power approaching 50 kilowatts, bandwidths approaching 30 percent, gains of 35 db, and efficiencies of 40 percent and to conduct theoretical and experimental investigations of other related microwave devices.

1. Electron Tubes
2. Electron Guns
3. Electron Multipliers

I. RADC Project 5573, Task 557303

II. Contract AF30(602)-2575

III. Microwave Laboratory, W.W. Hansen Laboratories of Physics, Stanford Univ., Stanford, Calif.

IV. In ASTIA Collection